Dissertation zur Erlangung des Doktorgrades
der Fakultät für Chemie und Pharmazie
der Ludwig-Maximilians-Universität München

Mechanisms of secretory cargo sorting at the *trans*-Golgi network

Mai Ly Tran

Aus

Schkeuditz, Deutschland

2022

Erklärung

Diese Dissertation wurde im Sinne von § 7 der Promotionsordnung vom 28. November 2011 von Herrn Prof. Dr. Klaus Förstemann betreut.

Eidesstattliche Versicherung

Diese Dissertation wurde eigenständig und ohne unerlaubte Hilfe erarbeitet.

München, 26.04.2022 ....   Mai Ly Tran ....

Mai Ly Tran

Dissertation eingereicht am 10.02.2022……....................

1. Gutachter: ………………….....................................   Prof. Dr. Klaus Förstemann

2. Gutachterin: ………………….................................   Assoc. Prof. Dr. Julia von Blume

Mündliche Prüfung am 09.03.2022……...........................

Table of content

List of abbreviations

APs	adaptor proteins
SNCA	α-synuclein
APEX	ascorbate peroxidase
βGC	β-glucocerebrosidase
BIP	binding immunoglobulin protein, also known as GRP78, HSPA5
BirA	biotin ligase from Escherichia coli
Cab45	Ca^{2+}-binding protein, 45 kDa
Cab45-6EQ	Ca^{2+}-binding deficient mutant
Cab45KO	Cab45 knockout
Cab45wt-rescue	Cab45 wild-type rescue mutant
Ca^{2+}	calcium
CAML	calcium-modulating cyclophilin protein
CNX	calnexin
CRT	calreticulin
CPE	carboxypeptidase E
CL	cardiolipin
CARTS	CARriers of the TGN to the Surface
COMP	cartilage oligomeric matrix protein
CatD	Cathepsin D, gene: CTSD
CERT	ceramide transfer protein
CgA	chromogranin A
CgB	chromogranin B
CCV	clathrin-coated vesicle
CD9	cluster of differentiation 9
COPI, II	coatomer protein complex I, II
CFL-1	cofilin
CHX	cycloheximide
DAG	diacylglycerol
DBCO	diarylcyclooctyne
PDZ1/2	Domain found in post synaptic density protein (PSD95),
Drosophila	disc large tumor suppressor (Dlg1), zonula occludens-1 protein zo-1)
ERp57	Endoplasmic reticulum resident protein 57
ESCRT	endosomal sorting complexes required for transport
EQ	equinatoxin
EDEM1, 2, 3	ER degradation enhancing mannosidases 1, 2, 3
ERES	ER exit sites
ERAD	ER-associated degradation
ERGIC	ER-Golgi intermediate compartment
ERGIC-53	ER-Golgi intermediate compartment 53 kDa protein or lectin mannose-binding 1
ECM	extracellular matrix
ERK	extracellular signal-regulated kinase.
CREC	family of low affinity, Ca^{2+}-binding, multiple EF-hand proteins, reticulocalbin, ER Ca^{2+}-binding protein of 55 kDa (ERC-55), reticulocalbin-3, Cab45, calumenin

Fam20 C	Family with sequence similarity of 20, member C
FAK	Focal adhesion kinase
FTLD	Frontotemporal lobar degeneration
GALNT	GalNAc transferase
GM$_2$AP	ganglioside GM2 activator protein
GD	Gaucher's Disease
GLPs	glycerophospholipids
GGT	glycolipid glycosyltransferase
GL	glycolipids
GSL	glycosphingolipids
GPI	glycosylphosphatidylinositol
GT	glycosyltransferases
GA	Golgi apparatus
GM130	Golgi matrix protein 130
GRASP55/65	Golgi reassembly and stacking protein 55 /65
GGA	Golgi-localized, γ-ear Arf-binding proteins
GAP	GTPase-activating protein
GEF	guanine exchange factor
GDP-GTP	Guanosine-5'-di/triphosphate
Hsc70	Heat shock cognate protein, 70 kDa
HSP40,70,90	Heat shock protein 40, 70, 90 kDa
hiSPECS	high-performance secretome protein enrichment with click sugars
HRP	horseradish peroxidase
ICD	I-cell disease
IGF2RKO	IGF2 receptor knockout
ISG	immature secretory granules
IP$_3$R	inositol 1,4,5-triphosphate receptor
IGFII/IGF2	Insulin-like growth factor 2
ILV	intraluminal vesicle
KIF	kinesin family
LE	late endosomes
lgp	lysosomal (membrane) glycoprotein
LRP1	lipoprotein receptor-related protein-1
LAMP1	Lysosomal associated membrane protein 1
LIMP2	Lysosomal integral membrane protein 2
LMPs	lysosomal membrane proteins
LSD	lysosomal storage disorders
LyzC	Lysozyme C
M6P	mannose-6-phospate
M6PR, CI, CD	mannose-6-phosphate receptor, cation-independent, cation-dependent
MS	mass spectroscopy
MMP2	matrix metalloproteinase 2
matCTSD	mature cathepsin D
MAPK	mitogen-activated protein kinase
MVBs	multivesicular endosomes/bodies
GalNAc	N-acetylgalactosamine
GlcNAc	N-acetylglucosamine
Ac$_4$ManNAZ	N-azido-acetylated-mannosamine-tetraacylated labelling sugar

NPC	Niemann-Pick-disease
OST	oligosaccharyltransferase
ORP1L	OSBP related protein 1L
OPN	Osteopontin
OSBP	oxysterol-binding protein
PAUF	pancreatic adenocarcinoma upregulated factor
PC	phosphatidylcholine
PE	phosphatidylethanolamine
PG	phosphatidylglycerol
PI	phosphatidylinositol
PI(4.5)P$_2$	phosphatidylinositol 4.5-biphosphate
PI4P	phosphatidylinositol 4-monophosphate
PS	phosphatidylserine
PI3K/	phosphoinositide 3-kinases
PM	Plasma membrane
PMCA	plasma membrane Ca^{2+} ATPase
PPC	polypeptide chain
PTM	post-translational modification
proCTSD	pro-cathepsin D
PGRN	progranulin
PSAP	prosaposin
PDI	protein disulfide isomerase
PKB/Akt	protein kinase B (PKB)
PKD	protein kinase D
BioID	proximity-dependent biotin identification
qRT-PCR	Quantitative Reverse Transcription PCR
RV	Recycling vesicles
RUSH	Retention-using-selective-hooks
RNA	ribonucleic acid
rER	rough endoplasmic reticulum
RyR	ryanodine receptor
SERCA	Sarco/Endoplasmic Reticulum Ca^{2+}-ATPase
SgII	secretogranin
SPCA1	secretory Ca^{2+}- ATPase
SP	signal peptide
SPP	signal peptide peptidase
SRP	signal recognition particle
SAPs	SL activator proteins saposins
siRNA	Small interfering RNA
SORT1	sortilin
SORT1KO	Sortilin knockout
SorLA	Sortilin-related receptor with A-type repeats
SM	sphingomyelin
SMS1	sphingomyelin synthase 1
SR	SRP receptor
SG	storage granules
SBP	streptavidin-binding protein
TA	tail-anchored
(TDP)-43	Tar DNA binding protein 43
TGN46KO	TGN46 knockout

TRC40	TMD recognition complex
TGN	trans-Golgi network
TGN38	trans-Golgi network protein 38
TGN46	trans-Golgi network protein, 46 kDa
TMD	transmembrane domain
TMP	transmembrane proteins
TRAPPI	TRAnsport Protein Particle1
UGGT	UDP-glucose:glycosyltransferase
GlcNAc-P	UDP-N-acetyl-D-glucosamin
UCE	uncovering enzyme
UPR	unfolded protein response
Vps	vacuolar protein sorting
VAPA	vesicle-associated membrane protein (VAMP)-associated ER protein A
VSV	Vesicular stomatitis virus
VTC	vesicular tubule complex
v-/t-SNAREs	vesicular/ target (soluble N-ethylmaleimide-sensitive factor attachment protein receptors
WT	wild-type

List of figures

Fig. 3.4: BioID time course with BirA-Cab45 indicates connection to TGN46.

Fig. 3.4.1: Influence of depletion of TGN46 on Cab45 secretion and client trafficking.

Fig. 3.4.2: Colocalization of EQSM-GFP and LyzC-mCherry in HeLa treated with control and TGN46 siRNA.

Fig.3.4.3: Loss of TGN46 slows trafficking of Cab45 and clients.

Fig. 4.8: Overview on Cab45 functions in sorting of soluble proteins.

Supplementary figures and table

Fig. S1 (related to Fig. 3.1.1): Primary set-up of conditions for secretion assays for sicontrol, siCab45 and Cab45KO cells.

Fig. S2A, B (related to Fig. 3.1.3D,E): Secretion assays in receptor KO cell lines under siRNA treatment.

Fig. S3 (related to Fig. 3.2.3E): Golgi exit assay of PSAP-mCherry RUSH in triplicates for HeLa (orange), Cab45KO (blue), Cab45wt-rescue (yellow) and Cab45-6EQ mutant (green).

Table S1 (related to Fig. 3.1.1E): hiSPECS MS results.

Summary

Protein sorting, processing and trafficking are central processes that maintain cellular functions, migration and homeostasis, ultimately defining health or disease of the organism. The secretory pathway comprises the compartments where these processes are realized. In this thesis the focus lies in particular on the last station of the Golgi apparatus (GA) and main sorting hub - the trans-Golgi network (TGN). There, proteins that have been modified post-translationally in earlier Golgi compartments, are sorted by their features, such as a transmembrane domain or a tag via certain receptors to intracellular destinations (e.g. endosomes, lysosomes) or for secretion (to apical and basolateral plasma membrane). Importantly, not all soluble secretory proteins are known to be recognized by a certain receptor, however, they are still sorted specifically to their final destinations. One mechanism involving the Ca^{2+}-binding protein Cab45 was reported to facilitate the sorting of some secretory soluble proteins in the TGN (von Blume et al., 2011, 2012; Crevenna et al., 2016; Deng et al., 2018, Hecht et al., 2020): Ca^{2+}-influx by secretory Ca^{2+}- ATPase (SPCA1) in the TGN lumen after activation via actin/cofilin, leads to oligomerization of Cab45, which can bind its cargo (client) proteins and form Cab45-client-complexes that cluster and remain in the TGN lumen. Upon phosphorylation by Golgi kinase Fam20C the clusters are broken down for packaging into SM-rich vesicles destined for secretion. However, how these Cab45-client complexes are recognized for packaging into specific vesicles is unclear. In this thesis one more component is added to the machinery, the transmembrane protein TGN46, found in proximity-labelling approaches (BioID, APEX ; Deng et al., 2018), and shown here to be involved in the sorting of Cab45 client Lysozyme C (LyzC) by possibly indirect interaction with Cab45. Depletion of TGN46 indicates a delayed formation of post-Golgi vesicles containing LyzC in Retention-using-selective-hooks (RUSH)-based experiments and missorting by reduced co-localization with sphingomyelin (SM)-rich vesicles. Results that are similar to the phenotypes described previously for dysfunctional Cab45 and depletion of other components of the Cab45-dependent sorting mechanism (Deng et al., 2016; Hecht et al., 2020). In addition to this secretion-delayed phenotype of Cab45 clients upon deletion of TGN46, a novel hypersecretion of lysosomal hydrolases was observed with depletion of Cab45 in secretome analysis with subsequent mass spectrometric analysis. Secretion assays confirmed the influence of Cab45 depletion on increased secretion of prosaposin (PSAP), progranulin (PGRN) and with lesser degree Cathepsin D (CatD) implying a new role of Cab45 in sorting of lysosomal proteins. Secretion assays using cells with loss of lysosomal protein receptor sortilin and cation-independent mannose-6-phosphate receptor (M6PR) and Cab45 siRNA treatment indicated an influence of Cab45 on receptor-cargo interactions necessary for correct sorting. This hypothesis was substantiated by RUSH-based live-cell imaging observing the TGN export of PSAP in Cab45 knockout, -Ca^{2+}-binding mutant and -wt rescue compared to control cells. Additionally, lysosomal positioning and co-localization of PSAP with lysosomes was altered with Cab45 deletion. The study gives evidence for the herein new

proposed role of Cab45 in receptor-dependent lysosomal sorting in addition to the already reported receptor-independent sorting of soluble secretory proteins, which is extended with TGN46 as a new component.

1 Introduction

Eukaryotic cells feature a high complexity of reactions, processes, and mechanisms on the molecular level to ensure proper functioning and maintaining cell integrity, homeostasis, cell-cell communication. Ultimately, it decides the fate of tissue and organism health, in particular interesting human health and disease. Just like the whole human body uses smaller units - organs - that perform their specific functions to regulate it, the single cell also regulates the underlying molecular mechanisms in units with functional identity, known as compartments.

Cellular compartmentalization is essential to spatially separate biochemical reactions and maintain a distinct environment with unique pH, ion and protein composition - the functional identity - a prerequisite for the localized macromolecules to function properly. While compartments can also be membrane-less, the membrane-bound organelles like endoplasmic reticulum (ER), Golgi apparatus (GA), mitochondria, lysosomes and the nucleus are more often associated with the term cellular compartments, since they define biological key systems like the endolysosomal system and the secretory pathway (Aguilera-Gomez and Rabouille, 2017). Since each organelle is defined as a compartment with enclosed lipid-bilayer membrane, the exchange of materials between those requires a fundamental concept of vesicular carriers for signaling and transport of macromolecules (Aguilera-Gomez and Rabouille, 2017). Even though the functional identity of organelles is not impaired by exchange via vesicular carriers, the protein composition relies on them. However, transport of longer distances requires a more complex system to modify, prepare and sort the de novo synthesized proteins to their respective destination. The principle of vesicular transport is reflected throughout the secretory pathway: in the transport of *de novo* synthesized proteins from the ER to the GA, the transport throughout the GA in scope of the vesicular transport model and also in transition to other pathways, i.e. when post-Golgi vesicles travel to the endolysosomal system.

About 30% of all proteins undergo transfer through the secretory pathway, independently if they are secreted from or retained within the cell (Guo et al., 2014; Pakdel and von Blume, 2018)(Fig. 1). After their synthesis in the ER, proteins with a signal sequence can enter the ER and are then routed to the Golgi apparatus. They are translocated to the ER-Golgi intermediate compartment (ERGIC) before they enter the GA in coatomer protein complex II (COPII) coated vesicles on the cis-Golgi network during the anterograde transport. During the travel through the Golgi stacks they gain posttranslational modifications including glycosylation and phosphorylation. The modified proteins reach the trans-Golgi network, the main sorting station of the secretory pathway, to be packed into specific secretory vesicles that enable transport to different destinations including the basolateral or apical plasma membrane (Fig.1). For non-secretory proteins, the recognition by receptors enables the separation into vesicles destined for the endolysosomal system, secretory granules and other organelles, including the ER during the retrograde transport. In addition to this, some proteins are

sorted by unknown mechanisms to their final destination as non-secretory or secretory proteins. Within the scope of this thesis the trafficking of secretory and lysosomal proteins from the ER to the GA in the secretory pathway are explained in greater detail in the following, starting with the largest membrane bound organelle - the endoplasmic reticulum.

1.1 the secretory pathway - preparation and modification of secretory and resident proteins
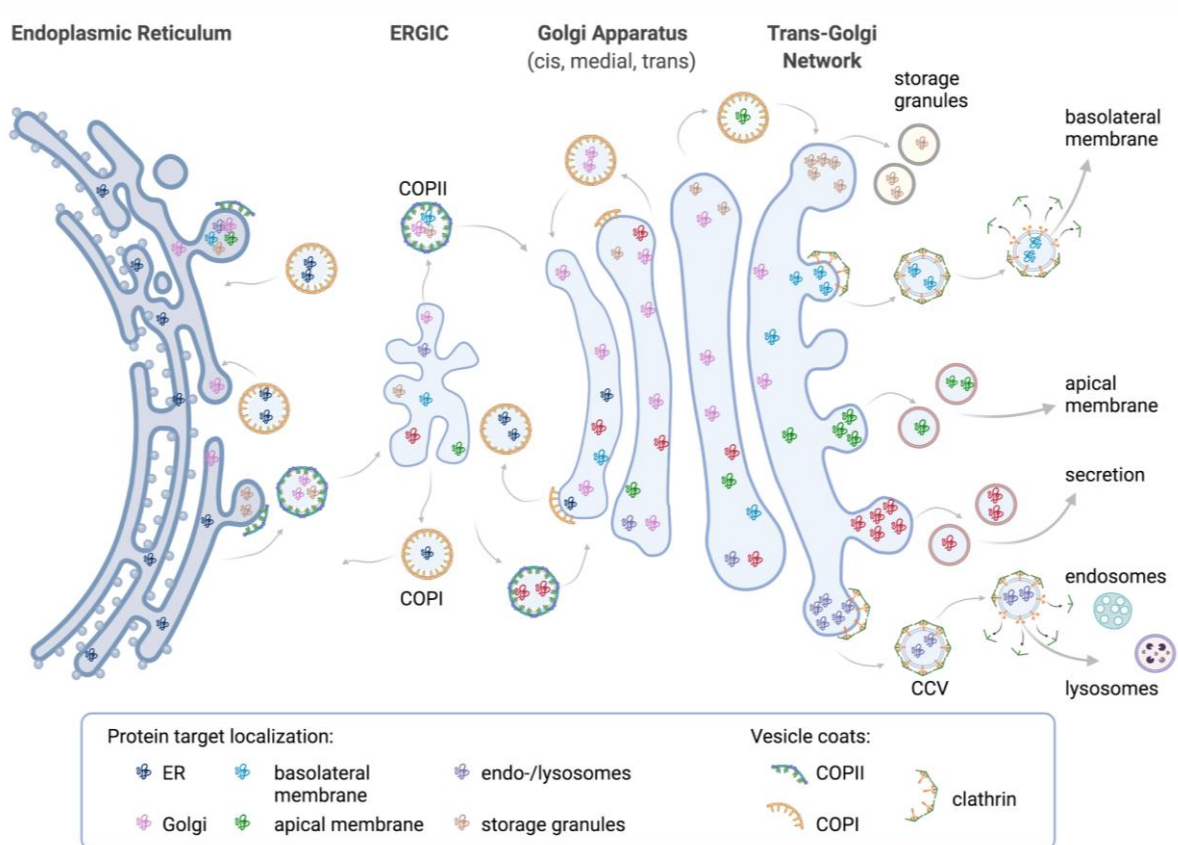
Fig. 1: The secretory pathway at a glance. Proteins synthesized in the rough endoplasmic reticulum (rER) are translocated into the ER lumen and prepared for anterograde transport passing the ER–Golgi intermediate compartment (ERGIC) in coatomer protein complex (COP)II coated vesicles and enter the Golgi apparatus on the cis-face. After migration through the Golgi stacks, they enter the trans-Golgi network to be sorted either into transport carriers destined for storage granules or travel towards basolateral or apical membrane including secretion as well as to the endolysosomal system. Retrograde transport is managed by COPI coated vesicles, while travel from the trans-Golgi network is mediated for example by clathrin-coated vesicles (CCVs), that uncoat before fusing with the target membrane. The figure was created with biorender according to Pakdel and von Blume, 2018.

1.1.1 Protein biosynthesis and translocation in the Endoplasmic Reticulum (ER)

The largest organelle with a complex structure of interconnected membranes, tubules, and cisternae with continuous intracellular lumen, bordering the nucleus, is the endoplasmic reticulum (Voeltz et al., 2002; Lippincott-Schwartz et al., 2000). The ER has a broad range of functions such as protein biosynthesis, protein folding and quality control, detoxification, lipid biosynthesis and calcium (Ca^{2+}) regulation. These processes are occurring in the rough, transitional and smooth ER, respectively (Alberts et al., 2002, Lippincott-Schwartz et al., 2000, Voeltz et al., 2002). Ribosomes line the cytoplasmic surfaces of ER membranes of the rough ER, and act as a factory for de novo synthesis of proteins in the ER lumen - the main function of the ER. The smooth ER is only featured in specialized cells like steroid synthesizing cells, liver cells or neurons (Voeltz et al., 2002).

One third of the cellular proteome (Fagerberg et al., 2010), including all transmembrane and secretory proteins are synthesized in the rough ER, where the transitional ER harbors enzymes important for translocating the protein out of the ER. Due to the localization of ribosomes on the cytosolic site of the ER membrane, proteins are synthesized in the cytosol. To enter the secretory pathway, however, proteins need to enter the ER lumen by translocation across the ER membrane (Fig. 2A). Proteins that are destined for the ER present a N-terminal signal peptide (SP) localizing the protein synthesis to proximity of the ER membrane, where the signal recognition particle (SRP) is located (Zhang and Shan, 2014; Alberts et al., 2002, Heijne, 1984). The SRP recognizes the SP and binds the nascent chain, before the nascent polypeptide chain (PPC) is synthesized completely, which stalls further translation. With formation of the SRP-ribosome complex the ribosome, release of the hydrophobic PPC into the cytosol is prevented by proximity to the ER membrane. There, the SRP receptor (SR) interacts with SRP via its cytosolic domain to pull the complex towards the translocon. The translocon, the sec61 complex, is a multidomain aquatic pore complex spanning the ER membrane. It features a binding site for the signal sequence of the nascent PPC that induces opening of its pore channel towards the ER lumen (Voorhees and Hedge, 2016). As soon as the ribosomal nascent tunnel and the pore align, the opening to the cytosol is sealed with the ribosome and SRP detaches, which leads to continuation of the ribosomal protein translation into the ER lumen. In contrast to proteins translocated via SRP co-translationally, secretory and tail-anchored (TA) membrane proteins contain their transmembrane domain or tail-anchor region at the C-terminus and are therefore post-translationally translocated (Fig. 2C). After release from the ribosomal exit tunnel they are exposed to the cytosol, before being recognized for ER membrane translocation by the TMD recognition complex TRC40 (Johnson et al., 2013). The TRC40 delivered TA proteins are translocated via tryptophan-rich-basic protein ER receptor in presence of calcium-modulating cyclophilin protein (CAML) (Yamamoto and Sakisaka, 2012). Even though secretory proteins contain a signal sequence which is recognized by SRP for co-translational entry into the ER lumen, the chain length of some of

the targeting signals are too short to be efficiently bound by SRP. For those proteins post-translational translocation is assisted by cytosolic chaperones HSP70 or TRC40 to capture the de novo synthesized protein preventing aggregation before guiding them to the sec61 translocon (Zimmermann et al., 1988; Johnson et al., 2012)(Fig. 2B).
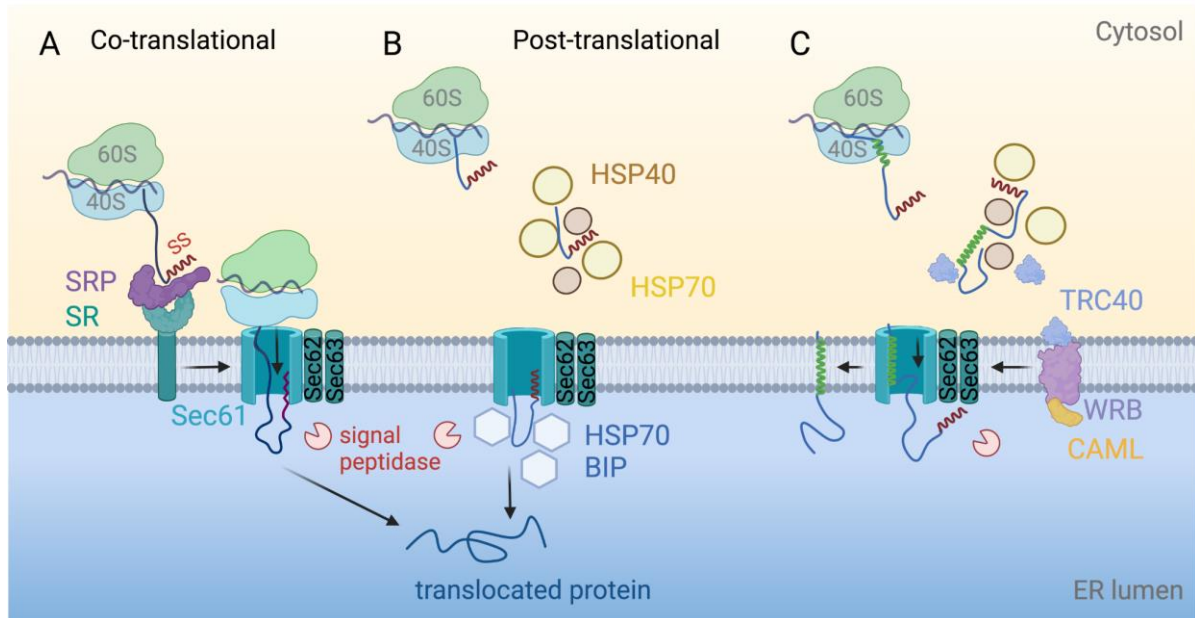
Fig. 2: Schematic representation of ER signal sequence (SS, red) targeted protein translocation from the cytosol into the ER lumen. A. Co-translational translocation for soluble proteins with long polypeptide chains (PPC) for recognition by signal recognition particle (SRP), which binds to its SRP receptor (SR) and stalls ribosomal translation. Transfer of the ribosome with the PPC under GTP hydrolysis onto Sec61 translocon associated with Sec62/63, closes the pore and continues ribosomal translation while pushing the nascent PPC into the ER lumen, where signal peptidase cleaves the SS to receive a translocated protein. **B.** Post-translational translocation for soluble proteins with short PPC that cannot be bound by SRP is immediately supported by heat shock proteins HSP40/70 to prevent aggregation after synthesis into the cytosol. Translocation occurs via Sec61/62/63 into the ER lumen, where HSP70 BIP interacts with the nascent chain and pulls the PPC into the lumen where the SS is cleaved. **C.** Post-translational translocation of transmembrane or tail-anchored (TA) domain (green) containing proteins after their synthesis in the cytosol. The PPC is bound by HSP40/70 and recognized via transmembrane domain recognition complex (TRC) 40 which delivers proteins to tryptophan-rich basic protein (WRB) and calcium-modulating cyclophilin ligand (CAML) (similar to Get1/2), the transmembrane protein can be inserted under ATP hydrolysis into the ER membrane or transferred on Sec61/62/63 for insertion. Figure was created with biorender according to Kunze and Berger, 2015; Johnson et al., 2012 and Akopian et al., 2013.

1.1.2 Processing, folding, modification of proteins in the ER lumen

The translocation of a protein from the cytosol into the ER lumen comes with the drastic change in the redox conditions due to high abundance of oxidoreductases like (protein disulfide isomerases) PDIs, electron donor-acceptor pairs, such as glutathione/glutathione disulfide (Margittai et al., 2015, Kleizen and Braakman, 2004). To prevent aggregation in a reductive milieu, Heat shock proteins (HSP), such as HSP70/BiP bind hydrophobic regions within the protein, stabilizing the protein, while PDIs, in addition to the oxidizing environment, initiates formation of disulfide bonds (Feige and Hendershot). Once the protein enters the ER lumen, it is exposed to several enzymes, among those the intramembrane cleaving protease signal peptide peptidase (SPP) which cleaves the SP at Gly-X-Gly-Asp motifs (Voss et al., 2013) and the oligosaccharyltransferase (OST) that adds GlcNAc (N-acetylglucosamine) to the N-terminus (Barlowe and Miller, 2013). Subsequently, glucosidases I and II enzymes process those N-glycosylations, while UDP-glucose:glycosyltransferase (UGGT) re-binds substrate glycoprotein (Kleizen and Braakman, 2004). During the glucose trimming, UGGT acts as a sensor to the innermost GlcNAc moiety in misfolded glycoproteins (Schrag et al., 2003) and re-glycosylases with a terminal glucose. The trimmed glycoprotein is recognized by lectin chaperones calreticulin (CRT) and calnexin (CNX), which retain the unfolded protein in the lumen in the iterative folding cycle until the protein is completely folded (Tatu and Helenius, 1997; Barlowe and Miller, 2013; Adams et al., 2020). The characteristic high calcium concentration in the ER lumen, which is maintained by calcium-dependent CRT/CNX among others (Meldolesi and Pozzan, 1998; Carrera-Sureda et al., 2018), influences the folding process by maintaining the stability of BiP-substrate complexes (Suzuki et al., 1999; Preissler et al., 2015, 2020), folding state of some ER clients (Fass et al., 1997), and regulating the unfolded protein response (UPR) (Carreras-Sureda et al., 2018). Besides aiding protein folding, CRT/CNX interaction recruits co-chaperone ERp57, a protein disulfide isomerase (PDI)-like oxidoreductase to mediate oxidative folding (Kleizen and Braakman, 2004; Jessop et al., 2009; Ellgaard and Helenius, 2001). The cycle of glycosylation and folding is finalized by ER mannosidase I activity at the A-branch of the glycosylated, correctly folded protein, which prevents further binding by CRT/CXN or re-glycosylation by UGGT (Adams et al., 2020).

1.1.3 Degradation or exit - protein folding control checkpoint

Correct folding is controlled in several steps by chaperones, which keep the folding loop until folding is successful. To not overextend the machinery's efficiency with endless folding iterations, terminally misfolded proteins that cannot be folded after prolonged time are removed from the folding pathway

(Kleizen and Braakman, 2004; Barlowe and Miller, 2013) by the ER-associated degradation (ERAD). This stringent regulation to reduce the amount of misfolded protein is crucial for maintaining the folding ability of the ER. When the folding capacity is saturated, ER stress occurs and activates a defense mechanism - the ER stress response. It combines the expression of ERAD components, supporting chaperones as well as downregulation of protein biosynthesis (Yoshida, 2006). To distinguish native and misfolded proteins a specific glycosylation signature is labelling them. Misfolded proteins are de-mannosylated at the B-or C-branch of the modified glycoprotein by ER-degradation-enhancing-mannosidases (EDEM1, EDEM2, and EDEM3) (Cherepanova et al., 2016; Adams et al., 2020) that generate a signal for ERAD and direct them back into the cytosol for degradation via proteasomal activity under involvement of BiP and PDI (Molinari et al., 2002, Adams et al., 2020; Olivari and Molinari, 2007). At the same time a heat-shock-response is triggered by an accumulation of misfolded protein in the cytosol, leading to upregulation of the gene expression for cytosolic chaperones (often heat shock proteins) that are required for protein refolding. The detection of an increased amount of misfolded protein in the ER activates the UPR that enhances gene expression of ER chaperones and enzymes needed for ERAD. A malfunction of this mechanism is associated with various diseases, among those neurodegenerative diseases like Alzheimer's disease and Parkinson's disease (Yoshida, 2006).

1.1.4 Synthesis of lipids and their transport

Besides harboring ribosomes as the main location for protein biosynthesis, the ER is also the main organelle for synthesis of all lipids, including sterols, sphingolipids and glycerophospholipids (GLPs). These are important for structure in cellular membranes, phospholipids that act as permeability barriers in membranes and matrices for catalytic processes as well as participant in signaling processes (Dowhan, 2017).
The general structure of lipids comprises a varying length of fatty acid chains containing a different amount of double bonds and varying types of head groups.
Within the scope of this thesis, structure and transport of amphiphilic lipids will be briefly discussed with the example of GLPs. Members of the GLPs are defined by the nature of their polar head group: phosphatidylcholine (PC), phosphatidylethanolamine (PE), phosphatidylserine (PS), phosphatidylinositol (PI), phosphatidylglycerol (PG), and cardiolipin (CL) (Hishikawa et al., 2014). A big variety of GLPs is necessary as the unique lipid composition differs qualitatively and quantitatively among organelles, cell types, inner and outer membranes and defines their specific function in signalling, trafficking and membrane fluidity (Hishikawa et al., 2014; van Meer et al., 2008).

After synthesis in the cytosolic leaflet of the ER in multiple steps, the phospholipid is translocated into the luminal leaflet of the bilayer by fast equilibration across the membrane mediated by scramblase (Alberts et al., 2002). From this point the transport is differentiated as non-vesicular and vesicular transport via COPII vesicles from the ER to the Golgi. Non-vesicular transport occurs at membrane contact sites either as lipid transfer with or against a concentration gradient. Ceramide transport via ceramide transfer protein CERT (Hanada et al., 2003) for example relies on the concentration gradient across ER and Golgi. When it arrives at the Golgi, an immediate conversion to sphingomyelin or glucosylceramide occurs, leading to the low level of ceramide in the Golgi compared to the ER (Funato et al., 2020). Additionally, studies suggest a role for phosphatidylinositol 4-monophosphate (PI4P) in ceramide trafficking (Balla et al., 2020, Stefan et al.,2017). Sterols on the other hand are postulated to require lipid transport proteins of the oxysterol binding (OSBP) family and hydrolysis of PI4P as energy expenditure for transport to the TGN (Funato et al., 2020). It is important to note that cellular lipid transport comprises a huge range of pathways with multiple roles for PI4P-dependent trafficking, discussed in reviews elsewhere but shall only be mentioned in this thesis (Lev, 2010; Stefan et al., 2017; Balla et al., 2020, Yang et al., 2018).

Vesicular transport of proteins marks another route how lipids are transported, since the vesicles are composed of defined lipids containing bilayers (Balla et al., 2020; Yang et al., 2018). With focus on the protein transport from the ER to the Golgi apparatus, the following section thereby explains COPII vesicle formation and trafficking.

1.1.5 From in ER to Golgi - transport in COPII vesicles

As described above proteins undergo quality control before entering the next step of the secretory pathway, which is the travel towards the Golgi apparatus. The anterograde transport from the ER to the Golgi apparatus is mediated by the well conserved COPII (coat protein complex II) vesicles in distinct zones of the ER - the ER exit sites (ERES)(Fig. 3). Once a cargo is recognized by export signals on their exposed cytoplasmic regions (Barlowe, 2003) the Ras-like GTPase Sar1 is activated and initiates COPII formation (Sato and Nakano, 2007). As GTPase, its function is dependent on a guanine exchange factor (GEF), which is fulfilled by Sec12, an ER-bound transmembrane GEF that is exclusively localized to the ER (Barlowe and Schekman, 1993; Sato and Nakano, 2007). Upon GDP-GTP exchange of Sar1p by Sec12, the conformational change exposes an n-terminal amphipathic α-helix of Sar1p, which is anchors it into the ER membrane (Kurokawa and Nakano, 2019; Lee et al., 2005).

The coat of the 'pre-budding complex' (Jensen and Schekman, 2001) forms stepwise with attachment of inner coat complex Sec23p/Sec24p and outer coat complex Sec13p/Sec31p together with

Sar1p+GTP (Barlowe, 1994; Bonifacino and Glick, 2004, Kurokawa and Nakano, 2019). Polymerization of these coat layers leads to formation of a cage that can adapt to the size of the cargo interacting with Sec24 (Venditti et al., 2013). The accumulation of cargo via capturing by Sec24 as well as the initial insertion of Sar1p's N-terminal α-helix is proposed to mediate membrane curvature and vesicle fission (Lee et al., 2005; Hariri et al., 2014, Sato and Nakano, 2007). Besides their function as coat proteins, Sec23/24 have a Sar1 GTPase-activating protein (GAP) activity, enhanced by Sec31 (Kurokawa and Nakano, 2019, Sato and Nakano, 2004), which allows dissociation of Sar1 from the COPII. GTP hydrolysis of Sar1p closes off the 'neck' of the vesicle bud and generates free COPII vesicles containing cargo which pinch off the ER membrane and deliver the cargo to the Golgi apparatus or in mammalian cells to the ER-Golgi-intermediate-compartment (ERGIC) (Appenzeller-Herzog and Hauri, 2006).
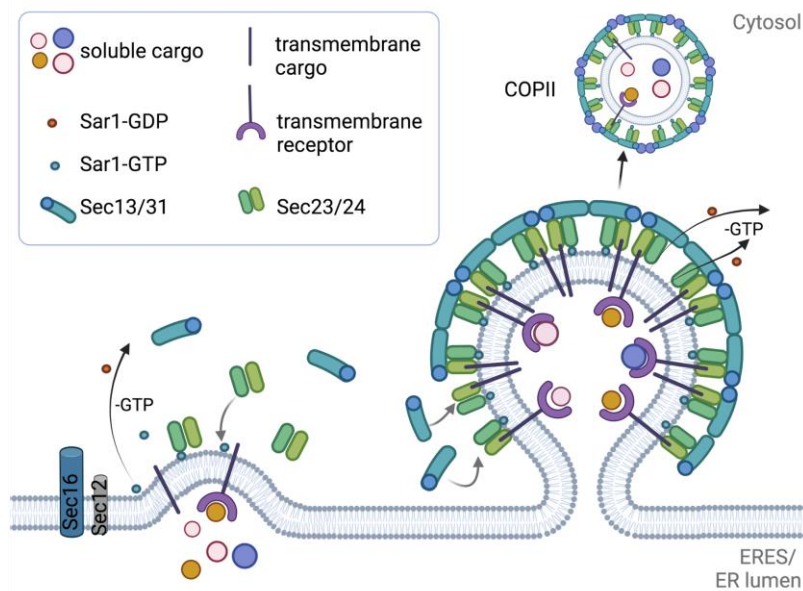
Fig. 3: Formation of coatomer complex II (COPII) vesicles at ERES positive for Sec16. Recognition of export signal on cargos activates Sar1-GTPase which initiates COPII vesicle formation upon GDP-GTP exchange with Sec12 GEF and leads to anchoring of Sar1-GTP in the membrane. Pre-budding complex formation by binding of Sec23/24 and association of Sec13/31 followed by polymerization of the coat proteins leads to cage formation, while Sar1-GTP promotes membrane curvature. GTPase activity of Sec23/24 and Sec13/31 dissociates Sar1-GTP, which finally results in budding and release of the COPII-vesicle transporting diverse cargo. The figure was created according to Venditti et al., 2013 and Mancias and Goldberg, 2005) using biorender.

In contrast to the historical view of vesicles being the transport carriers of proteins along microtubules, studies show a more complex vesicular tubule complex (VTC) based trafficking. Those VTC can directly form during COPII formation and vesicle budding, but also by homotypic fusion of new vesicles pinching off the ER (Watson and Stephens, 2005; Alberts et al., 2002; Lupashin and

Sztul, 2005). The carriers are initially captured by tethering factors (e.g., TRAPPI) before SNAREs (Soluble N-ethylmaleimide-sensitive factor attachment protein receptors) on the vesicle and the target membrane as well as small Rab GTPases induce a tighter docking (Lupashin and Sztul, 20050. Interaction between v-SNARE (vesicular) and t-SNARE (target) brings carrier and membrane in proximity and forms a SNARE-complex bundle, which drives membrane fusion (Bonifacino and Glick, 2004).

1.1.6 Retrograde transport for recycling of ER proteins

When COPII transport carriers fuse with the target membrane the protein is released into the lumen. In mammalian cells the first station of sorting is the ERGIC - a compartment in between ER and cis-Golgi positive for ERGIC-53 transmembrane protein (Ladinsky et al., 1999; Saraste and Marie, 2018). The transport of ERGIC-53 along with COPII coat proteins and ER-proteins back to the ER is mediated via COPI vesicles that contain proteins with an ER targeting signal - either a specific signal on their cytoplasmic tail or a KDEL sequence needed for recognition by KDEL-receptors. Retrograde transport occurs additionally between the Golgi stacks from trans to cis face. Similar to the formation of COPII vesicles, the insertion of a N-terminal amphipathic helix of a small GTPase induces the coat formation. Here, GTPase Arf1 is recruited by guanine exchange factor (GEF) GBF1 located in the cis- and the trans-Golgi. Upon activation to its GTP-bound form, conformational changes attach it to the membrane which allows recruitment of the coatomer complex (comprising subunits α-, β'-, ε-, β-, δ-, γ- and ζ-COP). Under activity of ArfGAP2/3 the complex stabilizes, while ArfGAP1 promotes membrane curvature. The vesicle scission is initiated by GTP hydrolysis at the vesicle 'neck', leading to budding and dissociation of most of the COPI machinery proteins with residual complex support targeting and docking to the target membrane (Arakel and Schwappach, 2018).

1.2 The processing complex of the secretory pathway

1.2.1 Structure and composition of the Golgi apparatus

As early as in 1898 Camillo Golgi observed and described a 'reticular apparatus' in neuronal cells by deposition of silver, making him the namesake of the Golgi apparatus (Golgi 1898, Klumperman 2011). With the cytochemical labeling of Golgi membranes (Novikoff and Goldfischer 1961) and

further development of the election microscope (EM) techniques over the past decades the Golgi architecture was revealed as stacked, disk-like membranes (cisternae) interconnected by tubules to a Golgi stack (reviewed by Klumperman 2011). There are different views on the origin of the Golgi apparatus (GA): either as outgrowth of the ER or as independent organelle as it can form de novo *in vitro* (Klumperman 2011). The GA is conserved in eukaryotic organisms, yeast and plants, however with differing structure and location. While vertebrate Golgi are localized near the centrosome (the main microtubule-organization point) via microtubule mediated interactions, the plant and fungi Golgi position depend on actin cytoskeleton rather than microtubules (Witkos and Loewe, 2016). In *Saccharomyces cerevisiae* the Golgi cisternae are not connected and stacked but distributed as ministacks throughout the cytoplasm, while *Pichia pastoris* features smaller stacks of Golgi cisternae resembling higher eukaryotes, however, not interconnected by tubules (Franzusoff et al., 1991; Papanikou and Glick, 2009; Preuss et al., 1992). Also, the plant Golgi apparatus is observed as small stacks of cisternae (dictyosomes) usually single or in small groups distributed throughout the plant cytoplasm with varying number of stacks and distribution dependent on the cell type (Dupree and Sherrier, 1998). Mammalian Golgi cisternae in the Golgi stack are distinguished as cis, medial, and trans-Golgi with cis being the periphery facing the nucleus (Dunphy and Rothman, 1985). For decades it has been controversial if these sub-compartments are formed independently or by maturation of the former, since the content within these stacks is distinctively different from each other (Glick and Luini, 2011; reviewed by Lujan and Campelo, 2021; Park et al., 2021) - a matter that will be discussed in detail in section 1.3. Due to its proximity to ERES, the cis-face of the GA serves as receiving compartment for COPII components before their retrograde transport and secretory proteins that travel further to the medial-Golgi. The most prominent and morphologically defining part of the GA is the lateral interconnection to flat cisternae of closely opposed membranes. This tubule-rich area, the tubular noncompact zone (Klumperman 2011), is known as Golgi ribbon (Xiang and Wang, 2011). Following the GA to the next step, proteins reach the trans-Golgi with its tubular membranes forming the trans-Golgi network (TGN), which acts as the sorting hub of the cell. As this compartment sorts, packs and also receives proteins in vesicles to and from the surrounding organelles or the plasma membrane, all three known types of coat components are found - COPI, COPII and clathrin (Klumperman 2001; Pelham and Rothman, 2000; Kirchhausen et al., 2014).
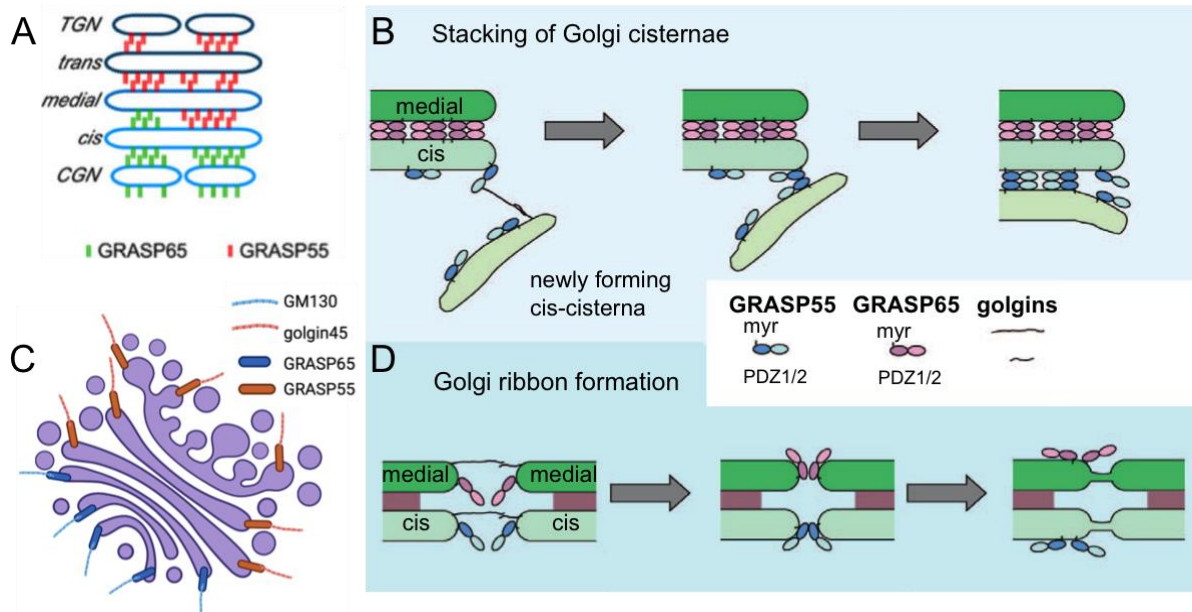
Fig. 4.: Golgi apparatus organization by GRASP55/65 and golgins. A. Golgi matrix proteins GRASP55/65 mediate cisternal stacking via cell-cycle regulated oligomers. The mechanism is shown in **B** by myristoylated (myr) GRASP55 (cis-Golgi) or GRASP65 (medial-Golgi) PDZ1/2 domains stacking on each other to form a new cis-cisterna. **C.** Organization of GRASP55/65 with their binding partners golgin45/GM130 to form 'Golgi ribbons' (**D**) via homotypic connections. Figure A is adapted from Xiang and Wang, 2011. Figure B and D is adapted from Lowe, 2010. Figure C is created with biorender according to Mendes et al., 2022.

Albeit, the constant trafficking of proteins, budding off and fusion of vesicles, the stacks of the GA remain well defined in structure. Besides the lateral tubules that interconnect the cisternae, the Golgi architecture features the 'Golgi matrix', containing several proteins essential for the structural organization of the Golgi (Klumperman 2011; Xiang and Wang, 2011). Among those are membrane associated proteins GRASP65/55 (Golgi reassembly stacking proteins) and their binding partners GM130 and Golgin-54 (Li et al., 2020) that tether Golgi membranes together. Depletion of GRASP leads to disassembly of the Golgi stack (Xiang and Wang, 2010). GRASP65/55 are peripheral membrane proteins attached to Golgi membranes via a myristic acid on their N-terminus and concentrated in the area where membrane stacking happens (Fig. 4). While GRASP65 and its partner GM130 serve as cis-Golgi marker, GRASP65 and Golgin-54 are found in the medial/trans-Golgi. Newer studies report an extension of the role of GRASPs in specific cargo transport, unconventional and noncanonical secretion and even glucose starvation-induced autophagy (Zhang et al., 2018; Li et al., 2020). Another main component of the Golgi matrix is the family of golgins. These coiled-coil proteins regulate vesicle tethering at the Golgi and its integrity of Golgi ribbons (Munro 2011; Gillingham and Munro, 2016) in association with small Rab GTPases. They feature a long C-terminus that allows peripheral attachment to the cytoplasmic face of the Golgi and can extend between 100 and 600 nm in distance to catch or tether vesicles in the cytoplasm (Witkos and Loewe, 2016). Length of C-terminal domain and the position depends on the specific golgin nature and its functions. In

vertebrates the set of golgins is more complex, as more cell types and specific trafficking events are regulated (Witkos and Loewe, 2016). The function of golgins is directly linked to the positioning of the GA as well: GM130 can bind microtubules to stabilize the proximity to the centrosome which controls positioning within the cell and equal distribution of Golgi membranes during mitosis, as mentioned above (Lippincott-Schwartz et al., 2000; Witkos and Loewe, 2016; Yadav and Linstedt, 2011).

1.2.2 Post-translational processing in the Golgi

Each compartment of the Golgi apparatus contains a unique set of enzymes, pH, ion concentration (e.g. Ca^{2+}) for sequential post-translational modification (PTM) of the proteins during their travel through the Golgi apparatus. Processing includes glycosylation, acetylation, palmitoylation, sulfation, phosphorylation, and proteolytic cleavage of the immature proteins, which is essential for functionality and recognition, ultimately sorting of the secretory protein to the right destination (Reynders et al., 2010). Defects of protein maturation lead to missorting or impaired protein function. The structurally impaired protein can accumulate or be secreted in premature form. Accumulation and missorting are associated with various neurodegenerative diseases such as Alzheimer's disease and Parkinson's disease or storage diseases like Niemann-Pick Disease and Gaucher's disease (Zempel and Mandelkow, 2014; Pagano et al., 2000; Abed Rabbo et al., 2021). Within the scope of this thesis, glycosylation, glycolipid biosynthesis and proteolytic processing will be explained in greater detail.

1.2.2.1 Glycosylation

As described in the earlier section 1.1.2 proteins obtain GlcNAc modifications in the ER to ensure correct protein folding and enter the Golgi apparatus on the cis-face as high-mannose-, hybrid-or complex N-glycans, however the main functional glycosylation occurs in the GA (Reily et al., 2019). Glycosyltransferases (GT) and glycosidases can remove and add sugars to the N-linked glycoproteins and modify their serine, tyrosine, threonine and hydroxylysine residues harboring the OH- (Hydroxyl) group (Stanley 2011). Other types of glyco-modifications comprise mannosylation of tryptophan's C2 atom, as well as the covalent attachment of Glycosylphosphatidylinositol (GPI)-anchor to a protein (glypiation) (Reily et al., 2019; Stanley 2011). In contrast to ER glycosylation, N-acetylgalactosamine (GalNAc; mucin-type-O-glycans) can be added by GalNAc transferases (GALNTs) to proteins resulting in extracellular (ECM) glycoproteins and those destined for secretion (Reily et al., 2019). The enormous number of types of GTs and glycosidases can produce complex polymers with up to

200 linked glycans (Stanley et al., 2011) in a highly regulated manner (Reynders et al., 2011). In fact, polarization of the cisternae is defined by the specific distribution of various glycosylation enzymes, which regulate their order of action (Pantazopoulou and Glick, 2019). In brief, the nucleotide precursor is transported by GTs to the specific Golgi membrane, travels from the cytoplasm into the Golgi lumen via nucleotide sugar transporters and is attached to the protein (Stanley et al., 2011, Berninsone and Hirschberg, 2000). Thereby, the ER-added mannose residues are removed to expose the mannosyl core of the glycoprotein, which gains additional GlcNAc modifications during travelling from cis to trans-Golgi face (Reynders et al., 2011). Subsequent modifications with GalNAc residues or other PTMs occur in different parts of the Golgi stack depending on defined pH and ion concentration (Reynders et al., 2011).

1.2.2.2 Membrane components made in the Golgi - Glycoproteins

Lipids are synthesized in the ER but gain possible modifications in the Golgi to fulfill their functions in the cell as component in internal membranes, vesicles and the plasma membrane for cellular signal transduction (Van Meer et al., 2008; Schuhmacher et al., 2020).
Similar to glycoproteins, also amphipathic glycolipids (GLs) are produced by addition of oligosaccharides via glycolipid glycosyltransferases (GGTs) to the hydrophobic ceramide moiety (Maccioni et al., 2011). One of the most abundant GLs are glycosphingolipids (GSLs) that gain their initial glucose or galactose residue at the lipid domain on the cytoplasmic face of the Golgi or ER, before flipping into the lumen for further modification by general GTs (Reily et al., 2019; Stanley 2011). Their nature is defined by the sphingolipid base with varying length and type of the hydrophobic sphingoid base backbone, the hydroxylation status of the N-acyl chain and polar head group (Harayama and Riezman, 2018). In mammalian cells up to 15% of the total phospholipids in different tissues are made up by sphingomyelin (SM) (Koval and Pagano, 1991), which is synthesized in the trans-Golgi by sphingomyelin synthase 1 (SMS1). The base molecule ceramide receives a phosphatidylcholine, while generating diacylglycerol as a byproduct (Maccioni et al. 2011). SMS1 serves as a regulator of cellular diacylglycerol (DAG) and ceramide levels that ultimately influence the selection of lipid messengers involved in cell proliferation (Hannun et al., 2002; Maccioni et al., 2011). Not only the control of ceramide and DAG levels are essential for cell homeostasis, but also the regulation of products of ceramide, such as sphingolipids. SM in Golgi membranes defines morphology of the Golgi cisternae as typical flat compartments (von Galen et al., 2014) and maintains transport carrier formation at the TGN (Duran et al., 2012; Campelo et al., 2017). In particular, the correct lipid organization relies on SM homeostasis to ensure the correct membrane thickness for insertion of transmembrane enzymes (von Galen et al., 2014; Munro 1995). As these and their glycosylated forms constitute PM and internal membranes, they are internalized for targeting various

organelles as well as for degradation in the endolysosomal system during turnover and production of ceramide, sphingosine and choline as second messengers (Pagano et al., 2000; Masanobu et al., 1993). The hydrolytic enzymes facilitating stepwise cleavage of ceramide to fatty acid and sphingosine are supported by SL activator proteins (SAPs, saposins). Their precursor prosaposin (PSAP) is the body of the study discussed in this thesis and will be described in detail in later sections.

1.3 Why is intra-Golgi trafficking a controversial topic?

Processing and modification in the Golgi depend on the presence of ions, certain pH and set of enzymes. Among those, especially glycosylation enzymes are used to classify the respective compartments (Pantazopoulou and Glick, 2019; Rabouille et al., 1995). Bidirectional transport to and between the Golgi stacks is mediated via COPI/COPII vesicles (see 1.1.5 and 1.1.6) and ensures recycling of Golgi proteins to prior stacks. With evolving studies on the secretory pathway, the view from seeing the GA as a static, yet polarized assembly of stacks (Farquhar and Palade, 1981) with defined environment shifted to describing the Golgi as a dynamic assembly of cisternae over the last decades. A debate is ongoing on how intra-Golgi trafficking combines efficient vesicular protein transport while maintaining distinct conditions and sets of enzymes in cis-, medial-, trans-Golgi and TGN, but allows fast redistribution of Golgi resident proteins (Glick and Luini, 2011; Lujan and Campelo, 2021; Park et al., 2021, Pantazopoulou and Glick, 2019). Different models developed that explain intra-Golgi trafficking, of which three models are briefly explained in the following.

1.3.1 The classic - the vesicular trafficking model

The vesicular trafficking model is based on the idea that the Golgi cisternae are stable compartments, which receive new cargo proteins by COPII mediated anterograde transport from the ER or ERGIC (Lujan and Campelo 2021; Bonifacino and Glick, 2004). Retrograde transport as well as the transport along the cis-trans stacks are COPI dependent (Pelham and Rothman, 2000) and occur at the rim of the cisternae. This vesicular or also rim progression model explains the polarized nature of the Golgi stack and the enhanced concentration of specific Golgi-resident enzymes at steady locations in certain cisternae nicely. However, large cargos (60-90nm) cannot be packed into the same vesicles that move along the rims of the cisternae, due to size restrictions. In a complement model idea, the cisternal progenitor model, this problem is overcome by the action of RabGTPases that support homotypic fusion of adjacent cisternae (Pfeffer 2010). Similar to large cargos, transport of very small secretory protein is not sufficiently addressed with the premises in this model. The transport with vesicles

would need to be unrealistically fast with each cisternae producing hundreds of vesicles per second (Glick and Luini, 2011) to align with observed quick intra-Golgi transport of small secretory proteins.

1.3.2 The dynamic cisternal maturation

As the name already suggests, this model proposes the de novo formation of cisternae as dynamic entities with fast turnover rate within minutes (Glick and Luini, 2011; Lujan and Campelo, 2021). The homotypic fusion of ER derived COPII vesicles forms the cis-Golgi, which matures gradually in the different Golgi cisternae, the TGN that finally disintegrates into carriers such as secretory vesicles (Lujan and Campelo, 2021; Glick and Luini, 2011, Pantazopoulou and Glick, 2019). Here, COPI coated carriers are not packed with cargoes for anterograde transport during maturation but mediate intra-Golgi recycling of resident Golgi proteins from older to younger vesicles as well as retrograde trafficking to the ER (Pantazopoulou and Glick, 2019). This dual functionality was reflected in the description of two types of COPI vesicles - COPIa and COPIb (Donohoe et al., 2007), yet none of them seems to be responsible for primarily transport of glycosylation enzymes as those were reported to be depleted in COPI vesicles (Glick and Luini, 2011). Another weakness of this model lies in the lack of explaining the exponential kinetics of differential export rates of secretory cargo exiting the TGN and general Golgi region.

An extension of the model introduced tubules that connect cisternae by heterotypic fusion in addition to the homotypically fused horizontal cisternae connecting tubules (Papanikou and Glick, 2014). Small secretory cargoes can be transported in a fast intra-Golgi trafficking that align with exponential kinetics of Golgi exit (Beznoussenko et al., 2014; Glick and Luini, 2011). Although, the extension still lacks to explain how large cargoes, that were initially proposed to be sorted by cisternal progression (Patterson et al., 2008; Pfeffer 2010), can be transported as they are too large for diffusion via heterotypic tubules. How the gradient across maturating compartments is maintained in the presence of heterotypic membrane connections has yet to be explained.

1.3.3 The modern rapid partitioning model

Even though the vesicular trafficking and the cisternal maturation model are the most accepted types with many other theories deriving from them, recently a completely different idea has been proposed challenging the traditional views on the Golgi (Patterson et al., 2008, Glick and Luini, 2011). In the rapid partitioning model, the GA is seen as single compartment comprising two types of domains, one regulating export of cargo and therefore enriched in secretory proteins and the other mediating

processing with high concentration of glycosylation enzymes (Lujan and Campelo, 2021; Glick and Luini, 2011). Proteins here can exit the export domain of any cisternae while moving through the GA. The model especially features the trafficking of large secretory proteins and exponential kinetics of both small and large cargos, however discrete cisternae and Golgi compartment and glycosylation enzymes distribution which is specific to certain regions of the Golgi stack cannot be explained (Glick and Luini 2011).

Overall, the existence of different models reflects the complexity of secretory cargo transport in the Golgi stack. The details about further variations of these are discussed in detail elsewhere (Glick and Luini 2011; Park et al., 2021;Lujan and Campelo 2021)
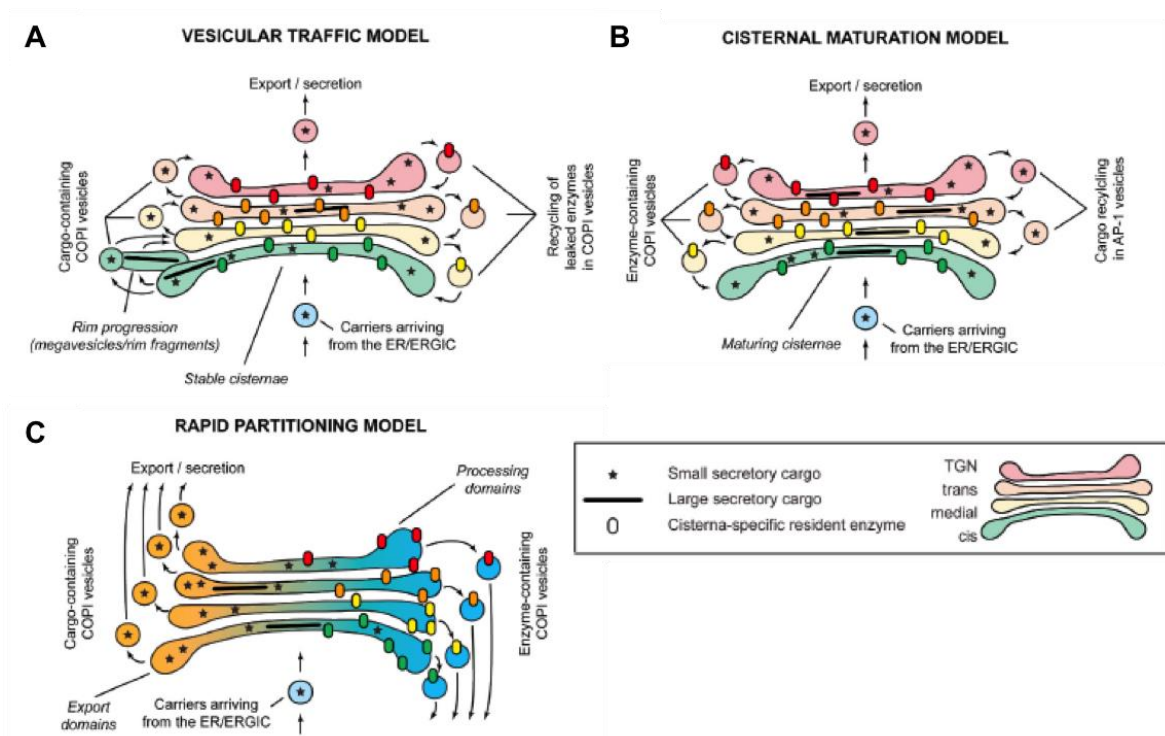
Fig. 5: Models of Golgi trafficking. A. Vesicular trafficking model transporting small (*) and large (--) secretory cargos in COPI coated vesicles in both anterograde and retrograde transport from the rim of the cisternae. **B.** Cisternal maturation model. Cargos from ER/ERGIC arriving in COPII-coated vesicles form the cis-Golgi, which gradually matures to the different stacks. COPI coated vesicles transport cisterna-specific resident enzymes back from older to younger cisternae. **C**. Rapid partitioning model showing the Golgi apparatus as single compartment with export domain enriched in small secretory cargo for COPI-mediated transport and processing domain comprising all cisterna-specific enzymes necessary for protein processing. The figure is adapted from Luhan and Campelo, 2021.

1.4 Logistics center of the secretory pathway - the trans-Golgi network (TGN)

Early EM studies of the Golgi apparatus already revealed a Golgi compartment with granules in its periphery (Farquhar and Palade, 1981) which are tubular membranes emerging from the trans-face of the Golgi stacks (Griffiths and Simons, 1986), later termed as trans-Golgi network. Widely accepted as the main sorting hub of the cell, the TGN is a region for sorting and packaging of proteins and lipids for post-Golgi destinations (Klumperman 2011; De Matteis and Luini 2008; Kienzle and von Blume, 2014). Matured proteins entering the TGN are recognized and packed into transport carriers depending on their properties, and then routed to apical and basolateral plasma membrane, the endolysosomal system or secretory granules, as well as back to the Golgi stacks during retrograde transport (Klumperman 2011; Pelham and Rothman, 2000). Since the TGN is not only the exit face of the GA but also receives cargo via endocytic events recycling from endosomes, its size and structure undergoes dynamic changes depending on the incoming and outgoing cargo molecules (De Matteis and Luini, 2008; Guo et al., 2014). To enable the GA exit of all sorts of secretory proteins and lipids, the mechanisms to recognize and sort the right cargo into specific transport carriers are complex and depend on cargo's targeting signal and structural properties, which are discussed in the following (Guo et al., 2014).

1.4.1 Transport carriers

Like cargo transport from the ER to the Golgi, within Golgi stacks or back from the Golgi to the ER, the trafficking from the TGN to the final destinations is also dependent on vesicular budding. Areas of the TGN where Golgi-resident proteins are absent, are enriched in cargo and components for the respective budding mechanism and termed 'exit domains' (Kienzle and von Blume, 2014; Gleeson et al., 2004). Even though COPI vesicles (see 1.1.6) are found at the TGN, the frequency is much lower than in the Golgi. Clathrin-coated vesicles, CARTS, sphingomyelin (SM)-rich vesicles (more details see 1.4.3.4) and lipid rafts are the main transport carriers budding from the TGN towards PM and organelles.

1.4.1.1 Clathrin coated vesicles

The formation and transport of cargo via clathrin coated vesicles (CCV) is well described as essential for most endocytic trafficking from the TGN, from endosomes as well as during the regeneration of synaptic vesicles (Milosevic 2018; Paraan et al., 2020). Several proteins are involved in the formation of CCV. The basic assembly unit of the vesicle surrounding cage is clathrin - a WD40β-propeller domain and zigzag domain 190 kDa protein with C-terminal trimerization unit. Three light and three

heavy chains form a clathrin triskelion which enables (i) *in vitro* self-assembly under acidic conditions into cages due to salt bridge formation between the three heavy chains (Kirchhausen et al., 2014; Paraan et al., 2020; Schein et al., 2009; Wilbur et al., 2010) and (ii) *in vivo,* in the presence of cargo recognition peptides and adaptor and accessory proteins, formation of cages with pentagonal, hexagonal and rarely heptagonal faces (Paraan et al., 2020). Once the cage is formed, adaptor proteins (APs) and epsin connect the cargo to the clathrin cage by interaction of their clathrin box motifs to the CHC N-terminal β-propeller domain of APs. Depending on the pathway different AP proteins promote and regulate clathrin coat formation. AP-1 is associated with Golgi-endosome trafficking while AP-2 mediates endocytosis (Paraan et al., 2020). AP complexes consist of 'clathrin box' motif-containing large subunits (adaptins α or γ and β) and small subunits (μ,σ), whose N-termini form the core complex. For AP-1 the γ subunit binds distinctively accessory proteins supporting the interaction with the receptors recognizing luminal cargo destined for transport to endosomes. For sorting to endosomes Golgi-localized, γ-ear Arf-binding proteins (GGA) bind to the TGN membrane and colocalize with AP-1 in CCVs (Dell' Angelica et al., 2000; Zhang et al., 2007). The mechanism will be covered in section 1.4.2.1 and 1.4.2.4. In endocytosis, AP-2 with its subunit termed α2 enables binding to the membrane by recruiting phosphatidylinositol 4.5-biphosphate [PI(4.5)P$_2$] additionally. These functions of AP complexes facilitate the nucleation of small, spherical CCVs or as more recently reported larger, often tubular clathrin coated transport carrier (Klumperman et al., 1993; Doray et al. 2002; Puertollano et al., 2001, 2003, Zhang et al. 2007). Further lattice growth, cage stabilization and closure require accessory proteins, e.g. epsins for transport to endosomes. Vesicle scission is driven by dynamin under membrane tension caused by actin polymerization. The budded vesicle travels towards the target membrane and fuses as a free vesicle after uncoating by Hsc70-ATP and auxilin (Fig. 6) (Kirchhausen et al., 2014).
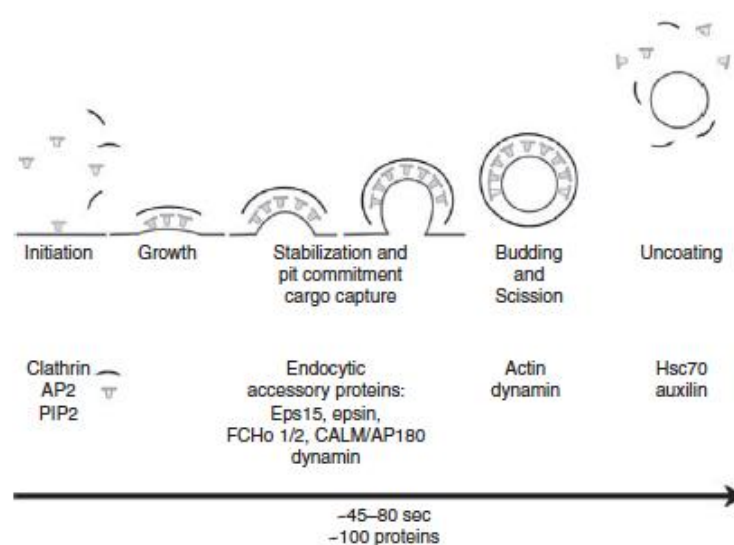
Fig. 6: Overview of clathrin-coated vesicle formation for endocytosis. Nucleation is initiated by recruitment of clathrin and AP-2 at the PM of cells, which is promoted by binding [PI(4.5)P$_2$]. Untethered clathrin from the cytosolic pool is recruited for lattice growth under presence of AP-2. Accessory proteins (eps15, epsin,FCHo ½,

CALM/AP180) support lattice stabilization and closure. Dynamin drives vesicle scission when the membrane is under tension due to action polymerization. The clathrin-coated vesicle can move towards the target membrane, where it loses its clathrin coat before fusion. Cytosolic heat-shock cognate protein Hsc70 binds hydrophobic peptides within the clathrin carboxy-terminus. Under the influence of the J-domain of auxilin, Hsc70 hydrolysis ATP to fasten a 'molecular clamp' leading to disassembly of the clathrin coat and fusion of the free vesicle with the target membrane. Figure is adapted from Kirchhausen et al., 2014.

1.4.1.2 CARTS

A novel group of bona fide transport carriers are CARTS - CARriers of the TGN to the Surface pathway - was more recently found to transport secretory and integral membrane proteins (Wakana et al., 2012, Pfeffer 2012; Ramazanov et al., 2021). Cargo molecules of CARTS are pancreatic adenocarcinoma upregulated factor PAUF and integral membrane protein desmoglein-1 (Wakana et al., 2012). Fission of CARTS is regulated by proteins like Rab6a and Rab8a, myosin II, while synaptotagmin II is involved in the correct targeting to the cell surface. Larger cargoes like collagen or Vesicular stomatitis virus (VSV)-G are excluded from transport via CARTS, which are with a size of 100- 250 nm bigger than CCVs (80-120nm) (Wakana et al., 2015; Paraan et al., 2020). CARTS requires protein kinase D (PKD) for biogenesis, but myosin II only for migration to the cell surface. The formation of CARTS was studied by monitoring TGN46 - a TGN-marker protein, that cycles between TGN and cell surface (see 1.4.4) - by addition of ATP and rat liver cytosol to permeabilized HeLa cells using digitonin. Centrifugation at high speed and immunoisolation enriched these TGN46-positive vesicles that only form in the presence of ATP and rat liver cytosol. Since PKD is prerequisite for CARTS formation, the SM pathway (see 1.2.3) is involved in CARTS biogenesis. In brief, ceramide is converted to SM and DAG, which recruits cytosolic PKD (Wakana et al., 2015).

1.4.2 Recognition of cargo proteins

1.4.2.1 Transmembrane proteins (TMP)

Similar to targeting signals of proteins in the ER to Golgi trafficking, many transmembrane proteins (TMP) contain a sorting signal at their cytosolic domain, which is recognized by adaptor proteins, which are recruited to the TGN by Arf GTPases. APs work in well-described complexes of three subunits (large, medium and small), where the N-terminal region of the large subunit form the core domain by wrapping small and medium units for binding Arf proteins, cargo and phospholipids (Guo et al., 2014). Accessory proteins interact with the C-terminus of the large subunit. Sorting signals of TMPs are tyrosine-based NPXY and YXXØ, where X represents a variable residue and Ø an amino acid with bulky hydrophobic side chain. While NPXY is specific for type I integral TMP displayed at

the cell surface, like β-integrin , YXXØ is contained in all types of membrane-spanning TMPs regardless of their localization at the cell surface or internal organelles (Bonifacino and Traub 2003). The YXXØ motif is generally recognized by the μ subunit of APs, however the affinity of different μ subunits depends on the particular YXXØ motif (Guo et al., 2014). Another group of sorting motif is di-leucine based [DE]XXX[LI] and DXXXL present in TMPs destined for specialized endolysosomal compartments, lysosomes and late endosomes (Guo et al., 2014; Braukle and Bonifacino, 2009). An example TMP for [DE]XXX[LI] is Lysosomal associated membrane protein 1 (LAMP1), present on many lysosomes and therefore commonly used as a lysosomal marker (Cheng et al., 2017; Pu et al., 2016). The other DXXXL motif is not only recognized by AP1, but also by Golgi-localized, γ-ear Arf-binding proteins (GGAs) (Dell'Angelica et al., 2000; Braukle and Bonifacino 2009, Bajaj et al., 2019) which signals the packaging into clathrin coated vesicles and the routing to the endolysosomal system. The transport and trafficking of lysosomal receptors will be discussed in detail below.

1.4.2.3 Soluble secretory proteins destined for storage granules

In specialized cells such as exocrine, endocrine and neuroendocrine or neuronal cells hormones (and precursors) or glycoproteins are stored in secretory storage granules (SG), which are released into the ECM upon fusion with the PM responding to an extracellular stimulus (Palade 1975; Tooze 1998). The initial model focuses on the environment in the TGN with pH 6.4 and high Ca^{2+} concentration which leads to aggregation of large protein complexes into clusters thereby distinguishable from smaller cargo proteins. An initial step is the formation of 'seeds' that promote the precipitation of regulated cargoes (Borgonovo et al., 2006). These clusters and aggregates interact with each other and accumulate in cholesterol-rich membrane domains in immature secretory granules (ISG) that bud from the TGN. Matured SGs are then as dense core post-Golgi structures observed in the cytoplasm, however, the mechanism of their maturation is elusive (Tooze 1998). Another model which describes maturation while still connected to the TGN, is postulated by the initial formation of ISG at the TGN including non-granule proteins. This 'sorting by retention' model does not exclude the aggregation effects stated in the 'sorting by entry' model but emphasizes the primary sorting machinery mediated by clathrin-coat formation and also recognition by receptors. Granule proteins are retained in the TGN while non-granule proteins are sorted away in the first step from the ISG bud during maturation of ISGs to SGs, which only contain the granule proteins. Proteins that remain as granules are for instance members of the granin family, like secretogranin (SgII), chromogranin A (CgA) and chromogranin B (CgB), which are proposed to aggregate in an acidic environment (Chanat and Huttner 1991; Cowley et al. 2000). The ability to aggregate into SGs can support other hormone peptides which cannot aggregate by themselves (Elias et al., 2010; Dittie et al., 1999, Kakhlon et al., 2006).

Technically, parts of the sorting to secretory storage granules are receptor mediated as well, SGIII for example interacts with cholesterol in the membrane and with carboxypeptidase E (CPE) which itself binds the granule membrane via an α-helical domain. Once CPE associates to the membrane, it is suggested to interact with cargo proteins like proinsulin, proenkephalin (Cool et la., 1998) and brain-derived neurotrophic factor (Lou et al., 2005). The classical receptor interaction within the frame of sorting comprises a tag attached to a protein which can be specifically recognized by a receptor. Especially well understood is the sorting of lysosomal hydrolases via receptors in the TGN membrane (Ghosh et al., 2003). Those include M6PR, sortilin (SORT1) and LIMP2. For M6PR and SORT1, which are partly localized within the TGN membrane, the mannose-6-phosphate modification on the N-terminus of lysosomal proteins are recognized by luminal domains via proteinaceous interactions (Saftig and Klumperman, 2009; Coutinho et al., 2012). To support capture of newly synthesized lysosomal proteins that escape the M6PR recognition (about 5-20% in non-tumor cells) or to bypass impaired M6PRs or M6P-tagging, M6P-independent sorting is being intensively studied (Braukle and Bonifacino, 2009). Sortilin for example, binds via a tunnel-like structure formed by the VPS10p β-propeller domain in the TGN to hydrophobic patches on the ligand proteins (Quistgaard et al., 2009; Braukle and Bonifacino, 2009; Saftig and Klumperman, 2009). While LIMP2 specifically recognizes β-glucocerebrosidase (βGC) via its heavily glycosylated coiled-coil domain (Reczek et al., 2007). After receptor binding of the ligand proteins, GGA and AP proteins are recruited to initiate the formation of clathrin coated vesicles, in which the lysosomal proteins are transported towards the endolysosomal systems (Puertollano et al., 2001; Klumperman et. al., 1993, Doray et al., 2002, Saftig and Klumperman, 2009, Bajaj et al., 2019).

Similar to other transmembrane proteins, M6PR and SORT's transport and trafficking rely on tyrosine-based sorting signals DXXLL to be recognized by GGAs, more precisely by their folded, globular VHS domain (Braukle and Bonifacino, 2009). GGAs are recruited to the membrane via ArfI GTPases (GTP-form) interaction with the GAT domain of GGAs. The largely unstructured hinge domain of GGAs on the other hand binds the N-terminal domain of clathrin heavy chain via its 'clathrin box' motif (Guo et al., 2014) as well as intramolecularly the VHS domain. The fourth conserved domain of GGAs, the GAE domain mediates the formation, movement and might also promote fusion of TGN-derived clathrin coated intermediate by recruiting accessory proteins (Braukle and Bonifacino, 2009). MP6Rs additionally contain conserved binding sites for AP-1 complexes for clathrin coat formation as described above.

1.4.3 Cab45-dependent sorting

Besides secretory proteins that contain a unique structural feature or modification that can be recognized by receptors, there are soluble secretory proteins without a common recognition motif or a known cargo receptor. These proteins participate in physiological relevant processes such as cell-cell communication, tissue integrity, homeostasis, and morphogenesis (Frantz et al., 2010; Blank and von Blume 2017), however, understanding of their sorting and trafficking still remains a challenge in the field. Recently, von Blume et al. described a receptor-independent sorting process for soluble secretory proteins in the TGN involving the luminal Ca^{2+}-binding protein Cab45. In brief, the 45 kDa protein oligomerizes upon local Ca^{2+} influx by SPCA1 binds to secretory protein molecules (clients) and thereby forms Cab45-client-complexes that can cluster and remain in the TGN lumen (von Blume et al., 2011, 2012; Crevenna et al., 2016). The Golgi kinase Fam20C, then specifically phosphorylates Cab45, to enable breakdown into smaller Cab45-client-complexes that can be sorted into sphingomyelin (SM)-rich carriers for trafficking of secretory proteins to the cell surface (Deng et al., 2018; Hecht et al., 2020).
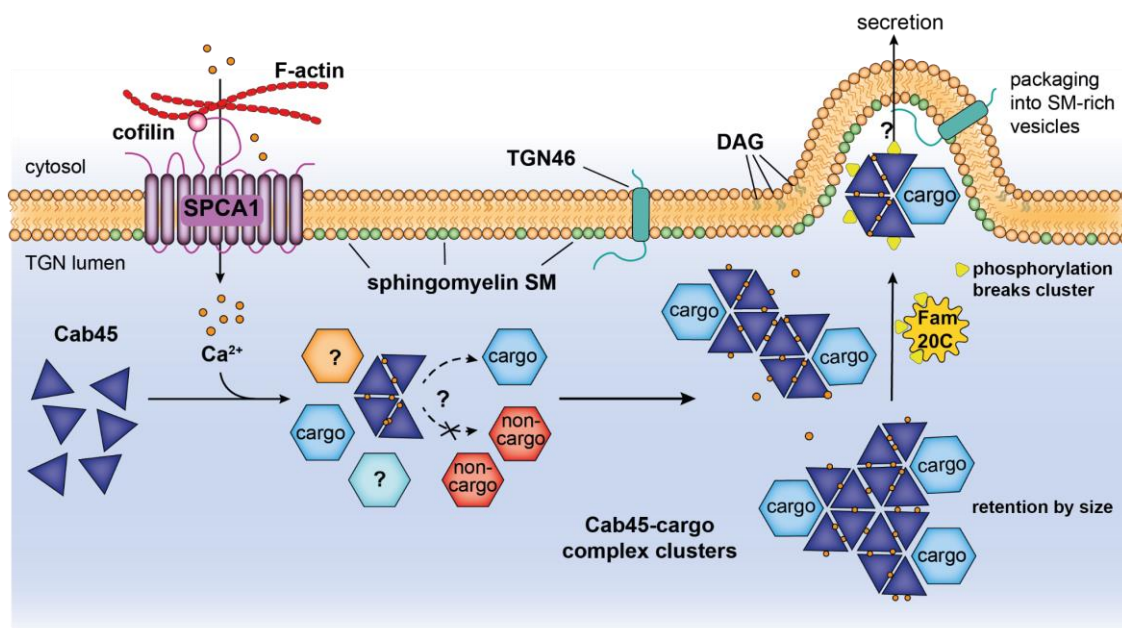
Fig. 7: Cab45-dependent sorting of soluble secretory cargo. The mechanism depends on Ca^{2+} influx occurring upon activation of the secretory pathway calcium ATPase 1 (SPCA1) by interaction of F-actin and cofilin. Cab45 in the TGN lumen binds Ca^{2+}, oligomerizes, binds and distinguishes cargo via an unknown mechanism and forms Cab45-cargo complexes that cluster and are retained by size in the lumen. The Golgi kinase Fam20C phosphorylates Cab45, thereby breaking down the clusters which can be recognized via an unknown process into SM-rich vesicles for secretion. Figure created according to von Blume et al. 2009, 2011, 2012; Crevenna et al., 2016; Deng et al., 2018; Hecht et al., 2020.

Among the proteins that have been associated with Cab45-dependent sorting are Lysozyme C (LyzC), cartilage oligomeric matrix protein (COMP) and matrix metalloproteinase 2 (MMP2) (Ramazanov et

al., 2021; Pacheco-Fernandez et al., 2019). LyzC facilitates the hydrolysis of β-(1,4)-glycosidic bonds leading to degradation of peptidoglycan in bacterial cell walls, therefore supports digestion in mammals as a digestive enzyme (Irwin 2015). Previous studies showed that LyzC trafficking is impaired in cells depleted of Cab45 or SM (Crevenna et al. 2016; Deng et al., 2018), showing the dependence on Cab45 for correct sorting and secretion. COMP and MMP2 trafficking via Cab45 is described in detail elsewhere (Hecht et al., 2020; Pacheco-Fernandez et al., 2019). The thesis focuses on understanding sorting mechanisms at the TGN, in particular focusing on the Cab45-dependent sorting of secretory proteins, which will be further explained in the next chapter.

1.4.3.1 Ca^{2+} in the secretory pathway

As Cab45 requires Ca^{2+} to sort secretory proteins like LyzC, this section will give a short overview on Ca^{2+} within the secretory pathway.

The signaling molecule Ca^{2+} is ubiquitously found in the cell, as it plays a key role in regulating cell proliferation, motility, development but also processes like secretion and cell-cell communication (Wuytack et al., 2002; Berridge et al., 2000). To provide enough Ca^{2+} to control cellular functions, compartments store calcium with concentration up to four orders of magnitude higher than those in the cytoplasm (Alonso et al., 2017). The local Ca^{2+} concentration is regulated by ATPase Ca^{2+} transporters that replenish calcium in storage compartments by pumping free cytosolic calcium against the calcium gradient into the organelle (Wuytack et al., 2002) and thereby restore the low resting Ca^{2+} level of about 100 nM in the cytosol (Vandecaetsbeek et al., 2011). Most of the stations of the secretory pathway feature high Ca+ concentrations, with the ER and its muscle sarcoplasmic reticulum being the main storage with about 400 µM Ca^{2+} while secretory vesicles contain approx. 80 µM Ca^{2+} (Pizzo et al., 2011; Alonso et al., 2017) (Fig. 8).

1.4.3.2 Ca^{2+} ATPases and release channels

In fact, a Ca^{2+} gradient exists across the secretory pathway that is maintained by Sarco/Endoplasmic Reticulum Ca^{2+}-ATPase (SERCA), inositol 1,4,5-triphosphate receptor (IP_3R) and ryanodine receptor (RyR) in the ER, additional secretory pathway Ca^{2+} ATPase (SPCA1) towards the medial-Golgi, and exclusively SPCA1 and RyR (in muscles and neurons) in the TGN (Pizzo et al., 2011; Vandecaetsbeek et al. 2011). Another Ca^{2+} pump is the plasma membrane Ca^{2+} ATPase (PMCA), which pumps Ca^{2+} into the extracellular space. IP_3R and RyR are Ca^{2+} release channels and especially important for fast increase of Ca^{2+} levels in the cytosol for Ca^{2+} signalling (Fig. 8). To enhance the speed of efflux of Ca^{2+} from storage compartments secondary messengers, such as IP_3 are generated which can bind open Ca^{2+}-channels (Lissandron et al., 2010). In case of RyR in the TGN, cells that do not express RyR simply take up Ca^{2+} by SPAC1 when cytosolic Ca^{2+} increases (Pizzo et al., 2011).

The mechanism by which SPCA1 transports Ca^{2+} is conserved within the P-ATPase family with SERCA and PMCA. They consist of three cytosolic domains: N- (nucleotide-binding), P (phosphorylation), which bind and hydrolyze ATP under phosphorylation of an aspartate in P-domain and A (actuator) domain that dephosphorylates the P-domain (Vandecaetsbeek et al., 2011; Vangheluwe et al., 2009; Kuhlbrandt et al., 2004). Ca^{2+} interacts with polar, negatively charged residues in the transmembrane domain, while ATP binds the N-domain, leading to a conformational change of the E1 state of the ATPase Ca^{2+} pump. In this conformation Ca^{2+} is trapped inside, ADP dissociates, causing a conformational change to a low affinity state E2. Ca^{2+} is released into the Golgi lumen. The A-domain dephosphorylation activity returns the ATPase to E1 state, high affine for a new Ca^{2+}-binding cycle (Vandecaetsbeek et al., 2011; Kuhlbrandt et al., 2004).
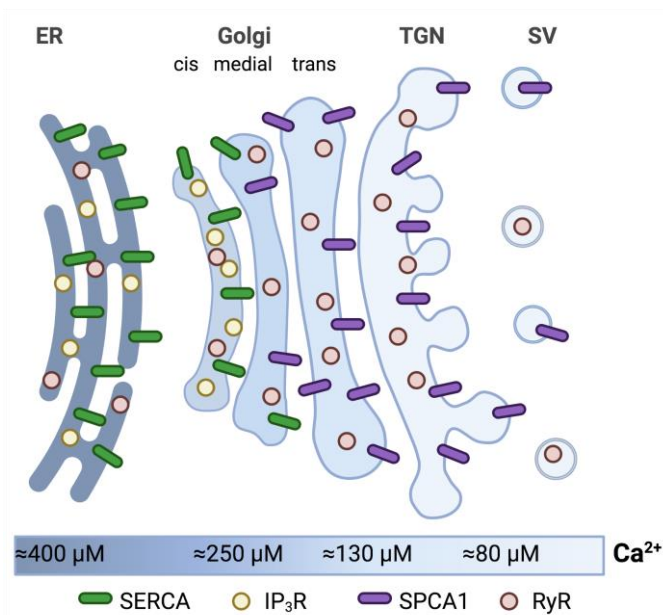
Fig. 8: Calcium gradient across the secretory pathway. The highest Ca^{2+} levels are in the ER, the main Ca^{2+} storage of the cell ($\approx$ 400 µM) and decreasing Ca^{2+} concentrations over cis-/ medial-Golgi ($\approx$ 250 µM) and trans-Golgi ($\approx$ 130 µM) towards the trans-Golgi network (TGN) ($\approx$ 80 µM). Ca^{2+} pumps SERCA (ER and cis-/ medial-Golgi) and SPCA1 (trans-Golgi and TGN) as well as Ca^{2+} release channels IP3R and RyR maintain Ca^{2+} concentrations. Figure created with biorender according to Pizzo et al., 2011.

1.4.3.2 Cab45's Ca^{2+}-binding and oligomerization

Ca^{2+} influx in the TGN is regulated solely by SPCA1, whose activity is influenced by interaction of F-actin and cofilin (CFL-1) (Kienzle et al., 2014). In the secretory pathway SPCA1 is the housekeeping Ca^{2+} and Mn^{2+} pump (Vandecaetsbeek et al., 2011, Wuytack et al., 2002). Interestingly, CFL-1 depletion leads to a change of secretion of proteins, including hypersecretion of Cab45 (von Blume et al., 2009). Further immunoprecipitation experiments with CFL-1 indicated actin and SPCA1 as potential interaction partners (von Blume et al., 2011; 2012; Kienzle et al., 2014). SPCA1 activity

pumps Ca^{2+} in the TGN lumen, where Cab45 binds it via its EF-hand pairs. EF-hand domains are a common feature of proteins that bind Ca^{2+} in a helix-loop-helix structure with pentagonal bipyramidal binding pocket (Honore and Vorum, 2000). Golgi localized Cab45, herein, contains beside an N-linked glycosylation on N39, six EF-hand motifs, which enable low affinity Ca^{2+}-binding in pairwise manner (Scherer et al. 1996; Blank and von Blume, 2017). It is therefore grouped together with reticulocalbin, ERC-45 and calumenin to form the CREC family of low affinity Ca^{2+}-binding proteins (Honore and Vorum, 2000; Vorum et al., 1999; Yabe et al., 1998). Upon Ca^{2+}-binding, Cab45 changed its conformation to a more α-helical secondary structure (Deng et al. 2018). This enables the assembly of Cab45-oligomers of varying sizes that can specifically interact with clients like LyzC and COMP (Crevenna et al., 2016; von Blume et al. 2012). While the structural details of the assembly of these clusters are unknown so far, it is certain that Ca^{2+} is essential for Cab45's client binding: the expression of a Ca^{2+}-binding deficient mutant (Cab45-6EQ), where glutamic acid is replaced by glutamine, was not able to oligomerize and bind clients (Crevenna et al., 2016; Blank and von Blume, 2017).

1.4.3.3 Phosphorylation of Cab45

Since Cab45-client-oligomers can assemble into bigger clusters, the packing into transport carriers requires the breakdown into smaller structures, which is achieved by phosphorylation of Cab45 via the Golgi kinase Fam20C (Hecht et al., 2020). Fam20C was recently discovered as the first and currently only Ser/Thr Golgi kinase in the secretory pathway (Tagliabracci et al., 2012, 2015) and to phosphorylate Cab45 specifically at five phosphorylation sites (Hecht et al., 2020). By mimicking the phosphorylated and non-phosphorylated state of Cab45 in alanine or glutamic acid mutants and by comparing these mutants to wild-type Cab45, the phosphorylated mutant cells localized in post-Golgi vesicles in steady state, accelerated TGN export of Cab45 clients and formed smaller oligomeric structures upon Ca^{2+} additions (Hecht et al., 2020).

1.4.3.4 Sorting into SM-rich vesicles

Soluble secretory proteins are sorted via receptor-mediated processes (e.g. lysosomal hydrolases see 1.4.2.4) or aggregation (e.g. granulins see 1.4.2.3) into CCVs for TGN export. The retention process for proteins destined for secretory granules is in fact similar to that of Cab45 oligomerization based sorting. Members of the granulin family accumulate near the membrane region where ISG formation is initiated. Similarly, Cab45 is not homogenous localized in the Golgi but more concentrated at SPCA1 rich sites, where oligomerization upon Ca^{2+}-influx can accumulate clients. In addition,

formation of transport vesicles in Cab45-dependent sorting in proximity to SPCA1, occurs in membrane regions enriched with SM (Deng et al., 2018). A property which was known for the transport of glycosylphosphatidylinositol (GPI)-anchored proteins - a group of proteins that cannot directly interact with coat proteins for vesicular trafficking, but oligomerizes to increase the affinity to cholesterol-sphingolipid microdomains (Deng et al., 2016; Ramazanov et al., 2021). While GPI-anchored proteins use the lipid microdomains as sorting platform at the TGN, the mechanism for how Cab45-client-complexes interact with SM-rich membrane regions is unclear. Findings so far proof that SM is closely associated with SPCA1 and controls its Ca^{2+}-flux activity and therefore Cab45-dependent sorting, which is further confirmed since SM colocalizes with Cab45 and its client in post-Golgi vesicles and depletion of SM synthesis leads to a kinetic delay of Cab45-client sorting (Deng et al., 2018). However, how the Cab45-client complexes are specifically targeted and recognized for sorting into SM-rich vesicles remains unclear and could involve so far unknown adaptors and TGN membrane localized proteins.

1.4.4 Trafficking of TGN46

One candidate who could be involved in such recognition or targeting processes to specifically pack Cab45 and its client into vesicles, is TGN46. The single span transmembrane protein (TMP) is prominent as a marker of the TGN, where it is exclusively integrated in the membrane, apart from constitutively cycling between the TGN and the cell surface (Stanley and Howell, 1993; Banting et al., 1998, Towler et al., 2000).

Historically TGN38, the rat homolog of TGN46, was described as TGN marker (Luzio et al., 1990) important for TGN morphology and formation of secretory vesicles at TGN exit sites (Ponnambalam et al., 1996; Stanley and Howe, 1993; Banting et al., 1998; Jones et al., 1993). Human TGN46 shares similarities with the rat homolog (Banting and Ponnambalam, 1997; van Galen et al., 2014) in function and structure (Banting et al. 1998). Both type I glycosylated integral membrane proteins share a highly conserved N terminal (including targeting signal (peptide), SP) and C terminal region (comprising part of the luminal domain, the membrane spanning region and cytoplasmic tail). The luminal domain which contains the repeat region, however, is different: TGN38 features 6 tandem repeats of an 8mer, whereas TGN46 comprises 14 tandem repeats of a 14mer sequence (Ponnambalam et al., 1996). Within the scope of the thesis the following part will focus on the human TGN46.
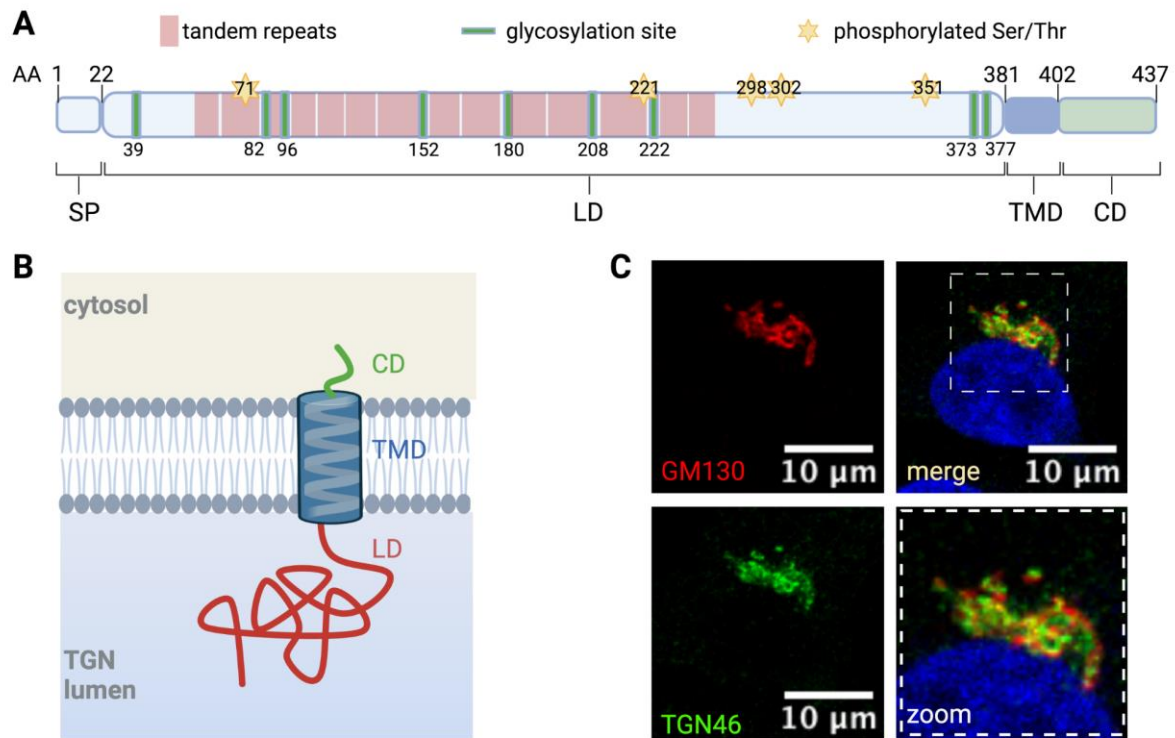
Fig. 9: Schematic sequence, structure and localization of TGN46. A. TGN46 is encoded in the gene TGOLN2, comprising targeting signal (peptide) SP to target to the secretory pathway, short cytosolic domain, single span transmembrane domain and long luminal domain with 14 tandem repeats (red shade), 9 glycosylation sites (green) and 5 Ser/Thr (stars) for phosphorylation by Golgi kinase Fam20C. **B**. The transmembrane domain with 20 residues is predicted to be based on an α-helix located in the TGN membrane, while the luminal part containing repeats are proposed to form helical or coiled-coil structures of repeating 7mer motif (Ponnambalam, 1996). **C**. Immunofluorescence images with GM130 and TGN46 antibodies on HeLa cells reveal the cis-Golgi and trans-Golgi network (TGN) as separate compartments and show TGN46 as marker of the TGN. Figures are created with biorender. IF images are taken on LSM700 in permeabilized, fixed HeLa cells.

TGN46's core has a molecular weight of 46 kDa, but runs at around 110 kDa in gel-electrophoresis (Prescott et al., 1997) due to various glycosylations gained in the ER and Golgi (Fig. 9). In the TGN the fully processed TGN46 is additionally sialylated by sialyltransferase (ST) (von Galen et al., 2014). Interestingly, upon perturbation of the SM pathway, by exchanging endogenous SM with a short form SM, the organization of the TGN is impaired and TGN resident enzymes (e.g. ST) fail to interact with their substrates (e.g. TGN46) (von Galen et al., 2014). In this case, TGN46 transported to the cell surface either after direct transport from earlier Golgi compartments or the TGN in its non-sialylated state (von Galen et al., 2014). Fully processed TGN46 localizes to the TGN via the targeting sequence

in its N-terminus, similar to other Golgi-resident proteins (Ponnambalam et al., 1996), while a conserved tyrosine-containing internalization motif in the cytosolic domain, regulates the cycling to the cell surface and return via endosomes (Ponnambalam et al., 1996). This 'SDYQRL' motif can additionally interact with the µ2 chain of the core of AP-2 complexes to initiate CCV formation (Banting and Ponnambalam, 1997; Banting et al., 1996; Chapman and Munro, 1994), however whether TGN46 is reaching the cell surface in CCV is debated (Ohno et al., 1993; McCrossan et al., 2001).

1.4.4.2 Recycling of TGN46

The recycling of TGN46 from the cell surface via endocytosis depends on GTPase activity of dynamin I (Banting et al., 1998). Strikingly, expression of a GTPase defective dynamin I mutant did not result in accumulation of TGN46 at the cell surface and did not influence TGN46 distribution in the cell, which leads to the result that TGN46 does not return directly from the cell surface to the TGN and that the transport to the cell surface is mediated by endosomes (Banting et al., 1998; Reaves et al., 1998). Indeed, TGN38/46 was shown to traffic from the cell surface to early endosomes, and then to the Golgi, thereby bypassing late endosomes (Mallet et al., 1999; Puri et al., 2002). The half-life of the TGN-to-PM trafficking of TGN46 was calculated with 45 to 60 min duration (McCrossan et al., 2001; Banting and Ponnambalam, 1997), however, internalization into the TGN is quick while exit is slower, resulting in observation of TGN46 mostly in the TGN. Although TGN46 is a ubiquitous used marker for the TGN and its recycling has been described, its function is unknown (Pfeffer 2012) which makes it an interesting target for the second part of the thesis.

1.5 Final destination - endolysosomal system

After the previous chapter elaborated on how secretory proteins reach the sorting hub and are sorted, the focus is set on the different destinations: the endolysosomal system, other organelles and the lateral or basal PM, respectively. Regarding the studies presented in the first part of this thesis, especially lysosomes will be explained in greater depth.

1.5.1 Lysosomes - waste disposal in many forms

Known as the molecular 'waste disposal' of the cell (de Duve, 2005), the 0.2-0.3 µm in diameter spherical lysosomes comprising a variety of about 50 luminal hydrolytic enzymes which are enclosed

in a membrane containing about 25 lysosomal membrane proteins (LMPs) (Trivedi et al., 2020; Saftig and Klumperman, 2009; Ni, Canuel and Morales, 2006). Already in 1963, a vacuole containing acid-dependent hydrolases was characterized and firstly termed 'lysosome' (Greek for 'digestive body') due to its ability to degrade internalized and endogenous macromolecules (Kornfeld and Mellman 1989; de Duve 2005). Because of their variations in contents due to their origin from biosynthetic or endocytic pathways or maturation of fused endosomes, their nature is morphologically heterogeneous and complex (Fig. 10). By definition the terminology for lysosome includes residual and multivesicular bodies, autophagosomes, primary and secondary lysosomes which are more precisely (i) organelles with acidic pH (about pH 5) that is optimal for contained degradative enzymes, which are (ii) hydrolyzing substrates in (iii) membranes accommodating specific glycosylated membrane-associated proteins, such as LAMP1, but feature (iv) a lack of non-lysosomal proteins, like M6PR (Luzio et al., 2007; Saftig and Klumperman 2009; Cheng et al., 2017).
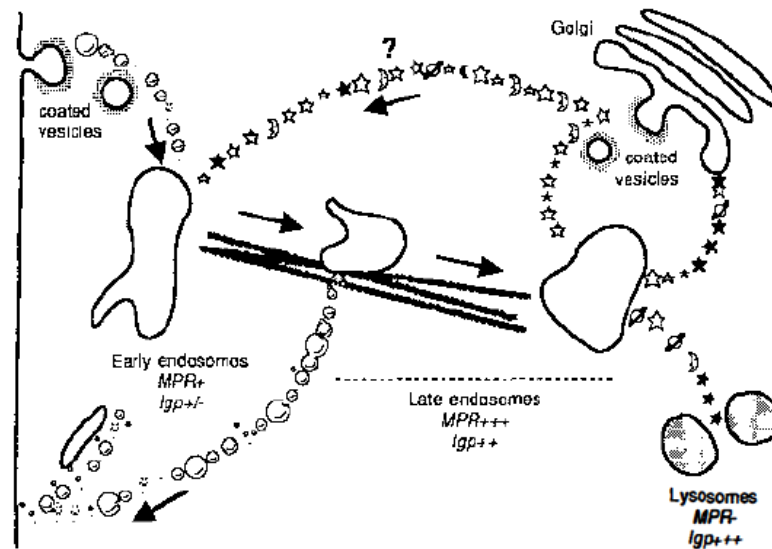
Fig. 10: Historical overview on pathways of lysosomal biogenesis from 1989, which still holds true. Shown is the endocytosis where lysosomal proteins cycle in a rapid constitutive pathway between endosomes and cell surface (vesicle transport is represented as bubbles) and coated vesicles contain MPR and lgp. The early endosomes (pH approx. 6-6.3) translocate via microtubules to the perinuclear region, while maturing to distinct late endosomes with higher MPR to membrane ratio since the distance to receive endocytosed membranes is too far. Due to their proximity to the Golgi, endosomes can receive input from endogenous lysosomal proteins from the secretory pathway (containing recycled or new MPR and lgp). At that point the direct transport from endogenous lysosomal proteins to early endosomes is not known. In this stage late endosomes can fuse with each other, with lysosomes or other existing late endosomes. Due to acidification within the late endosomes (pH < 5.5), the pH lowers leading to dissociation of MPR from their ligand, leaving mature lysosomes, which contain matured enzymes for diverse cellular functions. Figure adapted from Kornfeld and Melman, 1989. Abbreviations: MPR = mannose-6-phosphate-receptors, lgp = lysosomal membrane glycoprotein)

1.5.2 Biogenesis of lysosomal enzymes

Like general protein biosynthesis, endogenous soluble lysosomal enzymes are synthesized at the rER, following steps described earlier (see 1.1.1). With export from the rER the M6P modification - unique to lysosomal proteins - is added in stepwise fashion. Phosphorylation is initiated after ER resident glucosidase I and II trimmed glucose residues during initial processing in the rER, about 15-20min after synthesis for a duration of another 40-80 min (Goldberg and Kornfeld 1983). In the ERGIC, UDP-N-acetylglucosamine–lysosomal enzyme N-acetylglucosamine-1-phosphotransferase (simplified phosphotransferase) catalyzes the reaction of UDP-N-acetyl-D-glucosamin (GlcNAc-P) and lysosomal-enzyme-D-mannose to UMP lysosomal-enzyme N-acetyl-D-glucosaminyl-phospho-D-mannose. The process of GlcNAc-P residue transfer continues in the cis-Golgi (Dittmer and von Figura, 1999; Rohrer and Kornfeld 2001). The critical activity of the phosphotransferase is specific for all lysosomal enzymes but not occurring in non-lysosomal glycoproteins (Lang et al., 1984). It relies on the three-dimensional position of lysine residues derived from different regions in proximity to each other (shown for cathepsin D), which is the recognition domain (James and Siedecki 1986; Kornfeld and Melman 1989). In addition to this, α-1,2-linked mannose units on Asn-linked oligosaccharide serve as a recognition site for phosphotransferase as well. The produced phosphodiester intermediate is converted to an active phosphomonoester by N-acetylglucosamine-1-phosphodiester α-N-acetylglucosaminidase, called 'uncovering' enzyme (UCE) (Reitman and Kornfeld, 1981; Varki and Kornfeld 1981; Kornfeld and Melman, 1989; Rohrer and Kornfeld 2001). Due to the localization of UCE in the TGN, the final step to generate M6P modifications on lysosomal hydrolases is thought to happen in the TGN, where also M6PRs reside (Rohrer and Kornfeld 2001).

1.5.3 Intracellular trafficking of lysosomal proteins
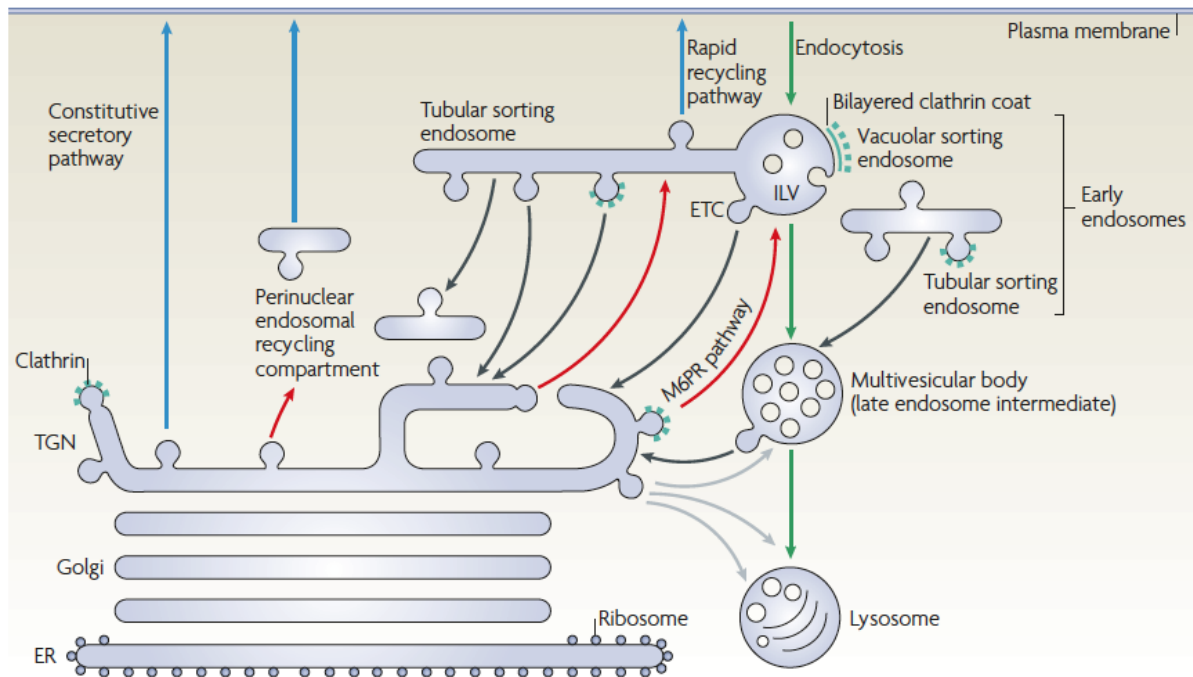
Fig. 11: Schematic overview of the biosynthetic and endocytic pathway, adapted from Saftig and Klumperman. 2009. In the biosynthetic pathway, lysosomal enzymes are synthesized, processed and recognized in the secretory pathway, before following the constitutive secretion to the plasma membrane and reaching endosomes and lysosomes via endocytosis (blue arrows) or follow the direct route to the endolysosomal system (red arrows). The endocytic pathway (green arrows) comprises intermediate stations like the intraluminal vesicle (ILV), formation of multivesicular bodies, which contain late endosomes and finally terminating in the lysosome. Black arrows represent retrograde pathways for recycling proteins.

1.5.3.1 Lysosomal hydrolases

As described earlier the sorting of lysosomal hydrolases is based on the receptor-ligand interaction with subsequent clathrin-coat formation initiation (see 1.4.2.4). After the newly generated CCV buds from the TGN, there are several options for delivery and sorting of enzymes destined for lysosomal degradation or recycling: fusion with each other, fusion with pre-existing early endosomes, or direct fusion with late endosomes (Saftig and Klumperman, 2009; Sachse et al., 2002; Trivedi et al., 2020). Early endosomes feature a vacuolar part that serves as the basis for emerging multi-branching tubules, so-called tubular sorting endosomes/ tubular endosomal network (Tooze 1991). During maturation early endosomes are acidified, resulting in dissociation of M6PRs from their ligands and recycling of the receptors by entering the tubular sorting endosomes (Bonifacino and Rojas, 2006; Saftig and Klumperman 2009). The recovery of M6PRs from the endosome to the TGN is mediated by retromers, a penta-unit structure comprised of sortin nexin dimers and a trimeric core of several

vacuolar protein sorting (Vps) proteins (Trivedi et al., 2020; Doray et al., 2002; Abubakar et al., 2017). The association of retromers with early endosomes is controlled via Rab GTPase Rab9 and effector TIP47 (Braukle and Bonifacino, 2009; Wandinger-Ness and Zerial, 2014).

1.5.3.2 Endosome and Lysosome maturation and fusion

Remaining proteins in early endosomes contain a sorting signal, ubiquitination, that can be recognized by endosomal sorting complexes required for transport (ESCRT), leading to biogenesis of intraluminal vesicles (ILVs), accumulation of those, which forms multivesicular endosomes/bodies (MVBs) (Trivedi et al., 2020; Saftig and Klumperman, 2009). Those vesicles fuse or fission driving structural remodeling and formation of globular late endosomes and lysosomes (Fig. 12). Key process for the maturation of early endosomes to late endosomes is the replacement of Rab5 to Rab7, which drives the movement of maturing endosomes from the cell periphery towards the cell center, while losing Rab5 and gaining Rab7 in the membrane of late endosomes (Trivedi et al., 2020; Bonifacino and Neefjes, 2017). Mutations in Rab7 cause accumulation of CI-M6PR and CatD in early endocytic compartments, proofing the exchange of Rab5 to Rab7 as crucial for lysosomal maturation (Press et al., 1998). Lysosomal and endosomal movement is depending on the cell state (nutrient state) (Parton et al., 1991; Trivedi et al., 2020; Pu et al., 2016) and mediated by dynein/dynactin (towards perinuclear, retrograde transport) and motor proteins of the kinesin family (KIF) (towards periphery, anterograde transport), along microtubules (Hirokawa and Noda, 2008; Paschal and Vallee, 1987; Trivedi et al., 2020; Pu et al., 2016).
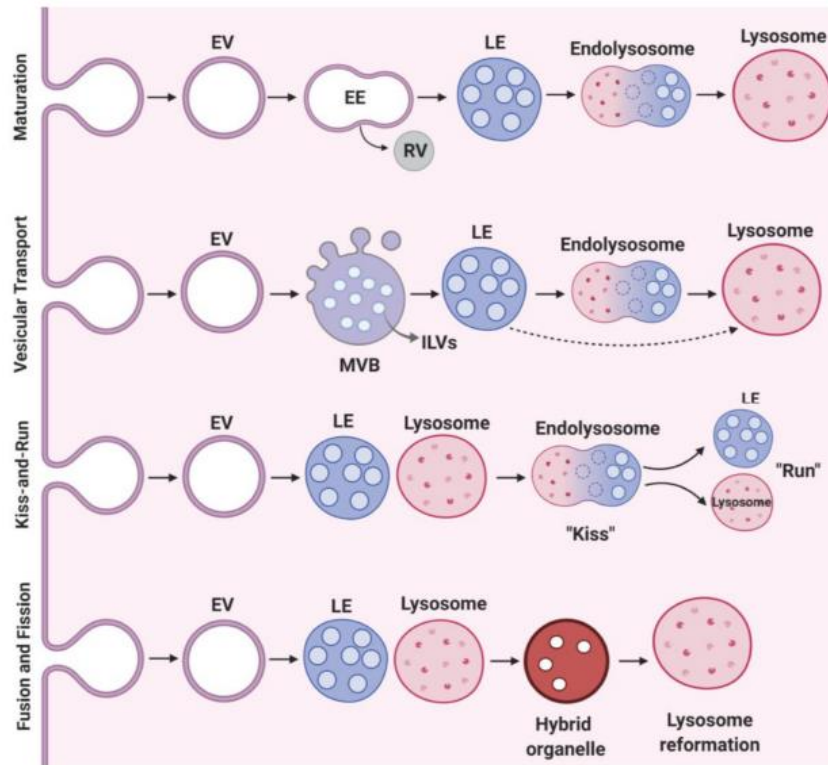
Fig.12: Possible fusion and fission events for endocytic vesicles (EV) that internalize from the plasma membrane. Recycling vesicles (RV) transport the cargo for retrograde transport to the TGN, while remaining proteins destined for degradation mature stepwise to late endosomes (LE), endolysosomes and finally lysosomes. Vesicular transport involving multivesicular bodies (MVBs) and intraluminal vesicles (ILVs) is similar to that described in the main text, where ILVs fusion and fission events lead to structural remodeling to late endosomes and lysosomes. The Kiss-and-run mechanism can occur on both the biosynthetic as well as endocytic route (Saftig and Klumperman, 2009), and describes the formation of contact sites between LE and lysosomes, conversion into an endolysosome intermediate for cargo transfer before dissociation in LE and lysosome. In fusion and fission events, heterotypic fusion between LE and lysosomes occurs while generating a hybrid organelle that reforms lysosomes. Figure is adapted from Trivedi et al., 2020.

When budding from the TGN, the CCV lumen displays similar properties like the TGN lumen with a pH of 6.3. Early endosomes that mature to late endosomes and finally lysosomes, however, contain a distinct pH < 5 and high Ca^{2+} (up to 500 µM) in lysosomes (Mindell 2012). The acidification is achieved by activity of several pumps and ion channels, among those v-ATPase (vacuolar H^+-ATPase protein pump), Ca^{2+}/H^+ exchangers, that maintain the lysosomal pH and ion homeostasis necessary for lysosome function (Mindell 2012, Pryor et al., 2000; Futai et al., 2019).

1.5.4 Lysosomal membrane proteins and receptors

In addition to the trafficking of lysosomal enzymes, the transport of membrane proteins like LAMP1 and 2 is not only important for lysosome motility but also indicate roles in cell signaling, as they show increased expression on cell surfaces of cytotoxic T cells and highly malignant tumor cells (Saftig and Klumperman, 2009). Apart from that, reduction of LAMPs by genetic downregulation or impaired transport, leads to a redistribution of lysosomes in the cell, therefore influence on lysosomal exocytosis (Trivedi et al., 2020) and accumulation of autophagosomes (Saftig and Klumperman, 2009). As transmembrane protein, LAMPs travel into endosomes and lysosomes directly from the TGN as described before (see 1.4.2.1), but also indirectly by travelling to the PM and return to the endolysosomal system (Braukle and Bonifacino, 2009). The existence of LAMPs is not static but are rather dynamic between membranes of lysosomes, endosomes and the PM (Cheng et al., 2017). Receptors of lysosomal hydrolases cycle between endolysosomal system and the TGN but are also found at the PM after secretion of lysosomal proteins or during endocytic uptake from the extracellular space (Saftig and Klumperman, 2009; Hasilik et al., 2009; Kornfeld and Melman, 1989). Some of the second group are exclusively localized at the PM, such as LRP1 (Hiesberger et al., 1998). However, the uptake of lysosomal proteins makes only about 5 - 10% of general lysosomal delivery. Also, the secretion of lysosomal enzymes happens in very low amounts and frequency in healthy cells, which defines the transport of macromolecules to the lysosome as a unidirectional process (Kornfeld and Melman, 1989).

1.5.4.1 Mannose-6-Phosphate receptors (M6PR)

There are two types of M6PR, the 46 kDa (MPR46) that works cation-dependent (CD) and the bigger 300 kDa (MPR300) that binds cargos independently of cations (CI) (Fig. 13a). The type I transmembrane glycoproteins share sequence similarity with their continuous repeats in the luminal domain and can interact with the same lysosomal proteins, which usually have a preference for either of the receptors. In this thesis, the CD-M6PR will only be described briefly. The small CD-M6PR consists of 251 residues with 167 residues forming an extracytosolic domain (Hasilik, 2008). It exists as a dimer in the membrane and can form tetramers in solution. Each functional dimer features two binding regions for M6P, that can be occupied by a single oligosaccharide with two M6P residues, particularly in the presence of Mn^{2+} (Kornfeld and Melman, 1989; Ni, Canuel and Morales 2006). CD-M6PR features a binding pocket for divalent cations which, when occupied with a metal ion (i.e. Mn^{2+}), shields its electrostatically negative region on Asp-103 and the phosphate moiety of the M6P-tagged protein, minimizing the repulsive negative interactions (Sun et al., 2005; Roberts et al., 1998). Even though the extracytoplasmic domain of CD-M6PR homologous to that of CI-M6PR, it does not

mediate endocytosis due to insufficient binding capacity at neutral pH (Gary-bobo et al., 2007; Hasilik 2008), and shows lower binding efficiency than CI-M6PR in lysosomal sorting therefore cannot completely rescue and prevent secretion of lysosomal enzymes once CI-M6PR is missing (Kornfeld and Melman, 1989).

The larger M6PR comprises two 2451-residue long transmembrane polypeptides containing an extracytosolic domain of 15 homologous repeats of 134-167 amino acids length, a short transmembrane region (23 aa) and a 43-residue domain similar to type II repeat of fibronectin (Hasilik 2008; Gary-bobo et al., 2009; Guo et al., 2014). It can bind two M6P molecules via domain 3 and 9, and one IGFII molecule in domain 11 (Hasilik 2008; Guo et al., 2014) or domain 13 (Gary-bobo et al., 2007), establishing CI-M6PR as IGF2R (Morgan et al., 1987; Kornfeld and Melman, 1989). The multifunctional binding protein participates in regulation of cell growth and apoptosis (Ghosh et al., 2003) and can compensate for loss of CD-M6PR (Kornfeld and Melman, 1989). The binding affinity of both M6PR for M6P is the same, but di-phosphorylated oligosaccharides are bound with higher affinity to CI-M6PR (Ni et al., 2006). Dysfunction of M6PRs leads to secretion of lysosomal enzymes (Guo et al., 2014; Qian et al., 2008).

1.5.4.2 Sortilin (SORT1)

Although M6PR-mediated sorting is the main pathway targeting lysosomal hydrolases (Saftig and Klumperman, 2009), M6PR-independent routes are necessary to compensate for impaired M6P-tagging, recognition or dysfunctional M6PRs. In fact, some lysosomal enzymes prefer sorting over receptors other than M6PRs. In I-cell disease (ICD) patients, M6P cannot be added to newly synthesized lysosomal hydrolases due to a mutation of GlcNAc-1-phosphotransferase (Reitman et al., 1981), yet the cellular levels of lysosomal enzymes are near normal levels in B-lymphocytes (Canuel et al., 2008; Hassan et al., 2004). In ICD fibroblasts most hydrolases are missorted and secreted, but not prosaposin and GM_2AP (Rijnboutt et al., 1991). Studies found that this is due to the preference of prosaposin and GM_2AP for the sortilin receptor (Lefrancois et al., 2003; Hassan et al. 2004; Ni et al., 2006). Originally described as low affinity receptor for neurotensin (NT), sortilin (SORT1) is also known as NT receptor 3 (Hu et al., 2010; Willnow et al., 2008). The type I membrane protein features a luminal part with Vps10 domain - which serves in yeast as sorting receptor for lysosomal hydrolases (Guo et al., 2014) (Fig. 13b). The mammalian Vps10 domain is essential for ligand interaction via its N-terminal propeptide and a conserved cysteine-rich C-terminus (Guo et al., 2014; Ni et al., 2006). The propeptide regulates sortilin transport to the TGN and inhibits interaction of the ligand with the immature sortilin and is cleaved by furin in the TGN (Ni et al., 2006; Guo et al., 2014). Following the propeptide region, a 10-bladed β-propeller fold forms a wide tunnel containing the binding sites for different ligands inside the tunnel to prevent multiple binding events at the same time (Quistgaard et

al., 2009; Guo et. al., 2014). Like CI-M6PR, sortilin is a multifunctional protein which binds also non-lysosomal proteins like precursors of TGF-β signalling (Guo et al., 2014) and can participate in endocytosis of lipoprotein lipase (Ni et al., 2006). Moreover, sortilin's cytoplasmic domain shares a homologous sequence with CI-M6PR, enabling binding to GGAs (Nielsen et al., 2001) as described earlier (see 1.4.2.4).

1.5.4.3 Other receptors

Besides multifunctional proteins like CI-M6PR and sortilin that mediate biogenetic and endocytic pathways of lysosomes, there are other receptor proteins that support lysosomal trafficking in a more specialized way. One is Low density lipoprotein receptor-related protein-1 (LRP1) which is solely expressed on the cell surface for endocytosis of exogenous proteins (Hiesberger et al., 1998). Also termed cluster of differentiation 9 (CD9), the transmembrane receptor is multifunctional, but mainly mediates the uptake of proteins, like saposins (Hiesberger et al., 1998), lipoproteins (Potere et al., 2019), neuronal amyloid-β-42 which influences lysosomal trafficking in neurons (Fuentealba et al., 2010).

Another receptor that works in M6PR-independent manner is Lysosomal integral membrane protein 2 (LIMP-2) mentioned earlier (see 1.4.2.4). It is a type III glycoprotein with two membrane spanning domains and a coiled-coil motif within the highly glycosylated domain in the lumen (Fig. 13c). Both N- and C-terminus face the cytoplasm. LIMP-2 is binding partner of βGC and interacts via its coiled-coil domain at neutral pH until dissociation in the acidic environment of late endosomes and lysosomes (Guo et al., 2014).
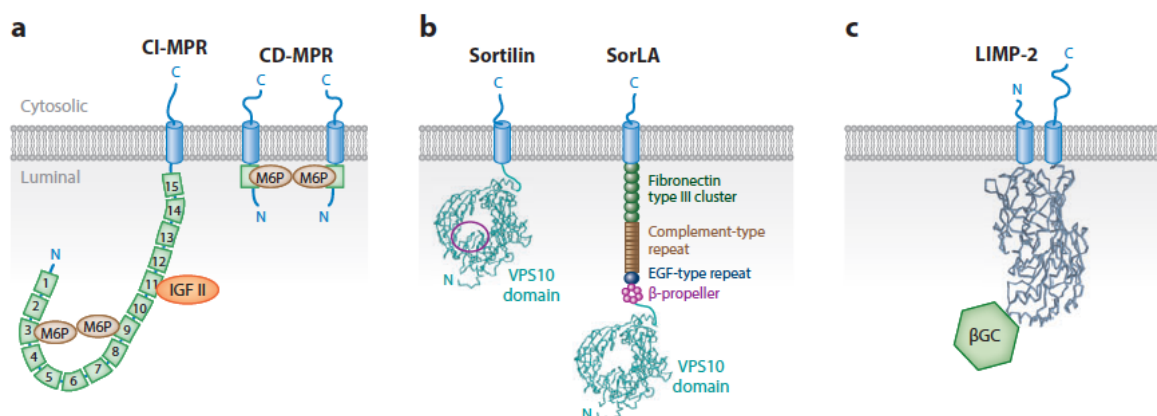
Fig. 13: Receptors of lysosomal enzymes. A. Mannose-6-phosphate (M6P) receptors binding cation-independent (CI) and cation-dependent (CD) to M6P-modified cargo proteins. CI-M6PR with 300 kDa consists of N-terminus (40 amino acids=aa), C-terminus as cytoplasmic domain (164 aa), 15 homologous repeats of 134-167 aa, and is inserted into the membrane via a 23 aa type I transmembrane domain. Binding sites for M6P and

IGFII are indicated on domain 3, 9 and 11. CD-M6PR with 46 kDa, comprises a 167-residue extracytosolic domain, N-terminus (28 aa) with signal sequence, C-terminal cytoplasmic domain (67 aa), a single transmembrane region (25 aa) and 159-residue luminal domain, with single binding site for M6PR, but exists as dimer in the membrane increasing the binding efficiency (Ni et al., 2006). **B**. M6PR-independent pathway receptor Sortilin and Sortilin-related receptor with A-type repeats (SorLA) as members of the type I integral membrane proteins and Vps10 superfamily. Sortilin forms a wide tunnel with a 10-bladed β-propeller fold which contains binding sites for ligands in its Vps10 domain in the lumen. SorLA is expressed mainly in the nervous system. The cytosolic domain SorLA contains several motifs to bind APs, retromer, GGAs that regulate shuttling between Golgi and endosomes. **C.** Lysosomal integral membrane protein 2 (LIMP-2), a type III glycoprotein with two membrane integral domains, cytoplasmic C- and N-terminus and highly glycosylated luminal domain with coiled-coil motif that binds specifically to β-glucocerebrosidase (βCG). Figure is adapted from Guo et l., 2014.

1.5.5 Prosaposin, progranulin and cathepsin D

About 50 different lysosomal enzymes are known, of which prosaposin (PSAP), progranulin (PGRN) and cathepsin D (CatD) will be in focus of this thesis. Even though they execute different proteolytic reactions, they are interconnected during sorting, maturation, processing and in physiological context (Tayebi et al., 2020).

1.5.5.1 Prosaposin (PSAP)

Prosaposin (PSAP) is the precursor of sphingolipid activator proteins (SAP, saposin) A, B, C, D, glycosylated and proteolytically processed in the endolysosomal system with the last step being cleavage by mature CatD in the lysosome (Tayebi et al. 2020). The sulfated glycoprotein was since its cloning (Kishimoto et al. 1992) intensively studied and structure and processing well described. PSAP exists as a 50 kDa form before glycosylation and modification to a major intracellular form of 68 kDa and a major extracellular form of 73 kDa (Kishimoto et al., 1992). Detection of prosaposin in various human secretory fluids (Hineno et al., 1992) was associated with PSAP's function as a neurotrophic factor promoting cell survival, ERK signalling, neurite outgrowth and differentiation (Meyer et al. 2014; Zhou et al., 2015). Secreted PSAP can be endocytosed via LRP1 and CI-M6PR (Hiesberger et al., 1998; Zhou et al., 2015). Intracellular PSAP is recognized by M6PR via its M6P modification (Qian et al., 2008; Tayebi et al. 2020) and additionally by SORT (Lefrancois et al., 2003; Hassan et al., 2004) which transport PSAP to the endolysosomal system. The protein is processed to SAP A-D which enhances various enzymatic reactions by interacting with the enzyme (SAP A, C, D) or with

the substrate (SAP B) (Hiraiwa et al., 1997). SAP A and C catalyze hydrolysis of glucocerebroside and galactocerebroside by causing a structural change in enzymes gluco-/galactosylceramidase. SAP B, however, interacts with the substrate, like GM1 ganglioside to support the enzyme acid β-galactosidase for hydrolysis. SAP D enhances sphingomyelinase activity and the hydrolysis of ceramide. Deficient PSAP processing therefore leads to accumulation of glycosphingolipids (e.g. gangliosides, cerebrosides) and causes a form of Gaucher's Disease (Kishimoto et al., 1992). Recently, PSAP was linked to neurodegenerative diseases as well due to its ability to facilitate sortilin-independent trafficking of progranulin (PGRN), a protein associated with Frontotemporal lobar degeneration (FTLD). The co-dependency includes that PGRN also bridges PSAP's interaction with SORT (Zhou et al., 2017a,b).

1.5.5.2 Progranulin (PGRN)

Progranulin (PGRN) is commonly associated with neurodegenerative diseases like frontotemporal lobar degeneration, the most prevalent form of early-onset dementia. One subtype is diagnosed with ubiquitin-positive inclusion bodies containing Tar DNA binding protein (TDP)-43 (Zhou et al. 2017b; Paushter et al., 2018). Mutations in PGRN's gene GRN lead to aggregation of ubiquitinated TDP-43. (Karamysheva et al., 2019). PGRN is an 88 kDa protein with N-linked glycosylation sites that account for heavy glycosylation (approx. 65 kDa without glycosylation) (Paushter et al., 2018). The unique structure comprises 7.5 granulin domains with each 55 residues long domain containing several cysteine motifs. It binds with high affinity to sortilin receptors and is processed by cathepsin B and L into individual granulins in a lysosome-dependent manner (Hu et al., 2010; Logan et al., 2021; Zhou et al., 2017b). Those granulins are implicated in cell growth and embryonic development (Evers et al., 2017; Nguyen et al., 2013b), however, their explicit functions are still elusive (Zhou et al., 2017c; Paushter et al., 2018; Karamysheva et al., 2019). Interestingly, in absence of a sortilin receptor, PGRN is still able to travel towards lysosomes by using PSAP as 'piggy-back' (Hu et al., 2010; Zhou et al., 2017b; Zhou et al., 2015).
Full-length PGRN is able to modulate MAPK/ERK, PI3K/Akt and FAK signaling pathways, which could be a result from its binding to receptor tyrosine kinase EPH receptor A2, that in turn activates the MAPK cascade (Paushter et al., 2018). Apart from that PGRN is involved in lysosomal homeostasis and morphology (Evers et al. 2017) not least by regulating CatD and glucocerebrosidase (GBA) activity and maturation (Butler et al., 2019; Zhou et al., 2017c; Paushter et al., 2018; Evers et al., 2017).

1.5.5.3 Cathepsin D (CatD)

Cathepsin D (CatD) is one of the best studied lysosomal proteases and belongs to a family of serine, aspartic and cysteine proteases, which are generally regulated by presenilin 1 (PS1) in the lysosomal membrane targeting v-ATPase for maintaining acidic intraluminal conditions (Trivedi et al., 2020; Zaidi et al. 2008). The aspartic cathepsin CatD is synthesized as a single polypeptide pre-pro-enzyme in the ER. Co-translational translocation leads to removal of the SP of the now inactive procathepsin D (52 kDa), which is further N-glycosylated before transport to the Golgi. There, modification of N-glycosylation and phosphorylation to M6P ensure recognition by CI-M6PR in the TGN for further trafficking to endosomes and lysosomes (reviewed in Zaidi et al., 2008). Apart from sorting by its M6P modification, CatD can reach the lysosome in a M6P-independent pathway via interacting with PSAP (Gopalakrishnan et al., 2004; Laurent-Matha et al., 2002) or completely independent of an adapter protein via binding by SORT (Canuel et al., 2008). After stepwise proteolytic maturation into an active intermediate form (48 kDa) by removal of the propeptide, CatD is processed into a two-chain form comprising a N-terminal light chain (14 kDa) and C-terminal heavy chain (34 kDa) by cathepsin L and B and also PGRN (Laurent-Matha et al., 2006; Butler et al. 2019; Tayebi et al. 2020). As matured CatD it degrades denatured or mutated proteins and supports further cleavage or processing of other lysosomal enzymes; among those is PSAP (Tayebi et al., 2020), which in turn also modulates the activation of pro-CatD - the Golgi-form of CatD (Gopalkrishnan et al., 2004) .

1.5.5.4 Interconnection between PSAP, PGRN and CatD

The previous sections indicated the interconnectivity of PSAP, PGRN and CatD. To summarize: CatD and PSAP, M6P-tagged proteins, are sorted via M6PR (Qian et al., 2008; Tayebi et al., 2020; Zaidi et al. 2008) and retrieved by CI-M6PR partially (Hiesberger et al., 1999; Zhou et al., 2015), but can also be recognized independently from other proteins by SORT in a M6P-independent process (Hassan et al., 2004; Canuel et al., 2008). PSAP in addition can interact with pro-CatD and helps its sorting in a M6P-independent way (Laurent-Matha et al., 2002) as well as modulates its activity. In turn CatD in its mature form is necessary for PSAP to be fully processed into SAP A-D (Tayebi et al., 2020). The maturation of CatD is aided (besides CatL and B) by PGRN via activation during cleavage of the propeptide. PGRN itself is sorted by SORT, but can, if that pathway is impaired, use PSAP as piggy-back to travel to lysosomes. Simultaneously, PSAP can bind SORT via PGRN as an adapter protein as well.
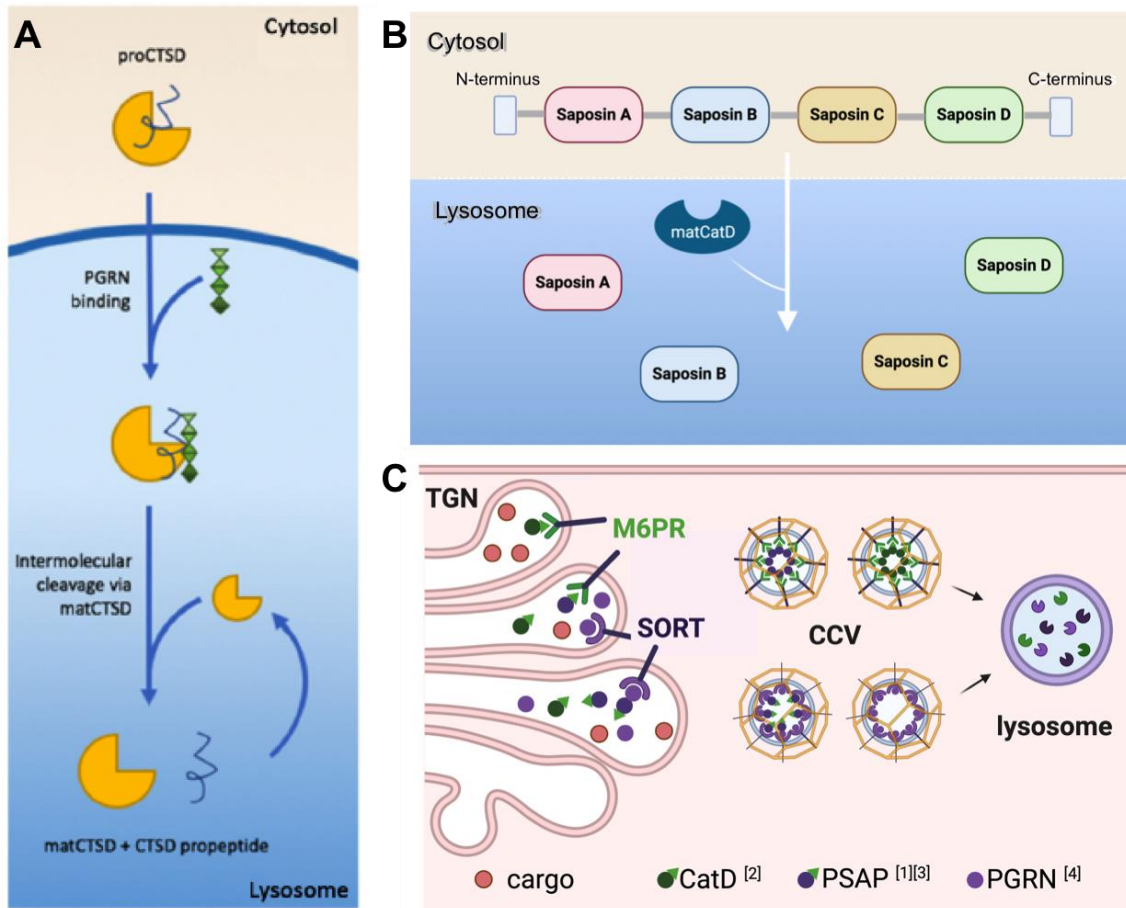
Fig. 14: Processing of procathepsin D, prosaposin and recognition of CatD, PSAP and PGRN in the TGN.
A. Activation of procathepsin D (proCTSD) to mature cathepsin D (matCTSD) by cleavage of the propeptide via progranulin (PGRN) activity in the lysosome. Figure adapted from Tayebi et al. 2020. **B**. Schematic overview of prosaposin (PSAP) maturation via matured Cathepsin D (matCatD) after transport to the lysosome into Saposins A-D. Figure was created by biorender according to Tayebi et al., 2020. **C**. Sorting of prosaposin (PSAP), progranulin (PGRN) and cathepsin D (CatD) with mannose-6-phosphate (M6PR) and sortilin (SORT) receptor. Transmembrane receptor M6PR recognizes M6P modification (green triangle) on CatD (green) and PSAP (dark purple), SORT binds PGRN (light purple) via proteinaceous interactions and indirectly PSAP which uses PGRN as adapter protein. Additionally, SORT can directly bind to PSAP as well. Other present cargo (red) remains in the TGN. Clathrin-coated vesicles (CCV) bud subsequently from the TGN and are processed to their matured form in lysosomes. Figure created with biorender based [1] Zhou et al., 2015; [2] Pohlmann et al., 1995; [3] Lefrancois et al., 2003; [4] Zheng et al., 2011.

1.5.5.5 PSAP, PGRN and CatD in health and disease

The function of lysosomes to recycle and degrade diverse macromolecules is a housekeeping function for cell homeostasis and mediated by a complex network of lysosomal enzymes. Malfunctioning of these, their processing and maturation or trafficking leads to >50 human diseases, generally termed as lysosomal storage disorders (LSDs) (Ferguson 2015). As the description of all these would

completely get out of frame of this thesis, only those linked to PSAP, PGRN or CatD are mentioned briefly.

The most common is Gaucher's Disease (GD), usually caused by mutation in the gene GBA1 encoding for β-glucocerebrosidase, which causes accumulation of glycolipids, glucosylceramide and glucosylsphingosine. Mutation or malfunctioning of the PSAP sorting processes causing secretion for example, can lead to lower levels of SAP A-D that can catalyze the hydrolysis of glucocerebroside resulting in subtypes of GD (Tayebi et al., 2020; Kishimoto et al., 1992). Interconnectivity of PSAP with PGRN proposed a link between PSAP and FTLD and neuronal ceroid lipofuscinosis (NCL), a neurodegenerative disease with lysosomal lipofuscin accumulation. (Tayebi et al., 2020; Zhou et al., 2017a; Zhou et al., 2015). Also, mutations in CatD results in NCL and causes neurodegenerative disorders, among those synucleinopathies. CatD normally acts in α-synuclein (SNCA) degradation as primary endopeptidase and ensures prevention of SNCA aggregates (Sevlever et al., 2008). Accumulation of SNCA found in Lewy bodies and neurites in Parkinson's Disease imply important roles for CatD and CatD associated enzymes PSAP and PGRN in processes in neurodegenerative diseases (Tayebi et al., 2020). The correct maturation in lysosomes, essential for their function, draws attention to the correct sorting mechanisms by their receptors in the TGN. Naturally, these enzymes can escape recognition mechanisms as described above and can be partly retrieved via CI-M6PR (PGRN, PSAP, CatD) and LRP1 (PSAP) from the extracellular space in endocytic events, even though with lower rate than biosynthetic delivery to the lysosomes (Bajaj et al., 2019; Hasilik et al., 2009). The principle of retrieval is currently studied in enzyme replacement therapies to treat GD, Fabry disease and Pombe disease, where missing lysosomal enzymes are added extracellularly via endocytosis (Desnick et al., 2012; Thurberg et al., 2006).

2 Aims

Correct processing, sorting, and transport of proteins is essential for maintaining cellular homeostasis, integrity, cell-cell communication, and migration. Previous studies have explained the mechanisms involved in sorting and trafficking of transmembrane proteins and M6P-tagged lysosomal proteins. The sorting of soluble proteins has been studied intensively in recent years but is still poorly understood. The molecular insights of Cab45-dependent sorting of secretory proteins were obtained by studying calcium-induced Cab45-oligomerization, Cab45-clients-complex formation, and its packaging into sphingomyelin-rich vesicles budding from the TGN to other destinations. However, mechanistic details of the trafficking and the nature of Cab45 clients and their recognition remains an enigma in the field.

The aims of my thesis, therefore, were formulated as follows:

- ★ Identification of additional clients of Cab45 in receptor-independent sorting
- ★ Recognition and packaging of Cab45-cargo-complexes into transport vesicles

During my doctoral studies, I identified a surprising new role of Cab45 in regulating lysosomal biogenesis, which was formulated as an additional goal:

- ★ Characterization of a novel role of Cab45 in targeting lysosomal enzymes via a receptor-dependent pathway.

3 Results

Cab45 is known to sort a subset of soluble secretory proteins, such as LyzC and COMP (von Blume et al., 2012; Crevenna et al., 2016; Deng et al., 2018; Hecht et al., 2020). A common structural domain or sequence that could serve as a potential recognition site for cargo interaction with Cab45 has yet to be found. It is essential to broaden the pool of Cab45 clients to gain insight into how Cab45 mediates its client binding and sorting mechanisms. Potential candidates can then be grouped according to their functional classes and if applicable conserved binding motifs. The first approaches to find proteins that play a role in or are sorted by the Cab45-dependent mechanism were performed as proximity-labelling based screening with a biotin ligase fused to Cab45 (termed BioID, Roux et al., 2012) and immunoprecipitation of tagged-Cab45 to pulldown potential interaction partner to determine direct or indirect interaction. With subsequent mass-spectrometric analyses a large number of proteins were identified but they could not be easily grouped by signaling network or functional activity (data not shown). Interactions between clients and Cab45 or within the Cab45 machinery could be transient and therefore challenging to preserve during long-time proximity labelling with BioID or complex immunoprecipitation experiments. Two major changes set the path for the investigations presented in part A and B of this thesis. Previously, we aimed to identify interaction partners of Cab45 by looking into proteins which could directly take part in the mechanism. In part A (3.1 - 3.3), I addressed the question in a different way - by focusing on the functional outcome, in particular, secretion of proteins with secretome analysis. Intriguingly, the secretome analysis revealed a group of potential clients that exposed an unexpected role of Cab45 in the transport of lysosomal hydrolases. The second change regards the APEX labelling, which is similar to BioID proximity-based, but requires a short labeling time and is therefore more precise (Rhee et al., 2013). The results published by Deng et al. (2018) revealed Cab45 to be sorted in SM-rich vesicles together with clients and TGN46, a transmembrane protein located in the TGN membrane. Part 2 (3.4) of this thesis therefore investigates the interconnection between TGN46 and Cab45 and is an extension of the mechanistic insight in the Ca^{2+}-dependent receptor-independent sorting published from this lab (von Blume et al., 2012; Crevenna et al., 2016; Deng et al., 2018, Hecht et al., 2020).

Part A - A novel role of Cab45 in lysosomal trafficking and positioning

3.1 Identification of lysosomal hydrolases as potential additional Cab45 clients

For the first aim, which targets the identification of Cab45 clients, the secretomes of HeLa cells treated with control or Cab45 siRNA were analyzed using hiSPECS (Tueshaus et al., 2020, in collaboration with S. Lichtenthaler). Then, promising hits were validated in secretion assays and quantitative real-time polymerase chain reaction (qRT-PCR) to assess the influence of Cab45 knockdown on protein secretion and mRNA expression.

3.1.1 hiSPECS results revealed increased secretion of lysosomal proteins in cells treated with Cab45 siRNA compared to control siRNA.

Von Blume and colleagues described a role of Cab45 for sorting of soluble secretory proteins previously, thus, we screened for proteins whose secretion is altered in cells deficient of Cab45 using high-performance secretome protein enrichment with click sugars (hiSPECS) (Fig. 3.1A) (Tueshaus et al., 2020). The method allows analysis of cell supernatants in presence of serum, thereby avoiding starvation effects and allowing the study to resemble physiological conditions more closely.
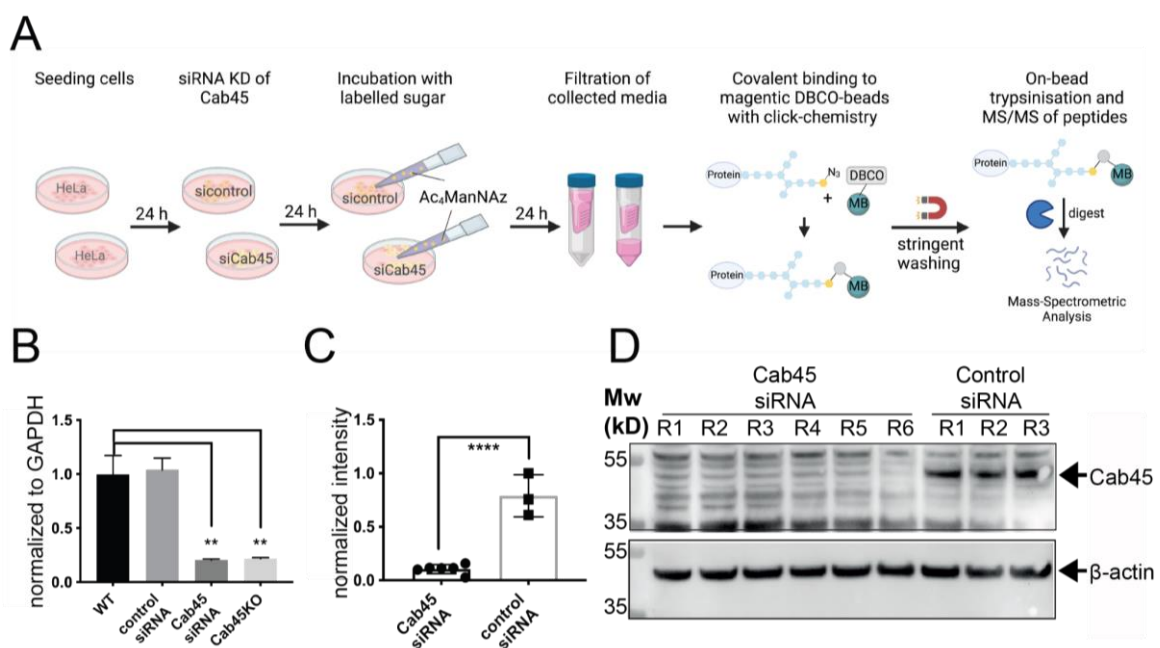
Fig. 3.1.1A-D: High-performance secretome protein enrichment with click sugars (hiSPECS) method for screening of potential interactors by secretome analysis of Cab45 siRNA and control siRNA treated cells.

A. Overview of the method. In brief, N-azido-acetylated-mannosamine-tetra-acylated labelling sugar (Ac$_4$ManNAZ) was added in media of cells treated with siRNA, filtrated to prepare for click reaction to DBCO magnetic beads. The labelled (glycosylated) proteins undergo on-bread trypsinization and peptides analyzed by mass spectroscopy (MS). **B.** Result of qRT-PCR show significantly decreased transcript levels in Cab45 siRNA treated cells, similar to those in Cab45KO. **C**. Quantification of western blot in **D** verifying significantly decreased protein levels in Cab45 siRNA treated cells compared to control siRNA cell lysates.

To compare the effects of Cab45 expression on secretion, we treated HeLa cells with control and Cab45 siRNA for 24h before adding the N-azido-acetylated-mannosamine-tetraacylated labelling sugar (Ac$_4$ManNAZ) to the cell media. Efficient knockdown of Cab45 was confirmed by observing protein and transcript abundance by immunoblotting and on transcript level by qRT-PCR respectively (Fig. 3.1B, C, D). Comparison of qRT-PCR results in HeLa wild-type (WT), control and Cab45 siRNA with Cab45KO showed a significant decrease of Cab45 transcript levels in Cab45 siRNA compared to control siRNA treated cells and WT cells, similar to levels in Cab45KO cells. Western blotting demonstrated the effective depletion of Cab45 in lysates of Cab45 siRNA treated cells of all six replicates by decrease of intensity of the protein band at 45 kDa, marking the size of Cab45, compared to lysates from control siRNA treated cells. Quantification of western blot signal of Cab45 confirmed the significant depletion of Cab45 protein levels upon Cab45 siRNA treatment (Fig. 3.1C). β-actin signal in the blot below showed similar intensities of the expected protein band at 42 kDa, confirming an equal loading of cell lysates (Fig. 3.1. D). While cell lysates were used for confirmation of Cab45 knockdown efficiency, the cell supernatants of control and Cab45 siRNA treated cells were collected and cleared from cellular debris by filtration. Subsequently, an *in vitro* click reaction of glycosylated proteins to DBCO magnetic beads was performed. On-beads trypsinization of glycoproteins yielded in peptides that were analyzed by mass spectrometry (MS). The MS results of hiSPECS are shown in a volcano plot with threshold below log2. On the left side are proteins with reduced secretion in Cab45 deficient cells, whereas on the right side proteins with higher secretion in Cab45 depleted cells are presented. A complete list of all significantly different secreted proteins can be found in the supplementary table 1.

E
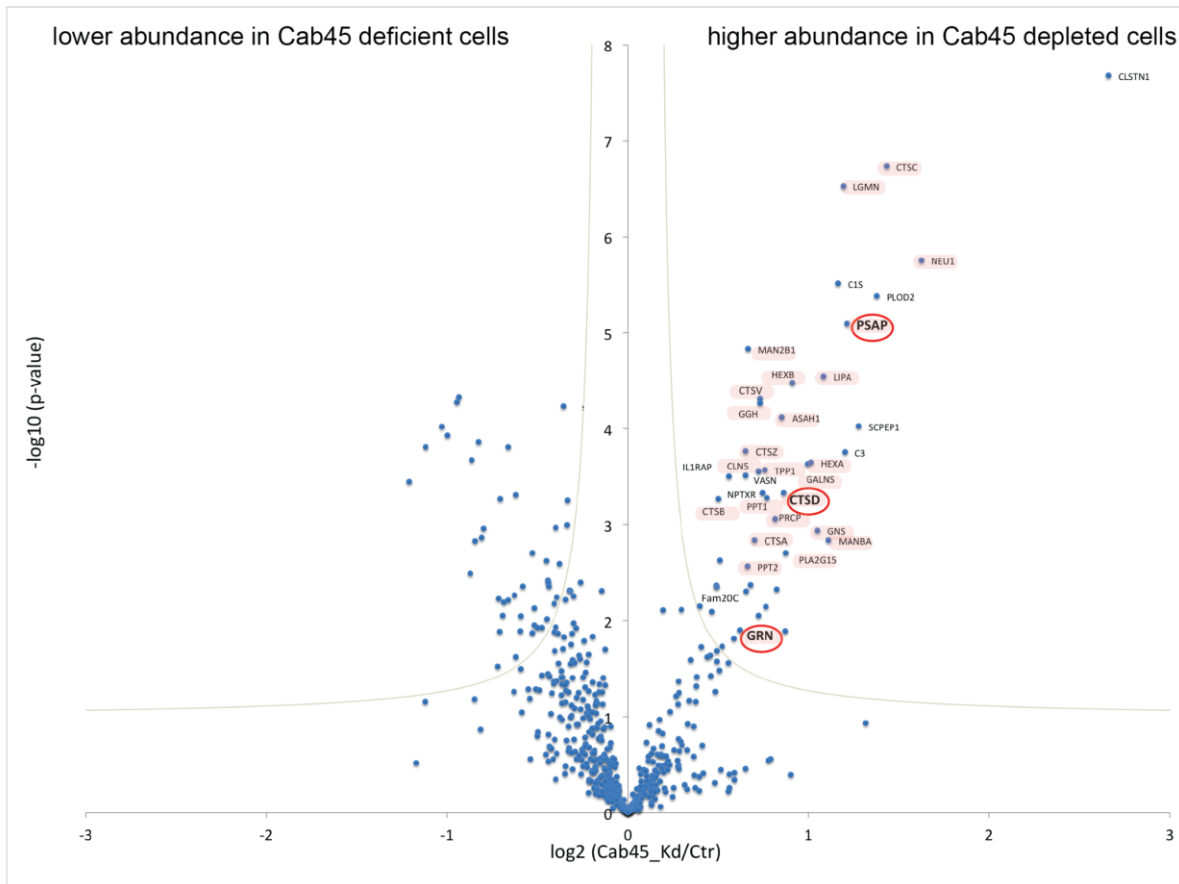
Fig. 3.1.1E: Volcano plot representing hiSPECS with MS analysis correlating p-value (-log10) versus Cab45 knockdown (KD)/ control (log2). Results show proteins in supernatants of Cab45 deficient cells compared to control cells with significantly lower or higher abundance (left: 44 of 551 hits, and right: 46 of 551 hits with gene names, respectively). The majority of proteins with higher abundance in Cab45 deficient cell supernatants are lysosomal proteins (shaded in pink) with examples chosen for further analysis prosaposin (PSAP), progranulin (GRN) and cathepsin D (CTSD) highlighted with a red circle.

Proteins that were found at lower levels in the cell supernatant of Cab45 deficient cells compared to control cells, comprised those from diverse functional and structural backgrounds, that could therefore not be grouped into one class of proteins. However, surprisingly, higher levels of lysosomal proteins were secreted from Cab45 siRNA treated cells compared to control siRNA treated cells. In fact, a majority of 70% of the total number of proteins found with significantly higher levels in supernatants of Cab45 depleted cells, are lysosomal enzymes (Fig. 3.1E, pink).

A similar higher secretion (hypersecretion) of cathepsin D in cells depleted of ADF/cofilin has previously been observed in cells that are depleted of ADF/cofilin, treated with F-actin modulating drugs or deficient of SPCA1 and Cab45 (von Blume, 2011, 2012). In agreement with this data, and in validation of our high-throughput hiSPECS methodology, our secretome analysis identified cathepsin D (CTSD) to be present at higher abundance in supernatants of Cab45 deficient cells. Among others,

prosaposin (PSAP) and progranulin (PGRN) were also hypersecreted in Cab45 siRNA treated cells intriguingly, these two proteins have recently been reported to function in a network together with cathepsin D (CatD) (Tayebi et al., 2020). PSAP is a binding partner and substrate of CatD while PGRN influences its activity (Gopalakrishnan et al., 2004; Laurent-Matha et al., 2002; Zhou et al., 2017c; Tayebi et al., 2020). PSAP and PGRN on the other hand can interact to enable their recognition by both receptors, M6PR as well as SORT1 (Zhou et al. 2015; 2017a, b; Tayebi et al., 2020). An impairment of recognition and processing or mutation of each one of these lysosomal proteins leads to the formation of lysosomal storage diseases (Tayebi et al., 2020).

Because of this interconnection between CatD, PGRN and PSAP, as well as the availability of commercially available reagents for these targets, I selected these lysosomal proteins for further validation experiments.

3.1.2 Immunoblotting validates hypersecretion of lysosomal proteins in Cab45 deficient cells

Since the screening for potential interactors of Cab45 was performed by analysis of the secretome of HeLa cells treated with Cab45 and control siRNA, secretion assays and immunoblotting were subsequently carried out as validation experiments. Firstly, secretion assays were optimized to allow clear detection of protein bands intensity in western blot for the available antibodies.

To verify that the proteins are secreted in the first place, the secretion assay was combined with a 20°C block assay, which allows the accumulation of proteins in the Golgi at 20°C before release for trafficking to the plasma membrane and secretion at 37°C (Ladinsky et al., 2002; Saraste et al., 1986) (Fig. S1). The experiment was performed with a 2h block before release for 4h in HeLa cells treated with control and Cab45 siRNA and Cab45KO cells. PSAP immunoblotting shows a strong double band representing the lysosomal saposin precursor form (65 kDa) and the secreted form (70 kDa) of PSAP (Meyer et al., 2014; Tayebi et al., 2020)(Fig. S1) in cell lysates after block at 20°C. As expected, the level of PSAP decreases in the cell lysates after release at 37°C, implying either processing in lysosomes or secretion of the protein. After 4h of release the PSAP bands in cell lysates are faint (Fig. S1), while in the supernatant no signal for PSAP is detected (data not shown). Prolonging the secretion to 24h, enabled detection of a clear quantifiable protein band for PSAP in western blot of supernatants.
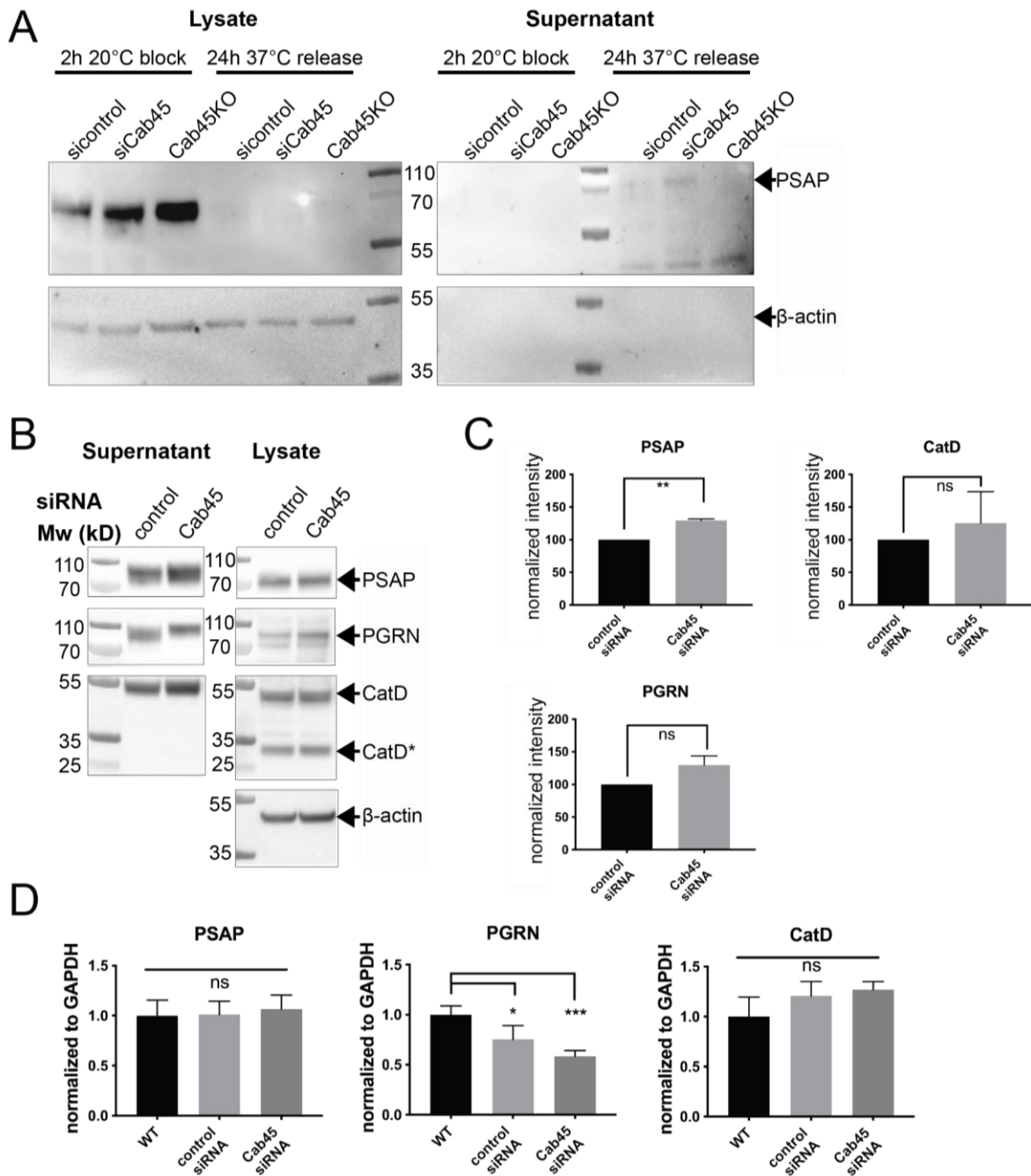
Fig. 3.1.2: Validation experiments of hypersecretion phenotype observed in hiSPECS. A. Primary set-up of conditions for secretion assays by 20°C block experiment to accumulate protein in the Golgi apparatus and subsequent release at 37°C for 24h, which was chosen as the time period for further assays. **B**. Representative immunoblot of cell culture supernatant and lysate after 24h secretion of in Cab45 siRNA and control siRNA treated cells demonstrating detection of more intense protein bands for PSAP, PGRN and CatD. CatD* depicts a form that is sorted correctly from the TGN to be processed into the heavy chain of mature CatD (34 kDa) **C**. Quantification verifies the hypersecretion phenotype for PSAP with 1.3-fold higher intensity (**) and shows a tendency for higher secretion (1.3-fold, non-significant) for PGRN and CatD. **D**. qRT-PCR quantification of

PSAP, PGRN and CatD transcript levels in wild-type (WT) control siRNA and Cab45 siRNA treated cells. Transcript levels are similar in PSAP and CatD between WT, control and Cab45 siRNA cells, whereas PGRN mRNA levels are reduced in both control and Cab45 siRNA treated cells. All statistical analyses were performed using GraphPad Prism7 with Welch's test.

After defining the conditions for secretion assays via western blotting, we analyzed the secretion of CatD, PSAP and PGRN in cells treated with control siRNA compared to those with Cab45 siRNA (Fig. 3.1.2B). Immunoblotting for PSAP in supernatants, across three individual experiments revealed a 1.3-fold higher PSAP level in Cab45 siRNA compared to control siRNA (Fig. 3.1.2B). Although PGRN and CatD secretion appeared slightly increased in Cab45 siRNA treated compared to control cells, the quantification of the protein bands shows non significance with a trend towards hypersecretion in Cab45 depleted cells (Fig. 3.1.2C). Endogenous levels of PSAP and CatD in cell lysate of control cells and Cab45 siRNA treated cells appear similar, whereas PGRN protein levels are slightly increased in Cab45 depleted cells. Notably, a thick band (probably a double band) is observed for CatD in lysate and supernatant of siCab45 treated cells, depicting the active intermediate (48 kDa) which is found in the endolysosomal system and the proenzyme pro-CatD - the Golgi localized inactive form (52 kDa). The processed form of CatD (34 kDa) is not found in the supernatant. To test if the increased secretion is due to a different transcript level of PSAP, PGRN and CatD, we performed qRT-PCR in HeLa WT, control siRNA and Cab45 siRNA transfected cells (Fig.3.1.2D). PSAP and CatD show similar transcript levels. However, levels of PGRN mRNA are strongly decreased in Cab45 siRNA treated cells compared to WT; nevertheless, in control siRNA treated cells there is also a significantly lower PGRN transcript levels observed compared to WT.
The validation experiments verify that PSAP is significantly hypersecreted and increased secretion is observed for PGRN and CatD in cells depleted of Cab45 and that this is not due to upregulated transcript levels.

3.2 Cab45 influences trafficking of lysosomal hydrolases to lysosomes

The surprising relationship between Cab45 depletion and hypersecretion of lysosomal hydrolases, raises the question as to how Cab45 participates in the correct trafficking of lysosomal proteins to the lysosomes. The life cycle of lysosomal proteins begins with their synthesis as pre-pro-enzymes, translocation from the ER to the Golgi following under removal of their signal sequence, over the modification to become pro-enzymes addition of M6P-tags for recognition by their receptors and ends with the transport to the endolysosomal system for processing into their mature enzymatic form in the lysosomes. Since Cab45 is Golgi-localized and known to function within the lumen of the TGN, we

addressed the third aim of this thesis by studying the influence of Cab45 on the interaction of lysosomal proteins with their receptor.

Since the secretion of PSAP, PGRN and CatD is increased upon knockdown of Cab45, while mRNA levels are similar or, in case of PGRN, even decreased, we tested whether the recognition by the receptors of lysosomal proteins was responsible for the increased secretion phenotype in the Cab45-depleted cells. In particular we used cells deficient of sortilin (SORT1) or IGF2 receptor, two receptors recognizing lysosomal proteins, or both simultaneously (double KO) in secretion assays and compared the steady state secretion of PSAP, PGRN and CatD (Fig. 3.1.3A).

3.2.1 Cab45 depletion causes enhanced PSAP hypersecretion in IGF2 receptor KO cells
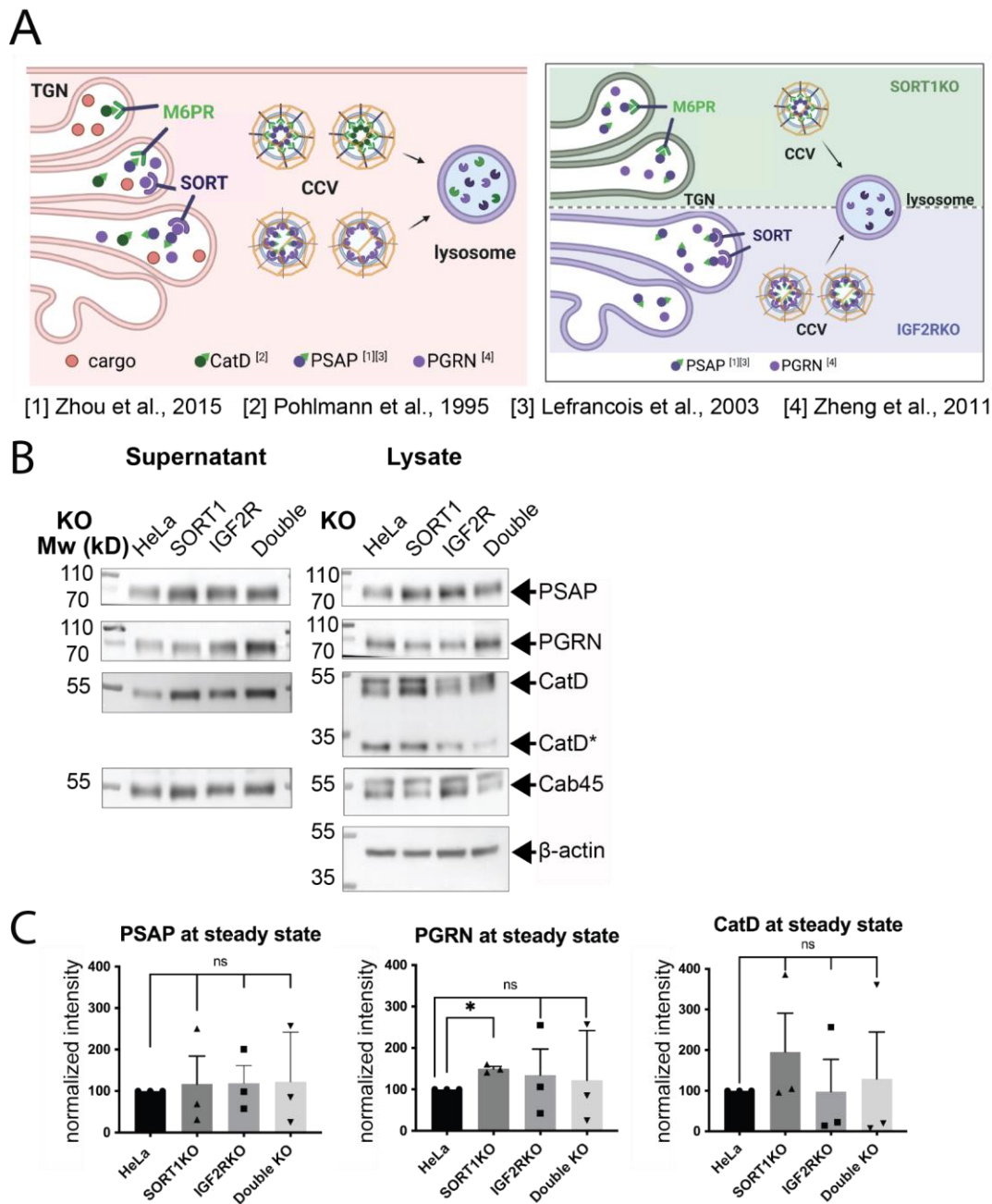
Fig. 3.2.1A-C: Direct transport of PSAP, PGRN and CatD to the lysosome via M6PR and SORT1 receptor. A. Schematic overview of the recognition of PSAP, PGRN and CatD by receptors M6PR and SORT1 in WT (left), and SORT1KO (CD-M6PR, right, top) or IGF2RKO cells (right, bottom). B. Immunoblot of 24h secretion assay in HeLa, SORT1KO, IGF2RKO and (SORT1/IGF2R) double KO cell supernatant and lysates at steady state. Antibodies for PSAP detect higher levels in SORT1-, IGF2R- and double KO cell supernatants compared to HeLa. PGRN levels appear highest in double KO cell supernatants. CatD antibodies show strongest protein bands in SORT1KO and double KO cell supernatant. With CatD* representing the heavy chain form of mature CatD, while the active intermediate form before processing in the lysosome is shown around 48 kDa. C. Quantification of western blots including B demonstrates non-significant changes in PSAP and CatD secretion

in HeLa SORT1KO, IGF2RKO and double KO cells, while PGRN secretion is significantly increased in SORT1KO cells. Each replicate is indicated as a symbol within the bar graphs that were statistically analyzed using Welch's test in GraphPad Prism9.

IGF2R-, SORT1-, and double KO cell supernatants show higher abundance of PSAP compared to HeLa cell supernatant, however, differences are not significant (Fig. 3.1.3B). PSAP is mainly sorted by IGF2R (Qian et al., 2008; Zhou et al., 2015), but can also use the SORT1-dependent route to the lysosome, either on its own (Zheng et al., 2011) or by interacting with PGRN (Zhou et al. 2017). A shut-down of both receptor pathways in SORT1/IGF2R double KO cells causes a similar increase in secretion like when either of the receptors is deleted. This suggests that PSAP could be recognized and routed to the lysosome by additional receptors. A significant increase in PGRN secretion is observed in SORT1KO cells compared to HeLa cells (Fig.3.1.3B), which is aligning with studies demonstrating increased levels of extracellular PGRN in cells with deficient or absent SORT1 receptor (Carrasquillo et al., 2010). It has to be noted that PGRN is present in its fully glycosylated form at 88 kDa as well as in its non-glycosylated immature 65 kDa form, which is observed more prominently (Fig.3.1.3B), however previous secretion assays showed the appearance of the higher molecular weight band as well, which could indicate that immature non glycosylated, partly glycosylated and fully glycosylated forms of PGRN are secreted. The nature of non-commercial SDS gels could also contribute to a slight change in observed molecular weight, especially with small molecular weight differences.

Interestingly, in SORT1KO cells the level of CatD is increased in supernatants, whereas IGF2RKO cell supernatants tend to have lower abundance of secreted CatD compared to SORT1KO cell supernatant, although differences are not significant compared to HeLa cells. The double band of CatD representing the active intermediate (48 kDa) in lysosomes and proenzymatic form (52 kDa) in the Golgi are more profound in lysate than in supernatants of all cell lines. From the similar molecular weights of the active intermediate and proenzyme form it cannot be certainly determined which form is secreted. The deletion of IGF2 affected CatD secretion surprisingly little compared to CatD secretion in cells absent of SORT1. A reason for the low secretion in IGF2RKO compared to SORT1KO cells is possibly based on the lower expression level of CatD in IGF2RKO cells as visible in lysates. In double KO cells additionally the cellular amount of mature CatD is reduced. Since CatD, a M6P-tagged hydrolase, is recognized and sorted by M6PRs (such as IGF2R), a loss of the main receptor suggests a highly increased secretion of unprocessed CatD. However, studies report that SORT1-dependent trafficking to the lysosomes enables the routing of CatD in absence of M6PR as well (Canuel et al., 2008).

From previous experiments, we expect that Cab45 acts in the same pathway as the recognition of lysosomal hydrolases by their receptors. To investigate the effect of Cab45 in SORT1KO, IGF2RKO

and double KO cells, we performed secretion assays of PSAP, PGRN and CatD after Cab45 siRNA treatment. Antibodies detected slightly lower levels of PSAP, PGRN and CatD after Cab45 siRNA treatment in SORT1KO cell supernatant and double KO cell supernatant (Fig. S2A, B).
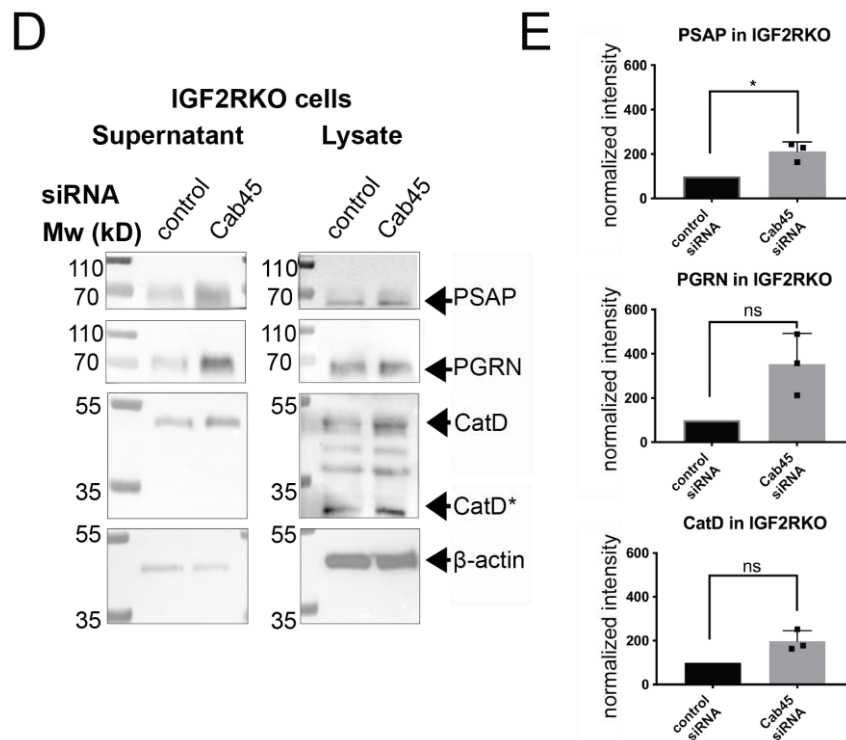
Fig. 3.2.1D, E: Influence of Cab45 depletion on IGF2RKO cell secretion of PSAP, PGRN and CatD. D. Representative western blot indicates hypersecretion phenotype of PSAP and PGRN with depletion of Cab45 in IGF2RKO cells. CatD levels are increased in supernatant and lysate. **E.** Quantification of three independent experiments revealed PSAP's increased abundance in the supernatant of IGF2RKO cells to be significant, while PGRN and CatD differences are reflected as non-significant tendencies.

Surprisingly, this is not the case for IGF2RKO cell supernatant after Cab45 depletion, where higher levels of PSAP, PGRN and CatD are detected. Quantification revealed the differences in PSAP to be significantly increased in cells treated with Cab45 siRNA compared to those treated with control siRNA (Fig. 3.2.1D, E). For CatD, the lysate showed more intermediate forms compared to previous secretion assays in both control and Cab45 siRNA treated cells. Since CatD is processed at multiple steps, it is not unexpected to find all forms in the lysate (see later discussion). In IGF2RKO cells, SORT1 partly takes over the trafficking of PSAP to the lysosomes. Possibly, the depletion of Cab45 impairs the binding or recognition of PSAP by SORT1, the interaction with the adaptor protein PGRN or other receptors of the lysosomal trafficking system.

3.2.2 Surface biotinylation shows no alterations in IGF2R presentation on the cell surface of HeLa compared to Cab45KO cells

Secreted lysosomal proteins that escape the recognition and binding by M6PR despite a functional M6P-tag, are reported to be retrieved by exocytosis via IGF2R (Bajaj et al., 2019) and LRP1 surface receptor (Hiesberger et al., 1998; Laurent-Matha et al., 2002). PSAP hypersecretion could, in addition to statements mentioned above, result from insufficient endocytosis of escaped PSAP by lower expression of IGF2R at the cell surface.

We performed cell surface biotinylation to test the influence of Cab45 levels on receptor expression on the plasma membrane (Fig. 3.1.4A, B). NHS-biotin-labelled proteins on the cell surface are enriched on Neutravidin Agarose beads (Pierce) and assessed by western blotting.
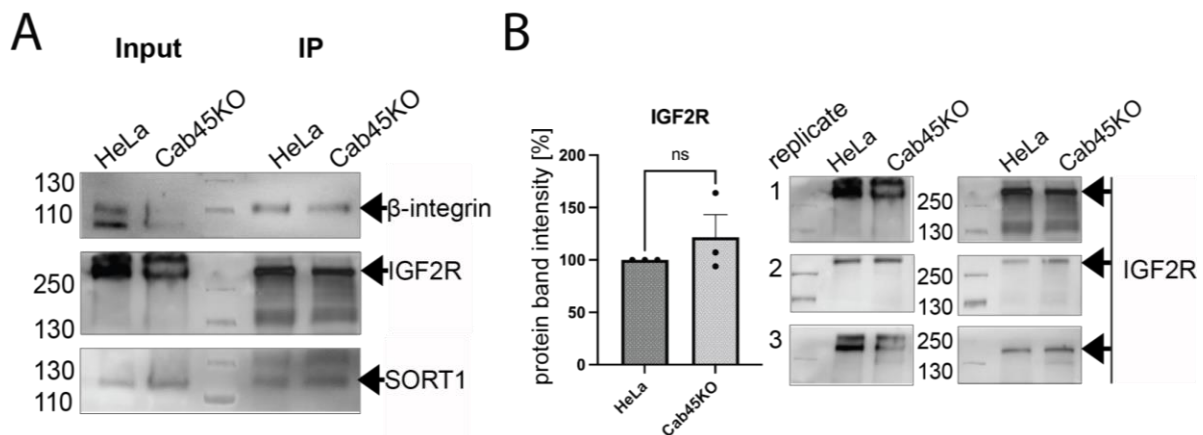
Fig. 3.2.2: Labeling of proteins expressed at the cell surface of cells with biotin and subsequent immunoprecipitation in HeLa compared to Cab45KO cells. A. Representative western blot shows similar IGF2R levels in immunoprecipitated samples of HeLa and Cab45KO cells, while integrin and SORT1 levels are indifferent as well. **B**. Quantification (left) of IGF2R detection on cell surfaces of HeLa and Cab45KO cells indicated in three independent experiments (B, right). Slight differences are non-significant in Welch's test (GraphPad Prism9).

The intensities of IGF2R and **β**-integrin, which serves as loading control, on the cell surface of Cab45KO are similar to those of HeLa, suggesting no influence of Cab45 depletion on IGF2R expression on the plasma membrane. The results indicate that a decreased exocytic retrieval of PSAP by IGF2R is not the cause of the increased abundance of PSAP in cell supernatants observed in secretion assays, but could be due to faulty trafficking to the lysosomes. Therefore, we hypothesized that Cab45 is directly or indirectly involved in a receptor-dependent sorting mechanism necessary for trafficking of PSAP and PGRN to the lysosome.

3.2.3 Depletion of Cab45 causes increased Golgi export of PSAP

Next, we investigated the influence of Cab45 on PSAP trafficking by using Retention-using-selective-hooks (RUSH) system-based approaches (Fig. 3.1.5A). The ER-hook, consisting of KDEL sequence and streptavidin, holds the streptavidin binding protein tagged fluorescent protein of interest at the ER, until released by the addition of biotin (Boncompain et al., 2012).
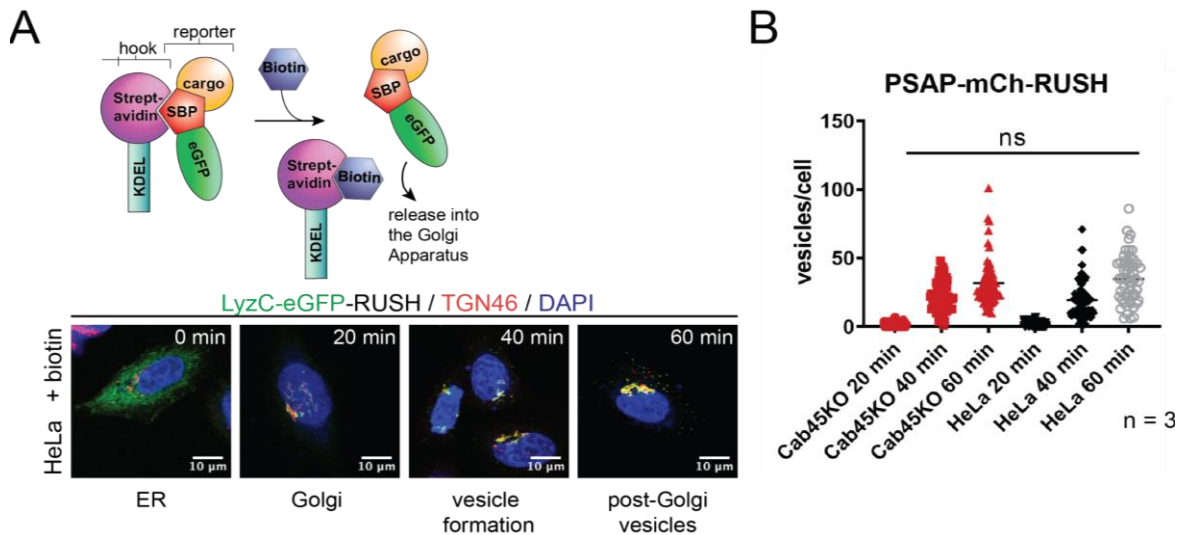
Fig. 3.2.3A, B: Trafficking studies of using PSAP-mCherry RUSH. A. Schematic of retention-using-selective-hooks (RUSH, Boncompain et al., 2012) system with confocal images using LyzC-eGFP RUSH in fixed HeLa cells at indicated time points. The cargo (LyzC) covalently bound to reporter eGFP and SBP (streptavidin-binding protein) is held by the KDEL-hook via streptavidin in the ER (0 min). Biotin addition results in competitive affinity-based replacement of SBP and releases the cargo (LyzC-SBP-eGFP) into the secretory pathway. Fluorescence in the Golgi apparatus (20 min post biotin addition), vesicle formation (40 min post biotin addition) and travel of post-Golgi vesicles after 60 min post biotin addition can be monitored and counted via confocal microscopy of fixed cells. **B**. RUSH assay using PSAP-mCherry RUSH for timepoints 20, 40 and 60 min after biotin addition in HeLa compared to Cab45KO cells. The number of post-Golgi vesicles are not significantly different from each other. Statistical analysis was performed using at least 50 cells with Kruskal-Wallis test in GraphPad Prism7.

Upon biotin addition a synchronized release of the protein of interest into the Golgi apparatus is achieved and its secretion can be monitored by analysis of the localization of the fluorescent tag in micrographs of fixed cells at the respective time points (Fig. 3.2.3A). Counting post-Golgi vesicles containing PSAP-mCherry RUSH in fixed cells revealed similar vesicle numbers across time points 20, 40 and 60 minutes post-biotin addition in HeLa and Cab45KO cells (Fig. 3.2.3B). However, this only represents the event after vesicular budding at defined time points. For a higher temporal

resolution and determination of the Golgi export of PSAP from the TGN, we combined RUSH of PSAP-mCherry with a co-expressed Golgi marker BFP-GalT1 in living cells (Fig. 3.2.3C).
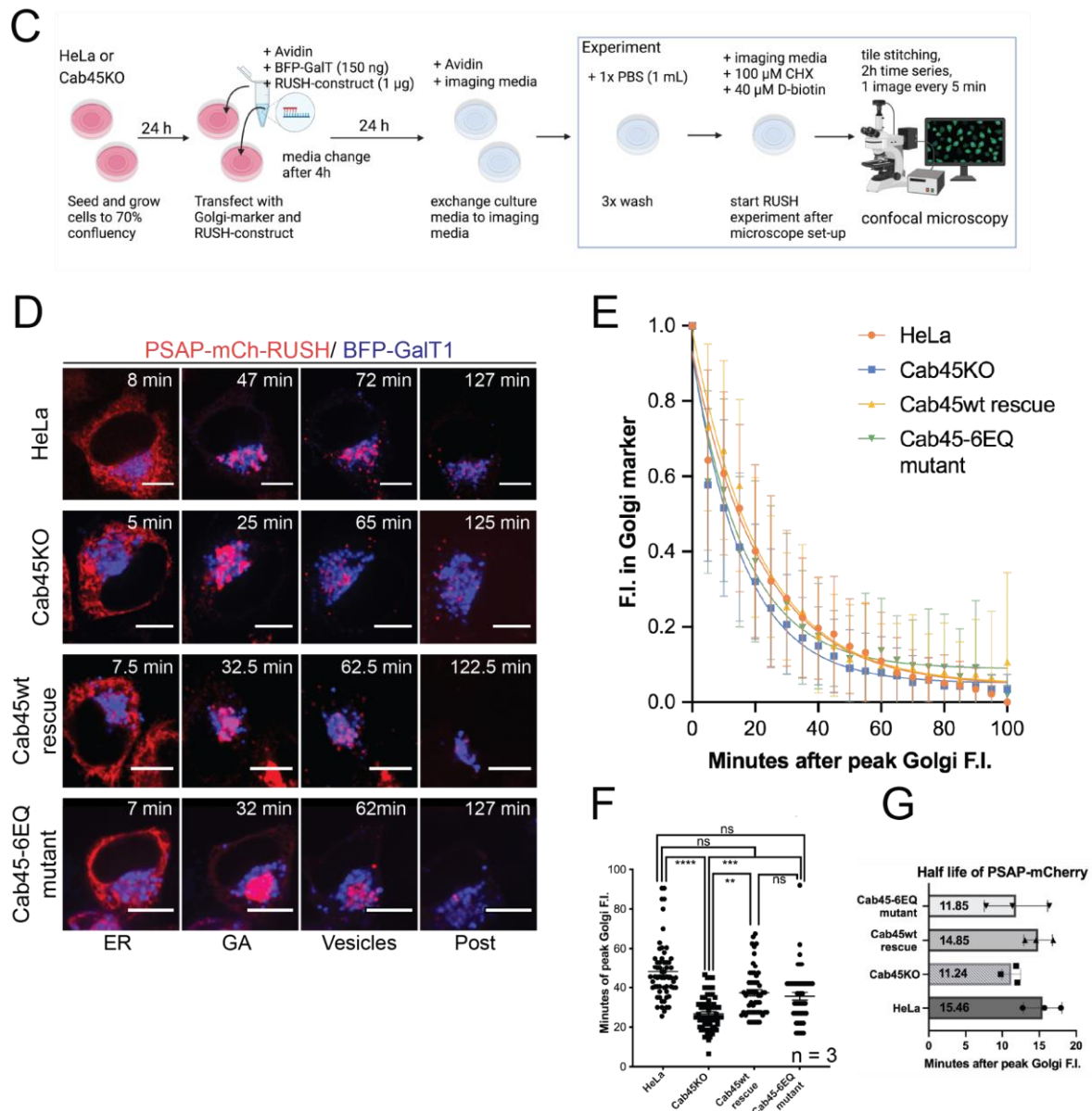
Fig. 3.2.3C-G: Studies of PSAP-mCherry RUSH trafficking in living cells. C. Overview of the workflow applied to investigate PSAP-mCherry export from the Golgi apparatus. In brief, cells grown on live-cell imaging glass dishes are transfected with PSAP-mCherry RUSH and Golgi marker BFP-GalT1 and prepared for imaging by replacing growth media to imaging media. With addition of biotin, images are taken after every 5 min for a total of 120 min in confocal microscopy. **D**. Micrographs are shown for PSAP-mCherry and BFP-GalT1 in HeLa, Cab45KO, Cab45wt-rescue and Cab45-6EQ mutant cells. Indicated time points represent when the PSAP-mCherry RUSH is located at the ER, reaches maximal fluorescence intensity in the Golgi apparatus, is present in budded post-Golgi vesicles and finally, the last frame after 120 min when the Golgi has been emptied of the RUSH cargo and the experiment is completed. **E**. Mean normalized fluorescence intensity (F.I.) of RUSH PSAP-mCherry in the Golgi marker (BFP-GalT1) region of interest (ROI) starting from t=0 when the maximal F.I. of PSAP-mCherry is detected in the ROI (peak Golgi F.I.). Graphs of HeLa (orange) compared to Cab45KO

(blue), Cab45wt-rescue (yellow), and Cab45-6EQ mutant (green) cells depict the decay of PSAP-mCherry F.I. and represent Golgi exit. Non-linear regression (exponential function) from three independent experiments of at least 50 cells was applied in the plot using GraphPad Prism9 built-in regression. **F**. Time points when maximal fluorescence intensity of PSAP-mCherry RUSH in the Golgi is reached are compared showing that for HeLa cells this occurs much later than Cab45KO (****) cells but are similar to those of Cab45wt-rescue and Cab45-6EQ mutant cells. Cab45KO cells indicate significantly earlier time points than those of Cab45wt-rescue (**) and Cab45-6EQ mutant (***), whose time points are not significantly different (Welch's test). Error bars show SEM. **G**. Comparison of half-life of cells in E, defined as the time when the decay of F.I. decreased to 50% of the peak F.I was calculated by using exponential curve analysis (one-phase decay) in GraphPad Prism9.

Micrographs of HeLa and Cab45KO cells show time points for localization in the ER, reaching the maximal F.I in GA, the beginning of vesicle budding at the TGN and the state of post-Golgi vesicles at the last time point of 120 min post release (Fig. 3.2.3D). The mean fluorescence intensity (F.I.) of RUSH PSAP-mCherry in the Golgi was recorded, utilizing the Golgi marker protein GalT to define the region of interest (Fig. 3.2.3D). Golgi export rates were obtained by measuring the decrease of F.I. of RUSH PSAP-mCherry within the area of BFP-GalT1. We plotted the Golgi F.I. at t=0, and observed a differential export rate of RUSH PSAP-mCherry in HeLa (orange) and Cab45KO (blue) cells (Fig. 3.2.3E). PSAP-mCherry Golgi exit from the GA is increased in Cab45KO compared to HeLa cells, demonstrated with a steeper exponential decay. To test if the increased Golgi exit of PSAP is specific to the loss of Cab45, we performed the assay with Cab45KO cells stably expressing Cab45wt (Fig. 3.2.3E, yellow). The exponential decay showed similarity to the results obtained from HeLa cells, indicating a successful rescue. For quantification we measured the half-life from three independent experiments (Fig. S3) as the time point when 50% of the maximal F.I of PSAP-mCherry was reached (Fig. 3.2.3G, left). The shortest half-life was obtained from Cab45KO (11.24 min), while HeLa and Cab45wt-rescue showed a similar longer half-life (HeLa: 15.46 min, Cab4wt rescue: 14.85 min). Since Cab45-dependent sorting depends on its Ca^{2+}-binding properties (Crevenna et al., 2016), we subsequently studied the Golgi exit of RUSH PSAP-mCherry in Cab45KO cells stably expressing a Ca^{2+}-binding deficient mutant of Cab45 (Cab45-6EQ, Crevenna et al., 2016) (Fig. 3.2.3E, F, G). The decay of the Golgi exit of RUSH PSAP-mCherry (Fig. 3.2.3E, green) for t<20 min with a half-life of 11.85 min is similar to those of Cab45KO cells. Interestingly, when comparing the time points when the peak Golgi F.I. of PSAP-mCherry is reached, Cab45KO cells show the earliest peak times, while the Cab45-6EQ mutant shows significant later time points similar to the Cab45wt-rescue (Fig. 3.2.3F). In HeLa cells the peak Golgi F.I. is reached latest and highly significantly different to Cab45KO but non-significant compared to Cab45wt-rescue and Cab45-6EQ mutant. The results of half-life calculations and peak time measurements indicate different processes involving Cab45 for accumulation in the Golgi prior to the exit from the Golgi.

Taking the previous secretion assay results with SORT1 and IGF2RKO cells into account, we propose that Cab45 influences trafficking of PSAP in a receptor-dependent manner. The results demonstrate a novel role of Cab45 in addition to its function to sort its specific clients (Crevenna et al., 2016, Deng et al., 2018).

3.3 Investigations on the role of Cab45 on lysosomal organization

Results from trafficking experiments showed an increase in Golgi export rate of PSAP which could be the cause for the hypersecretion phenotype identified in section 3.2. Hypersecretion of PSAP and PGRN - a result of missorting to the cellular surface - leads to lower levels of the mature forms of PSAP and PGRN in the lysosome. Ultimately, missing enzymes capable of hydrolysis of their substrates cause lysosomal storage diseases (Tayebi et al., 2020). Since missorting of PSAP and PGRN impairs lysosomal homeostasis (Evers et al., 2017; Ni et al., 2006, Tayebi et al., 2020), we hypothesized that Cab45 deficiency would also impair lysosomal homeostasis and investigated lysosomes in these cells.

3.3.1 Loss of Cab45 results in accumulation of lysosomes near the nucleus

LAMP1, a commonly used lysosome marker, shows spherical structures mostly spread throughout the cell (termed as peripheral) in multiple cell lines, including HeLa cells (Cheng et al., 2017).Surprisingly, when we examined LAMP1 localization in Cab45 siRNA treated cells, we observed lysosomes to be redistributed to the perinuclear region, although their size and structure was similar to those in HeLa cells. To quantify this lysosomal distribution phenotype, we manually selected the area covered by LAMP1- positive lysosomes, using the most peripheral to the nucleus as the region of interest boundary and expressed the area covered by lysosomes as a percentage of the whole cell area. The mean area covered by lysosomes in Cab45KO is significantly decreased compared to that in HeLa cells (Fig. 3.1.6B, 33.37% and 52.43%, respectively). Next, we studied if the change of lysosomal organization is specific to the loss of Cab45. We used LAMP1 antibody staining and calculated the mean area coverage of LAMP1 area in Cab45wt cells (Figure 3.1.6D).
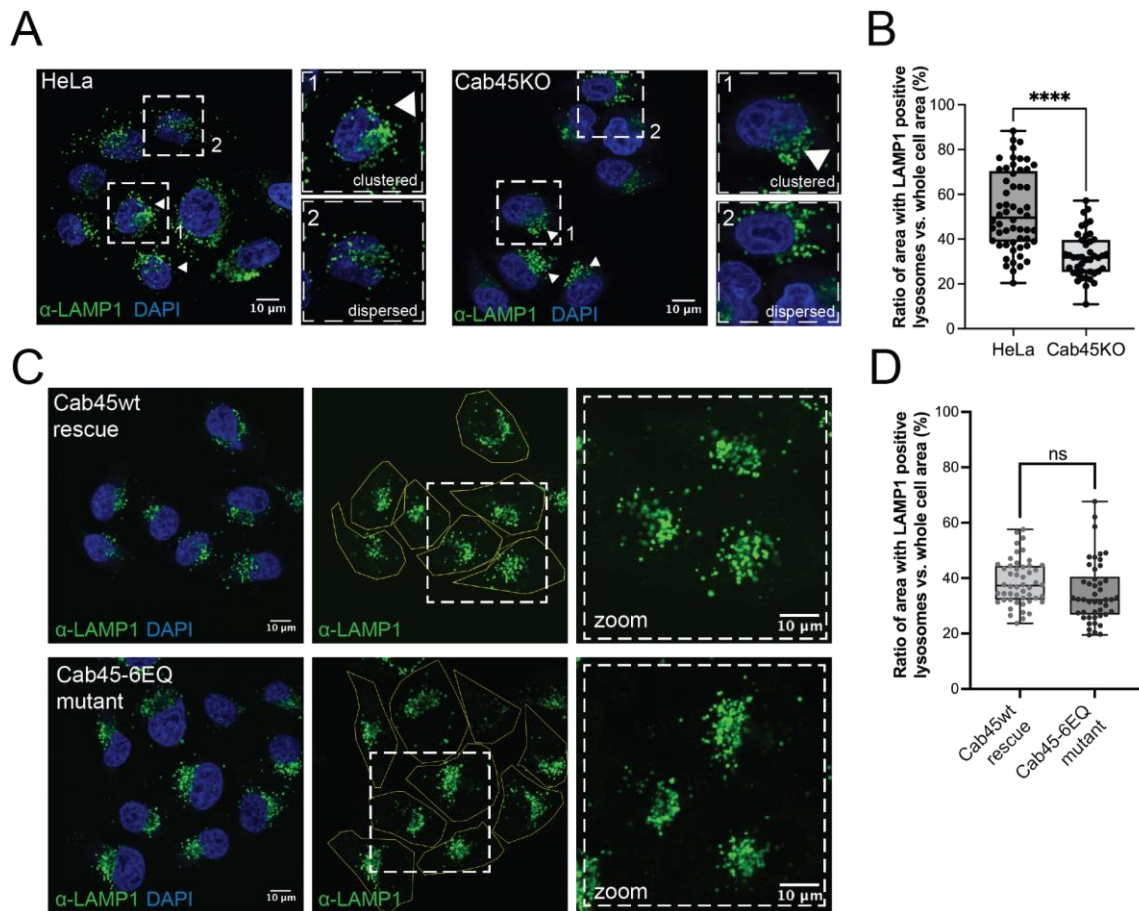
Fig. 3.3.1: Lysosomal organization in dependence of Cab45 expression using immunofluorescence with LAMP1 antibody. A. The phenotypes of LAMP1-positive lysosomes are represented as clustered (perinuclear) and dispersed (peripheral) localization in HeLa and Cab45KO cells. The ratio of area covered by lysosomes is quantified for at least 42 cells in HeLa and Cab45KO in **B** by dividing area covered by LAMP1-positive structures by area of the whole cell. The box plot demonstrates a higher number of cells with dispersed LAMP1 localization, depicted as significantly higher (****) mean area coverage of 52.43% in HeLa compared to Cab45KO with 33.37%. **C**. Representative confocal images depicting lysosomal localization in cells re-expressing Cab45wt, or Cab45-6EQ Ca^{2+}-binding mutant using LAMP1 antibody. Structure, size and localization of LAMP1-positive lysosomes appear similar between Cab45wt and Cab45-6EQ mutant cells, which is verified in quantification **D** of mean area coverage of LAMP1 structures in at least 46 cells as not significantly different.

Re-expression of Cab45 resulted in an increase of area coverage, demonstrating a rescue of the phenotype from perinuclear to peripheral lysosomes. To investigate the importance of Ca^{2+} for this effect, we analyzed the lysosome localization in Cab45-Ca^{2+}-binding mutant (Cab45-6EQ) cells as well. Both, the Cab45-6EQ and Cab45wt showed a similar perinuclear LAMP1-localization and area coverage of LAMP1-positive lysosomes (Fig. 3.3.1C, D; 34.82 % and 38.49 %, respectively). Since lysosome-covered areas of HeLa cells cover a large distribution (26.7 - 88.3%), statistics could have a low accuracy in representing the changes in lysosome positioning. The rescue is not completely

restoring the phenotype of spread lysosomes; however, the tendency is clearly showing more cells with peripheral lysosomes in cells expressing Cab45wt - similar to HeLa. Expression of the Ca^{2+}-binding mutant of Cab45 increases the number of cells with larger lysosomal area coverage slightly, but more similar to those in Cab45KO. Therefore, while Ca^{2+}-dependence is indicated, additional experiments to determine the influence of calcium have to be performed to verify this hypothesis.

3.3.2 Colocalization of PSAP and LAMP1-positive lysosomes is slightly affected by lysosomal organization

After observing the accumulation of lysosomes near the nucleus in Cab45KO cells, we asked whether the localization of lysosomal hydrolases is altered as well, in particular for PSAP. Immunofluorescence imaging with PSAP antibodies in Cab45KO, Cab45-6Q mutant and Cab45wt cells reveals a more perinuclear distribution of PSAP localization compared to HeLa cells.
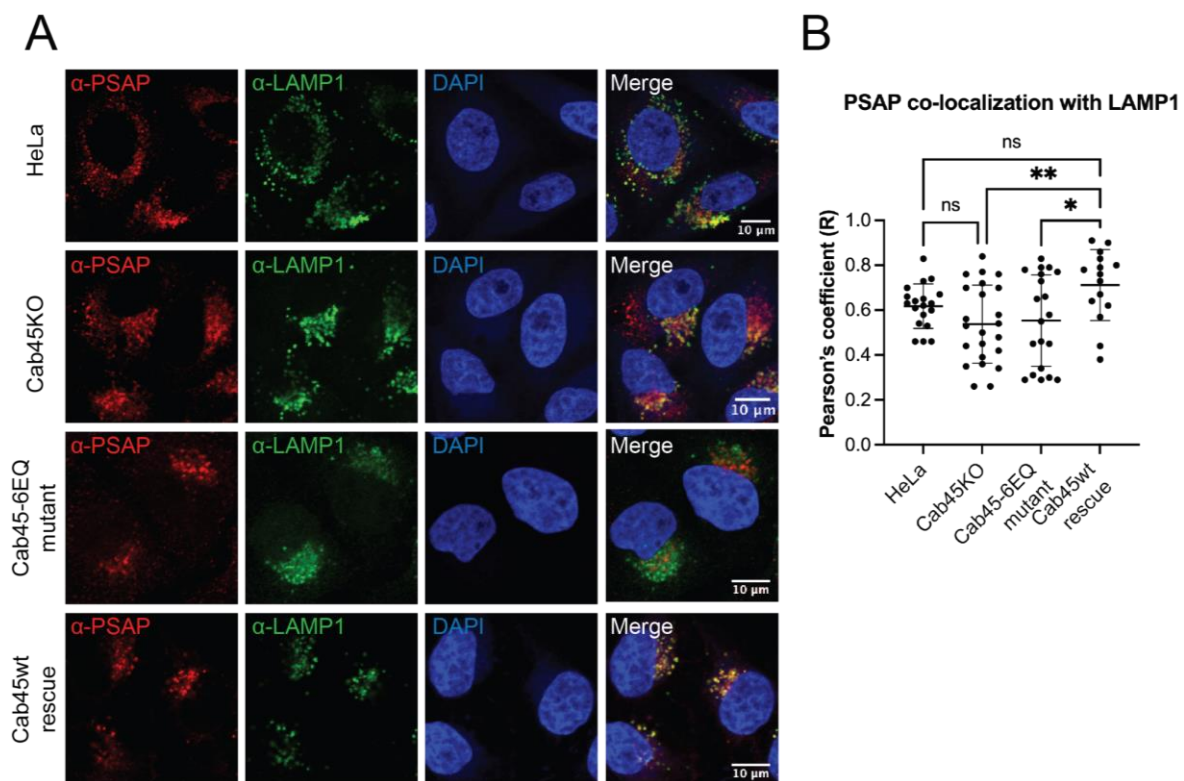
Fig 3.3.2: Colocalization of PSAP and LAMP1-positive lysosomes in dependence of Cab45. A. LAMP1- and PSAP antibodies in HeLa, Cab45KO, Cab45-6EQ mutant and Cab45wt-rescue show differences in overlapping fluorescence signal, which are further quantified in **B.** Pearson's correlation (Fiji plugin Coloc2) was applied to indicate the quantity of colocalization via Pearson's coefficient R, which shows complete colocalization for R = 1, no colocalization for R = 0 and perfect anti-colocalization for R = -1. Coefficients for

at least 20 cells of HeLa, Cab45KO, Cab45-6EQ and Cab45wt are shown in scatter plot B with error bars representing SD. Cab45wt-rescue and HeLa cells showed highest colocalization between PSAP and LAMP1, while loss of Cab45 in Cab45KO or dysfunctional Cab45 in Cab45-6EQ resulted in decrease of colocalization. Statistical significance is not achieved for the difference between HeLa and Cab45KO or Cab45-6EQ mutant, however for Cab45wt-rescue compared to Cab45KO and Cab45-6EQ mutant. Statistical analyses were performed using Welch's test in GraphPad Prism 9.

To assess if the change in PSAP localization is dependent on LAMP1-positive lysosomes, we co-stained and analyzed the signal overlap by Pearson's coefficient R (Coloc2 in Fiji), which would demonstrate a perfect co-localization with R=1. Despite both the PSAP and also the LAMP1 signal being accumulated in Cab45KO cells, the overlap is lowest, similar to the Cab45-6EQ Ca^{2+}-binding mutant. HeLa and Cab45wt cells show a stronger co-localization on average, with the rescued cells being highest and significantly different to cells expressing no or Ca^{2+}-binding deficient Cab45. Since the expression of the Ca^{2+}-binding mutant of Cab45 appears to have a similar impact on the colocalization of PSAP in LAMP1-positive cells which is significantly lower compared to that of the Cab45wt-rescue cells, the phenotype could underlie Ca^{2+}-dependence. Although the colocalization of PSAP and LAMP1 in HeLa is not statistically significantly decreased in Cab45KO or Cab45-6EQ mutant, the trend is obvious and supports the hypothesis that a loss of Cab45 leads to missorting of PSAP.

All in all, the results in this first part of my thesis demonstrate a new role for Cab45 as regulator of lysosomal positioning and trafficking of lysosomal hydrolases towards the endolysosomal system. The influence of Cab45 depletion caused a) hypersecretion of PSAP and PGRN, b) an increased rate of the Golgi exit of PSAP and c) accumulated perinuclear positioning of lysosomes with lower colocalization with PSAP.

Part B - TGN46 influences the sorting of Cab45-dependent clients into sphingomyelin-rich vesicles

In the previous section the function of Cab45 was extended to include the sorting of lysosomal hydrolases in a receptor-dependent manner. Cab45 was initially proposed to be a Ca^{2+}-dependent receptor-independent sorter of secretory soluble cargo in SM-rich vesicles (von Blume et al., 2012; Crevenna et al., 2016; Deng et al., 2018; Hecht et al., 2020). Recent studies have advanced the understanding of how Cab45 interacts with its cargo and is sorted into specific uncoated vesicles; however, the molecular components involved and how they contribute to vesicle formation is still unknown. In this section, the participation of TGN46, a TGN-resident type I membrane protein, in the trafficking events in Cab45-dependent sorting is examined.

3.4 Identification of TGN46 as potential player in Cab45-dependent sorting of secretory clients

Based on the premise that potential interactors of Cab45, which comprises clients as well as participants of the Cab45-dependent sorting mechanism, are proteins which are localized in proximity to Cab45, proximity-based labelling with immunoprecipitation was applied. First, the BioID method (Roux et al., 2012, Kim et al., 2014) where the biotin ligase BirA is fused to the protein of interest to biotinylate vicinal proteins was used (Kim et al., 2014). Cells stably expressing BirA-Cab45 were incubated for 3h, 6h or 22h with biotin and labelled proteins enriched on streptavidin beads. Western blotting demonstrates an increase of protein levels detected by TGN46 antibody in input samples (I) and immunoprecipitation samples (IP) with increasing biotin incubation time (Fig. 3.4). For longer incubation (6h, 22h) TGN46 is not detected in BirA-Cab45 cells incubated without biotin or Cab45KO cells with biotin, while for short incubation time (3h) a faint band is visible in BirA-Cab45 cells without biotin (Fig. 3.4), indicating inconsistency or transient interconnection between TGN46 and Cab45. Further experiments were performed by using 3-6h biotin incubation and analysis of immunoprecipitation (IP) by MS for increased sensitivity compared to immunoblotting (data not shown). However, no peptides of TGN46 were found in any sample. As a result of the variabilities when utilizing the BioID method, it was concluded that these data and techniques were unsuitable for further studies. Fortuitously, these data showing a role for TGN46 in the Cab45-dependent sorting of its clients, was independently verified using an APEX-proximity labelling methodology by Burd and colleagues (Deng et al., 2018), who found Cab45, LyzC and TGN46 to be specifically enriched in sphingomyelin (SM)-rich vesicles marked by equinatoxin (EQ) sphingomyelin (SM), an exogenous SM-binding probe.
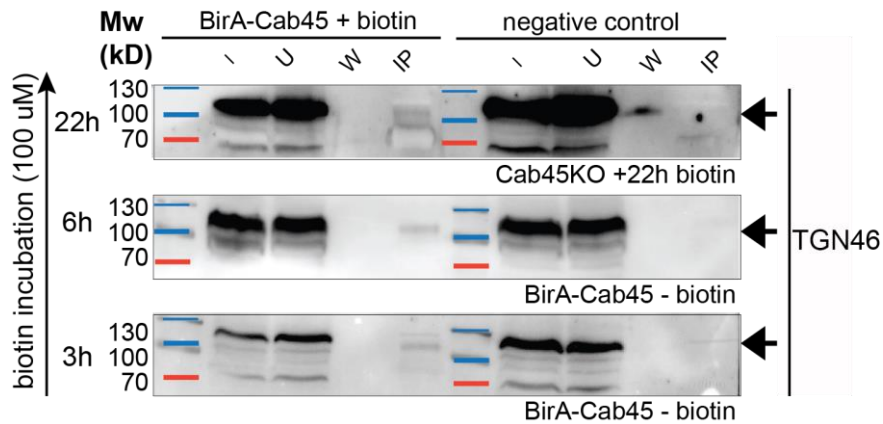
Fig. 3.4: BioID time course with BirA-Cab45 indicates connection to TGN46. Proximity labelling using biotin ligase BirA fused to Cab45 was performed with 100 µM biotin for 3h, 6h or 22h and cell lysates analyzed via immunoblotting. Input samples (I) show increased TGN46 levels with increased biotin incubation time. Unbound (U) and samples after first wash (W) are analyzed for quality control. In immunoprecipitation (IP) samples higher levels of TGN46 are detected with increasing biotin incubation time. Negative controls are analyzed simultaneously on western blot and show no (6h, 22h) or a faint detection of TGN46 (3h) in cell lysates of Cab45KO with biotin or BirA-Cab45 without biotin treatment.

3.4.1 TGN46 depletion influences the secretion of Cab45

TGN46 is commonly used as a TGN marker, since the transmembrane protein spans the TGN membrane (Luzio et al., 1990). Based on the identification of Cab45, LyzC and TGN46 in SM-rich vesicles (Deng et al., 2018), I hypothesized that TGN46 could serve as an interaction point between the Cab45-client-complex and the TGN membrane, possibly holding the complex prior to vesicular budding. Depletion of TGN46 could thus result in less stalling of Cab45-client-complexes prior to specific vesicle formation, possibly leading to increased secretion of Cab45 and clients from the TGN. Indeed, western blot analysis (Fig.3.41A) shows efficient TGN46 depletion in TGN46 siRNA treated HeLa compared to those treated with control siRNA, accompanied by a slight decrease in Cab45 levels in TGN46 depleted cells. To test if the observed decrease in Cab45 level in TGN46 siRNA treated cells is potentiated with controlled secretion, I performed a secretion assay with 2h block at 20°C to accumulate Cab45 in the Golgi before a synchronized release for 1h at 37C in control and TGN46 siRNA treated cells in the presence of cycloheximide (CHX). During the blocking stage, no Cab45 signal was detected in supernatant samples, demonstrating addition of CHX to the media effectively inhibits new synthesis of protein. Release at 37°C lowered Cab45 levels in cell lysates, with a concomitant increase in Cab45 levels in the supernatant. The abundance of Cab45 in TGN46 siRNA treated cell supernatants compared to those from control siRNA treated cells is observed with higher intensity protein bands in western blot (Fig. 3.4.2B). Notably, Cab45 levels in cell lysates of TGN46 depleted cells appear higher as well. Quantification, normalized to β-actin levels, show a smaller increase of Cab45 in cell lysates after TGN46 depletion compared to control cells, than the

increase of Cab45 in supernatants of cells depleted of TGN46. However, differences are not significant in Welch's test.

Next, the relationship between increased secretion of Cab45 and the depletion of TGN46 was examined by observing the trafficking of Cab45 client RUSH assay with LyzC-SBP-eGFP in control siRNA versus TGN46 siRNA treated cells (Fig. 3.4.1C).
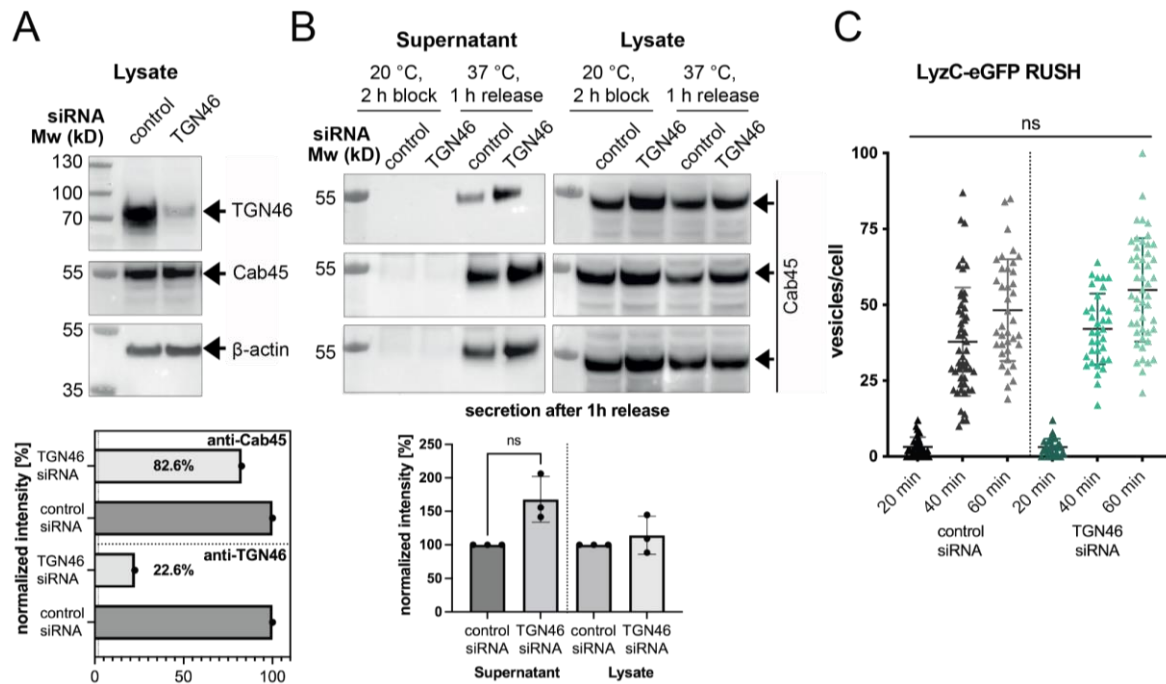
Fig. 3.4.1: Influence of depletion of TGN46 on Cab45 secretion and client trafficking. A. TGN46 siRNA effectively reduces levels of TGN46 in HeLa cells compared to control siRNA represented in western blotting. The quantification below shows a reduction to 22.6% in TGN46 siRNA treated cells, along with a slight decrease of Cab45 levels to 82.6% compared to levels in control siRNA treated cells. **B**. Secretion assay with 20°C block (2h) and 37°C release (1h) for supernatants and lysates of TGN46 siRNA treated cells compared to control cells under presence of CHX. With block at 20°C, proteins are accumulated at the Golgi and no Cab45 signal is detected in the supernatant. Synchronized release by temperature shift to 37°C leads to secretion of Cab45 in the supernatant, with Cab45 levels in TGN46 depleted cells appearing with higher intensity compared to those in control cells. Western blot signals of Cab45 show a slightly stronger intensity in lysates of TGN46 siRNA versus control siRNA treated cells. Quantification represents no significant difference in both supernatants and lysates after treatment with control or TGN46 siRNA. **C**. LyzC-eGFP RUSH in control and TGN46 depleted cells after 20, 40 and 60 min of biotin incubation analyzed via vesicle counting assay in fixed cells (Deng et al., 2018). No significant difference is observed for 20-, 40- and 60-min post biotin addition in control compared to TGN46 siRNA treated cells. Statistical analysis (Kruskal-Wallis test) was performed with GraphPad Prism 7, error bars showing SD.

The RUSH assay with LyzC-eGFP is well established and published in studies investigating LyzC-SBP-eGFP trafficking in regard to loss of Cab45 or its Ca^{2+}-binding ability of Cab45, as well as loss and mutation of the kinase Fam20C, that influences the phosphorylation state of Cab45 and therefore the binding to Cab45's clients (Deng et al., 2018, Hecht et al., 2020; Pakdel et al., 2021; Pacheco-Fernandez et al., 2021). Here, HeLa cells were treated with control or TGN46 siRNA and the trafficking of LyzC-eGFP monitored at 20-, 40- and 60-min post biotin addition in fixed cell confocal imaging (Fig. 3.4.1C). The number of post-Golgi vesicles increases with longer biotin incubation, as more vesicles bud from the TGN, although with a large spread of vesicle numbers between individual cells, likely influenced by the heterogeneity of siRNA treatment of HeLa cells. A similar post-Golgi vesicle number in control siRNA and TGN46 siRNA treated cells was observed for the respective timepoints, with TGN46 siRNA treated cells experiencing a slight tendency for increased vesicle numbers throughout the experiments.

Although the secretion of Cab45 was increased with depletion of TGN46, the overall level of Cab45 in the cell lysate was not decreased after release of Cab45 at 37°C, leading to the assumption that the higher secretion could be due to higher expression of Cab45 levels in TGN46 depleted cells (Fig. 3.4.1B). Despite, the increased levels of Cab45 secretion in TGN46 siRNA treated cells, Cab45-dependent trafficking was unaffected, as evidenced by the non-significant changes to the number of post-Golgi vesicles when following the trafficking of Cab45 RUSH client LyzC.

3.4.2 Depletion of TGN46 influences the correct sorting of Cab45 client LyzC into EQSM-rich vesicles.
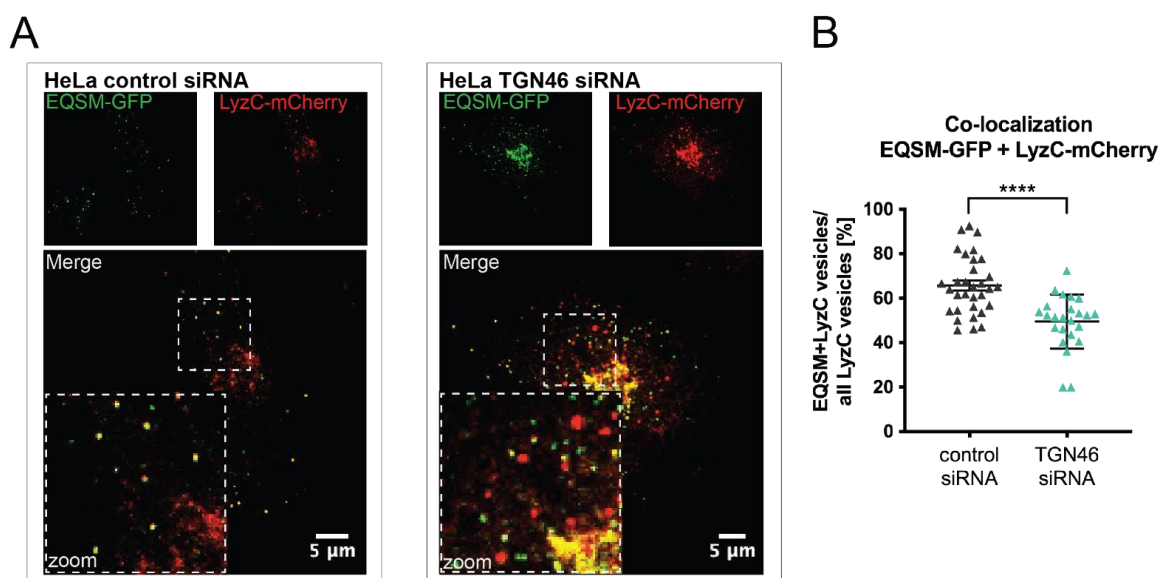
Fig. 3.4.2: Colocalization of EQSM-GFP and LyzC-mCherry in HeLa treated with control and TGN46 siRNA. A. Representative confocal image showing more vesicles positive for EQSM-GFP and LyzC-mCherry

in control compared to TGN46 siRNA treated cells. Box with dashed stroke indicates the area shown in zoom. **B**. Quantification of the portion of vesicles positive for both EQSM-GFP and LyzC-mCherry to all LyzC-mCherry positive vesicles in control and TGN46 depleted cells (32 and 24 cells, respectively). Statistical analysis (Kruskal-Wallis test) shows highly significant (****) decreased portion of colocalized vesicles with depletion of TGN46. Error bars represent SD.

The collaboration with Burd and colleagues (Deng et al., 2018) revealed that Cab45-cargo-complexes are budding from the TGN in SM-rich vesicles. They used a natural SM-binding protein, equinatoxin II (EQ) as non-toxic SM reporter protein. Evaluating the results in 3.4.1, it was considered whether TGN46 depletion leads to an influence on the sorting of Cab45-cargo complexes into SM-rich vesicles, rather than the post-Golgi vesicle number and overall secretion *per se*. To answer this question, I co-expressed EQSM-GFP and LyzC-mCherry in HeLa cells after treatment with control siRNA or TGN46 siRNA and analyzed their localization. In control cells EQSM-GFP and LyzC-mCherry colocalize more often in vesicular structures than in cells depleted of TGN46, where more individual EQSM-GFP or LyzC-mCherry punctae are observed (Fig.3.4.2A). Quantification was performed by dividing the number of colocalized vesicles by the total number of LyzC vesicles and verified that a higher number of control cells contain vesicles that are doubly positive for EQSM-GFP and LyzC-mCherry. This demonstrates that the depletion of TGN46 does not change the number of post-Golgi LyzC-GFP vesicles observed in the RUSH assay but influences the correct sorting into SM-rich vesicles.

3.4.3 Cab45 trafficking is slowed down with loss of TGN46

Since TGN46 depletion causes missorting of Cab45's client LyzC, but does not change the number of post-Golgi vesicles, the next step was to test LyzC trafficking in cells with loss of TGN46. LyzC-SBP-eGFP was expressed in TGN46KO and wild-type HeLa cells and the trafficking monitored as described previously.
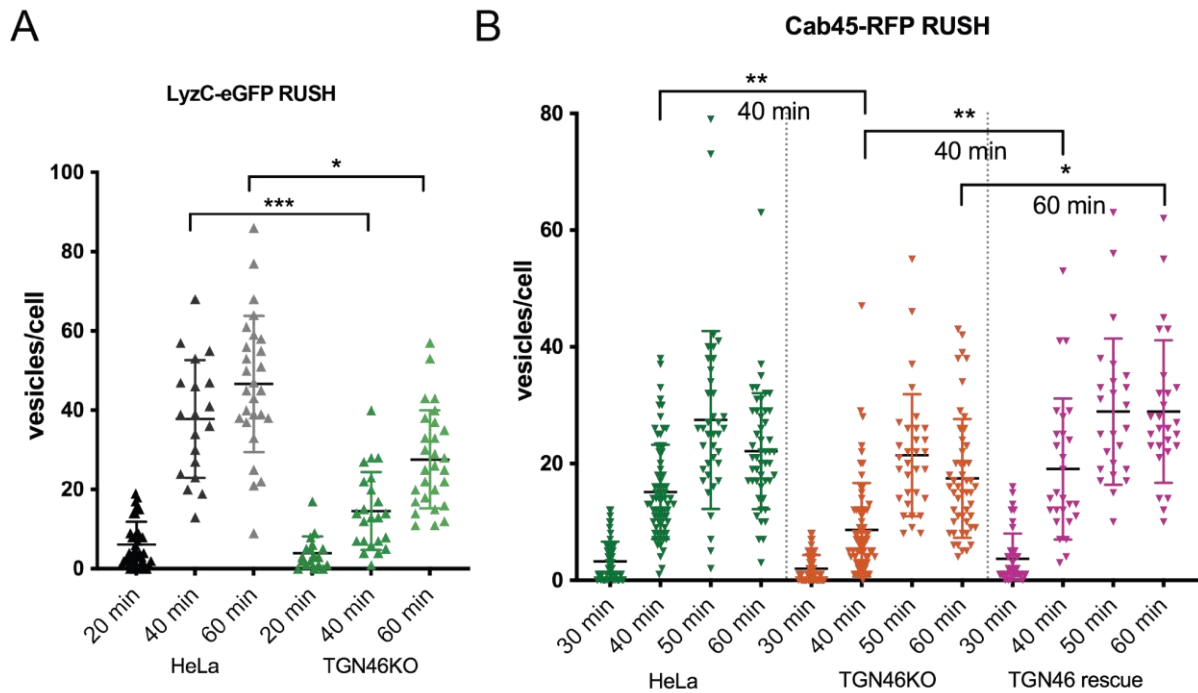
Fig.3.4.3: Loss of TGN46 slows trafficking of Cab45 and clients. A. RUSH assay with LyzC-eGFP in HeLa compared to TGN46KO cells for time points 20, 40 and 60 min. Quantification shows the number of vesicles per cell with higher values for HeLa cells than those in TGN46KO. 40 min and 60 min after biotin addition TGN46KO cells have significantly (***, *, respectively) lower number of vesicles. **B**. RUSH assay with Cab45-RFP in HeLa (green) compared to TGN46KO (orange) and TGN46 rescue (magenta) cells after 30, 40, 50 and 60 min after biotin addition. Quantification demonstrates vesicles/cell 40 post biotin addition to be significantly (**) lowest in TGN46KO, similar between HeLa and TGN46 rescue. Vesicle numbers 60 min post biotin addition in TGN46 rescue cells are significantly (*) increased compared to TGN46KO cells, but similar to those in HeLa. Statistical analysis with Kruskal-Wallis test was performed with GraphPad Prism7. Error bars show SD.

While the LyzC-SBP-eGFP RUSH assay showed no differences in the number of post-Golgi vesicles in HeLa cells treated with control or TGN46 siRNA (Fig. 3.4.1C), the same RUSH assay comparing wild-type and TGN46KO HeLa cells shows a significantly lower number of vesicles per cell (Fig. 3.4.3A). The strongest decrease (***) is observed 40 min of post-biotin addition in the TGN46KO cells, whereas 60 min post-biotin addition depicts a smaller decrease (*) of vesicles/cell between HeLa and TGN46KO cells. Since the timepoint at which the differences between wild-type and TGN46KO are most significant is at 40 min post-biotin addition, it seems likely that TGN46 is influencing events that happen within this timeframe. Usually, the formation of vesicles from the TGN starts around 40 minutes after biotin addition, demonstrating that TGN46 might play a role in the recognition of Cab45-client-complexes prior to vesicle budding. Loss of TGN46 slows the process of LyzC packaging into vesicles, the formation of vesicles or the budding from the TGN. To investigate if Cab45 trafficking is influenced in a similar way by TGN46 loss, Cab45-RFP was

expressed in HeLa and TGN46KO and the RUSH experiment performed as described before. Indeed, the loss of TGN46 leads to a decrease of the number of vesicles in general, with the strongest difference after 40 min of biotin addition (**) (Fig. 3.4.3B). Re-expression of TGN46 depicts an increase of vesicle numbers to a level similar to those in HeLa. The differences in vesicle numbers at 40 min post-biotin addition are significantly higher (**) than those in TGN46KO as well. After 60 min of biotin addition of cells re-expressing TGN46 the rescue effect leads to slightly higher vesicle numbers compared to HeLa, leading to a significant difference (*) when compared to TGN46KO.

The results in the second part of the thesis, reflect the complex influence of TGN46 on Cab45-dependent sorting with unexpected differences between Cab45 trafficking in cells with depleted TGN46 or complete loss of TGN46. The nature of TGN46 as transmembrane protein of the TGN as well as post-Golgi events like recycling of TGN46 or Cab45 after release of the client are further discussed in frame of a possible transient and indirect interaction between Cab45 and TGN46.

4 Discussion

Part A - A new role of Cab45 in lysosomal trafficking and positioning

Sorting of LyzC, COMP, MGP (matrix gla protein) and TSP-1 (thrombospondin 1) is mediated by Cab45 (Ramazanov et al., 2021), in a Ca^{2+}-dependent manner (von Blume et al., 2011, 2012; Kienzle et al., 2014, Crevenna et al., 2016; Hecht et al., 2020) in SM-rich transport vesicles (Deng et al., 2018).

Those clients of Cab45 are not structurally or functionally related to each other, yet they are missorted during Cab45 depletion - a puzzling result which led to the suggestion that Cab45 might not sort a distinct subset of proteins, but could serve as a general sorter of soluble secretory proteins. The findings in part A of this thesis indicate an additional, surprising, participation of Cab45 in the sorting and/ or trafficking of lysosomal hydrolases, PSAP, PGRN and CatD, as well as the positioning of lysosomes.

4.1 Lysosomal hydrolases are hypersecreted in Cab45 depleted cells

Since Cab45 influences sorting and secretion of soluble secretory proteins, secretion assays have been performed in previous studies successfully to reveal LyzC and COMP as Cab45 clients (von Blume et al., 2011), which were not secreted upon Cab45 depletion, but accumulated in the TGN. In those assays 2h of incubation in serum-free media was sufficient to detect LyzC and COMP via western blotting in the supernatant - with stark decrease compared to normal secretion in control cells (von Blume et al., 2009; 2011). Here, the time of secretion was much longer to compensate for the weak detection of lysosomal hydrolases PSAP and PGRN via western blotting. 24h incubation with serum-free media was necessary to detect the protein in supernatants and maintain comparability to hiSPECS results in experimental procedure. The fold change of up to 5 (PSAP) observed in hiSPECS with subsequent MS analysis could not be achieved by western blotting (fold change 1.3 for PSAP). Modest differences between amounts of protein detected in supernatants of control cells versus Cab45 KD cells could be results of long secretion times and higher sensitivity of MS compared to western blotting. Secretion assays are usually performed for shorter periods of time for higher visibility of differences between conditions. However, a significant hypersecretion of PSAP (both intracellular 68 kDa and extracellular 72 kDa form) could be observed as well as a tendency for increased levels of PGRN (immature form without full glycosylation 65 kDa) and CatD (intermediate 48 kDa and inactive 52 kDa form) in supernatants of Cab45 depleted cells compared to control cell supernatants. Interestingly, former studies already hinted at CatD as target for Cab45-dependent sorting, although

being contrary to how the trafficking of direct interaction partners - clients - LyzC and COMP was influenced by KD of Cab45 or other essential proteins in this sorting mechanism, like SPCA1 and its activators. In yeast (Curwin et al., 2012) as well as mammalian cells (von Blume 2011; 2012; Kienzle et al., 2014), the influence of silencing of SPCA1 (yeast orthologue: pmr1) and activators cofilin/ADF (yeast orthologue: cofl1) on protein secretion was observed. The Cab45 clients LyzC and COMP were not detected in supernatants, but CatD and carboxypeptidase Y (another vacuolar hydrolase) showed hypersecretion upon SPCA1 (pmr1) and ADF/cofilin (as a temperature sensitive mutant of cofl1) deletion (Okreglak and Drubin, 2007; von Blume et al., 2012; 2011; 2009; Curwin et al., 2012; Crevenna et al., 2016), which is similar to the results from secretion assays with Cab45 and control siRNA.

Because the sorting and trafficking of lysosomal hydrolases is based for the majority on mannose-6-phosphate-dependent mechanisms (Saftig and Klumperman, 2009; Bonifacino and Traub, 2003) lysosomal hydrolases were not studied in detail in frame of Cab45-dependent sorting, although CatD and carboxypeptidase Y were hypersecreted in their intermediate forms in SPCA1/cofilin depletion mutants (von Blume et al., 2011; 2012; Curwin et al., 2012). The secretome analysis presented in this thesis is the first experiment from which a direct conclusion can be drawn from the influence of Cab45 depletion on lysosomal hydrolases, instead of other components in the Cab45-dependent mechanism.

4.2 Deletion of lysosomal receptors lead to secretion of lysosomal hydrolases

The sorting of lysosomal hydrolases is well described to involve receptors that sort them into clathrin coated vesicles (CCV) to endosomes and finally lysosomes (Saftig and Klumperman, 2009). Among those receptors are cation-dependent (CD) and -independent (CI) mannose-6-phosphate receptors (M6PR) and sortilin (SORT1) (Kornfeld and Melman, 1989; Saftig and Klumperman, 2009). The studies on PSAP, PGRN and CatD secretion focused on the CI-M6PR, referred to as IGF2R (Hasilik et al., 2008; Guo et al., 2014), and SORT1. CI-M6PR is the more effective sorter of M6P-tagged proteins, such as PSAP and CatD (Kornfeld and Melman, 1989; Ni et al., 2006, Tayebi et al., 2020), while SORT1 is associated with M6P-independent sorting of CatD (Canuel et al., 2008) and PSAP (Lefrancois et al., 2003; Hassan et al., 2004; Coutinho et al., 2012) as well as main receptor of PGRN (Zheng et al., 2011; Tayebi et al., 2020). In section 3.2.1, I investigated the secretion of lysosomal hydrolases in cells deficient of IGF2R or SORT1 or both of these receptors. The steady state secretion in receptor KO cell supernatants was slightly elevated compared to those in HeLa, which is as expected since the depletion of receptors is known to cause secretion of lysosomal hydrolases (Qian et al., 2008; Guo et al., 2014). As described above the amount of PSAP in IGF2RKO, SORT1KO as well as their double KO cell supernatants is increased, although not significantly, but indicates the

compensation of the lost pathways by other receptors. LRP1, a receptor enabling PSAP uptake from the extracellular spaces, is therefore a promising candidate for further extending our studies (Hiesberger et al., 1998).

PGRN and CatD are both hypersecreted in SORT1KO cell supernatant (as seen in statistical analysis), which is expected since both can rely on SORT as a receptor for transport to the lysosome. In SORT1KO cells, other receptor pathways can compensate for the loss of SORT1, however, since PSAP serves as adaptor for PGRN's sortilin-independent trafficking, the hypersecretion of PSAP could slim the amount of intracellular PSAP for interaction with PGRN. On the other hand, secretion of PGRN can impact PSAP's ability to be sorted via SORT1 in IGF2RKO cells, since PGRN is shown to be the adaptor between PSAP and sortilin (Zhou et al., 2017a, b). Earlier studies have shown that PSAP is recognized by sortilin (Lefrancois et al., 2003, Hassan et al., 2004), implying a PGRN independent sortilin-mediated recognition of PSAP.

4.2.1 Depletion of Cab45 in IGF2 receptor deleted cells increase hypersecretion of PSAP

The additional depletion of Cab45 in IGF2KO cells led to significant hypersecretion of PSAP and PGRN in cell supernatants, which indicates that Cab45 participates in the sorting events of lysosomal hydrolases, especially in CI-M6PR independent sorting. In cells deleted of IGF2 other receptors compensate and re-route hydrolases usually sorted by IGF2 (Kornfeld and Melman, 1989). CD-M6PR can partially compensate by sorting M6P-tagged proteins, however, with lower efficiency (Kornfeld and Melman, 1989). Sortilin mediates both, PSAP and PGRN sorting (Lefrancois et al., 2003; Hu et al., 2010) and is not affected by IGF2R deletion. Since the treatment with Cab45 siRNA induces hypersecretion, the recognition of these lysosomal hydrolases is impaired by Cab45 via the following possibilities: (1) Cab45 supports the interaction between sortilin and PSAP or PGRN, and the depletion leads to decrease in recognition efficiency, (2) Cab45 impairs the trafficking/recycling of sortilin receptor leading to less receptor in the TGN that can bind PSAP or PGRN, (3) Cab45 influences other lysosomal receptors in their recognition or recycling. Since similar experiments with SORT1KO and the IGF2R/SORT1 double KO did not lead to significant hypersecretion upon Cab45 depletion, the likelihood of receptors other than IGF2R/SORT1 is lower, although still possible. If Cab45 depletion would target mainly another receptor, the effect of Cab45 siRNA treatment in IGF2RKO, SORT1KO and the double KO would be similar. Slight variations in the secretion of PSAP and PGRN in SORT1KO and double KO however indicates that a combination of receptors could be influenced by Cab45, leading to the possibility that not Cab45 itself, but it's properties might play the role in lysosomal hydrolase sorting. One of these properties involves it's Ca^{2+}-binding ability, which is crucial for binding of its clients after oligomerization (Crevenna et al., 2016; Deng et al., 2018). However, lysosomal proteins are not sorted via Cab45, as CatD did not immunoprecipitate with Cab45 (Kienzle et al., 2014; Crevenna et al., 2016) similar to PSAP (data not shown). The

interaction between CI-M6PR or sortilin and their ligands are also not dependent on Ca^{2+} (Saftig and Klumperman, 2009; Botta et al., 2009). Only recognition by CD-M6PR is influenced by divalent metal ions, but the receptor prefers Mn^{2+} for enhancing binding efficiency to M6P-tagged proteins (Sun et al., 2005).

4.2.2 Sortilin and IGF2 receptor expression on the cell surface is independent of Cab45

Secretion of lysosomal hydrolases happens under normal conditions on a very low level, which can be compensated by endocytosis as well (Kornfeld and Melman, 1989). In case of dysfunctional M6PR the secretion of lysosomal hydrolases is high and cannot be compensated completely by endocytic events which therefore leads to pathologies resulting in LSDs (Qian et al., 2008; Guo et al., 2014). Receptors that can bind exogenous hydrolases on the PM and bring them back to the lysosomes are CI-M6PR (Gary-bobo et al., 2007; Hasilik 2008), SORT (Hu et al., 2010) and LRP1 (Hiesberger et al., 1998; Potere et al., 2019). As IGF2RKO cells showed hypersecretion of PSAP during Cab45 siRNA treatment, the surface expression was analyzed (see 3.2.2) to check if Cab45 influences the recycling of the receptors from lysosomes to the PM. The levels of sortilin and IGF2 receptors on the cell surface were unchanged upon pulldown of surface biotinylated proteins in HeLa compared to Cab45KO cells. This indicates that Cab45 does not primarily interfere with the presence of receptor proteins on the cell surface.

4.3 Combination of live-cell imaging and RUSH to determine TGN export rates

Sorting of secretory proteins occurs in the trans-Golgi network (Klumperman 2011; De Matteis and Luini 2008; Kienzle and von Blume, 2014), before trafficking from the Golgi to the plasma membrane. With the introduction of the RUSH assay (Boncompain et al., 2012), the visualization of trafficking of secretory proteins from the ER to the Golgi, from the Golgi into vesicular carriers targeting the plasma membrane was possible. In our lab the RUSH assay is a well-established method to especially monitor trafficking processes after accumulation of proteins in the Golgi, upon entering the TGN for sorting into transport vesicles (Pacheco-Fernandez et al., 2021). The timepoints when post-Golgi vesicles appear were monitored and vesicle numbers obtained at these specific time points using fixed cells and confocal microscopy. Those vesicle-counting assays using RUSH enabled the comparison between snapshots when the protein is accumulating in the Golgi or when post-Golgi vesicles appear but could not give insights on the kinetics of the export from the Golgi. Indeed, the full potential of RUSH monitoring the synchronized protein release into the secretory pathway was not utilized in fixed cell analysis. Recently, live-cell imaging was combined with RUSH (Pakdel et al., 2021), however the analysis focused on counting of post-Golgi vesicles. In this study I used a

differential analysis focusing on the decrease of fluorescence intensity of the RUSH-protein, which equates to the export of the protein (Fig. 3.2.3). With simultaneous monitoring of a Golgi-marker protein BFP-GalT1, the exact F.I. of the RUSH-protein could be obtained within the Golgi region per single cell. In addition, visualization of the Golgi aided the selection of suitable cells with constant BFP-GalT1 F.I. throughout the experiment.

4.4 Lysosomal hydrolase PSAP is exported faster from the TGN upon Cab45-depletion

For RUSH-protein PSAP-mCherry in this study, the TGN export in control HeLa cells was compared to Cab45KO, Cab45-6EQ Ca^{2+}-binding and the corresponding Cab45-wt rescue mutant (Fig. 3.2.3C-G). The export curve of Cab45KO shows a stronger decrease in time, equaling a faster export of PSAP-mCherry. Half-life calculations in Cab45KO confirmed this with the shortest half-life in exponential decay of F.I among the observed cell lines. PSAP-mCherry RUSH in Cab45-6EQ (Ca^{2+}-binding mutant) showed a similar half-life time. An increased Golgi export rate of PSAP-mCherry in Cab45 depleted and mutated Cab45 cells was observed, indicating the influence of Cab45 on trafficking of lysosomal hydrolase PSAP in a Ca^{2+}-dependent manner. It is important to note that the time when the maximal PSAP-mCherry F.I. was reached (Fig. 3.2.3.D, F) is earliest in Cab45KO cells, but slightly later in Cab45-6EQ mutant, while latest in HeLa and Cab45wt-rescue. One possibility for the difference time points of maximal F.I. in the Golgi could be an altered transport from the ER to the Golgi, however during imaging the first F.I. in the Golgi was observed in HeLa, Cab45KO, Cab45-6EQ and Cab45wt after the same time after induction of RUSH. Since Cab45-6EQ mutant cells showed the same effect on PSAP-mCherry export rates, but not on time points of maximal PSAP-mCherry F.I. in the Golgi, it is unclear whether Cab45 mediates sorting and trafficking of PSAP-mCherry in Ca^{2+}-dependent or -independent fashion. Sorting and vesicle budding is a dynamic process, with coordinated budding occurring in parallel during sorting of new protein. Sorting and budding, however, are distinct processes that utilize specific machinery. For Cab45's participation in these processes, there are these options: (i) Cab45 influences sorting and vesicular budding of lysosomal hydrolases in the same way (ii) Cab45 influences sorting and vesicular budding of lysosomal hydrolases in separate successive processes. I suggest that the sorting of lysosomal hydrolases could happen via two independent actions mediated by Cab45: firstly, Cab45 influences the receptor-dependent interaction between PSAP and its receptor (e.g., SORT1) for sorting into clathrin-coated vesicles, and secondly, Cab45 influences the export mechanism including vesicle formation and budding.

In Cab45KO cells no Cab45 monomers exist that can bind and sequester Ca^{2+} in the TGN, which could lead to either increased free Ca^{2+} in the TGN lumen or changes in activity (or expression) of Ca^{2+}-pump SPCA1 or Ca^{2+}-release channel RyR to regulate Ca^{2+} levels. The *TGN export* is increased in cells depleted of Cab45 or expressing the Ca^{2+}-binding mutant Cab45-6EQ, meaning vesicle budding and packing into vesicles could occur faster. A cause for this could be missorting into receptor-independent, uncoated vesicles instead of clathrin-coated vesicles which in wild-type conditions mediate transport of lysosomal hydrolases to the endolysosomal system (Puertollano et al., 2001; Klumperman et. al., 1993, Doray et al., 2002, Saftig and Klumperman, 2009, Bajaj et al., 2019). Those uncoated vesicles could belong to the bulk-flow pathway, which soluble proteins by default without concentration or enrichment (Barlowe and Helenius, 2016; Ramazanov et al.; 2021). Typical bulk-flow proteins are either nonnative artificially induced proteins like GFP, HRP or bacterial proteins, but also endogenous ones like OPN (Deng et al., 2018; Hecht et al. 2020). However, bulk-flow occurs typically in lower secretion rates (Crevenna et al., 2016), which cannot explain the hypersecretion of lysosomal hydrolases in Cab45-depleted cells. The formation of clathrin-coated vesicles is initiated by GGA-domain containing proteins recruiting AP-1 molecules to the TGN membrane and binding of cargos in the lumen (Dell' Angelica et al., 2000; Zhang et al., 2007; Dittie et al., 1999, Kakhlon et al., 2006). When this interaction is impaired lysosomal hydrolases escape the recognition via their receptors and are secreted (Guo et al., 2014; Qian et al., 2008).

In Cab45KO cells the *time point of maximal PSAP-mCherry F.I. in the Golgi*, is much earlier than that in HeLa, Cab45wt-rescue but also Cab45-6EQ mutant cells. This means the protein export happens after a shorter period of sorting time. Even though sorting in the GA is a dynamic process, the protein first must enter the TGN and interact with receptors if any, before being packed and transported to the PM, which causes a short delay between accumulating protein and exporting protein at the TGN. From results described in secretion assays, it seems that Cab45 promotes the recognition of PSAP by the SORT1 receptor, since in Cab45 depleted IGF2RKO cells lysosomal hydrolases are missorted. The loss of Cab45 could partially be rescued by expressing the Cab45-6EQ mutant, indicating that the receptor interaction to its cargo is Ca^{2+}-independent.

Interestingly, the vesicle counting assay using the same PSAP-mCherry RUSH construct showed no differences in numbers of post-Golgi vesicles in cells not expressing Cab45, which is like former studies on CatD export.

Previously, Cab45 mutants (Ca^{2+}-binding, as well as phosphorylation-deficient mutants) showed no influence on the Golgi export, analyzed via comparing the number of post-Golgi vesicles containing CatD, exemplary for lysosomal hydrolases, in RUSH based assays (Crevenna et al., 2016; Hecht et al., 2020). Because CatD could not be immunoprecipitated and therefore does not directly interact with Cab45 (Kienzle et al., 2014; von Blume et al., 2012; Crevenna et al., 2016), it is proposed that the influence of Cab45 on CatD targets a different mechanism in comparison to Cab45-dependent

sorting of LyzC and COMP. The data obtained in the frame of this thesis confirm that the effects of Cab45 on CatD, observed in former studies, are not caused by individual properties of CatD but rather are a general effect of Cab45 on lysosomal protein sorting, trafficking and secretion.

4.5 Lysosomal organization is altered with depletion of Cab45

The maturation of lysosomal proteins happens during acidification of the early endosome towards the late endosome, via fusion with lysosomes and scission or via formation of a hybrid organelle (Trivedi et al., 2020; Saftig and Klumperman, 2009). Carriers of lysosomal pro-enzymes fuse with early endosomes and mature to late endosomes and lysosomes (Saftig and Klumperman, 2009). Maturation events often come with movement along microtubules (Trivedi et al., 2020). Also, mature lysosomes change their intracytoplasmic positioning in response to the cellular nutrient status (Triadi et al., 2020; Parton et al. 1991). Interestingly, the knockout of Cab45 led to change in LAMP1-positive endo-and lysosomal positioning. While in HeLa cells LAMP1 signal is peripherally distributed (dispersed) over the cytoplasm as expected (Trivedi et al., 2020; Cheng et al., 2017; Pu et al., 2016), it is accumulated near perinuclear regions in Cab45KO cells. A movement of lysosomes towards the nuclear region is associated with nutrient depletion (Korolchuk et al., 2011) and high cholesterol (Pu et al., 2016). The level of cholesterol influences the dynein/dynactin interaction to lysosomes (promoting retrograde transport to perinuclear regions). During low level of cholesterol oxysterol-binding protein (OSBP) related protein 1L (ORP1L) binds the ER protein vesicle-associated membrane protein (VAMP)-associated ER protein A (VAPA) that induces dissociation of dynein/dynactin from lysosomes (Pu et al., 2016; Rocha et al., 2009). Interestingly, accumulation of cholesterol in perinuclear endosomes is a hallmark of Niemann-Pick-disease (NPC), a neurodegenerative lysosomal storage disorder. PSAP levels were shown to be elevated and accumulated in NPC mutant mice leading to accumulation of glycosphingolipids which are normally proteolytically broken down under influence of SAP A-D (Sleat et al., 2012). In that study, the possibility is mentioned that the accumulation of lysosomal cholesterol in NPC could impede accessibility of glycosphingolipids rather than their degradation (Sleat et al., 2012). An interesting fact in frame of the increased accumulated (perinuclear) positioning of LAMP1-positive endo- and lysosomes in Cab45KO cells, which were shown in this thesis to missort and hypersecrete PSAP. Moreover, the co-localization of PSAP with LAMP1 is reduced in Cab45 depleted cells and rescued by re-expression of the Cab45 - functional as well as Ca^{2+}-binding deficient. Surprisingly, with expression of the Cab45wt-rescue mutant more co-localizing PSAP and LAMP1 punctae were observed, which could be a result of overexpression of Cab45. PSAP's localization appears more accumulated towards the perinuclear region in Cab45KO and -6EQ mutant, which was expected to co-localize in the same ratio with similarly perinuclear positioned LAMP1 punctae. The surprising decrease in co-localization indicates the presence of PSAP in non-

endolysosomal vesicles, as explained in the following: LAMP1 is commonly used as lysosomal marker, but strictly also labelling late endosome and other endocytic compartments (Cheng et al., 2017). For this reason, correctly sorted PSAP targeted to the endolysosomal pathway is expected to co-localize with LAMP1, but this is not the case for perinuclear accumulated PSAP observed in Cab45KO cells. Since LAMP1 labels also non-lysosomal compartments, no conclusion about the lysosomal activity of observed peri-nuclear punctae can be drawn at this point without using a co-labelling of markers of early and late endosomes, such as M6PRs and sortilin (Cheng et al., 2017). The findings indicate a role for Cab45 in lysosomal positioning, which can be linked to lysosomal homeostasis (Pu et al., 2016; Bonifacino and Neefjes, 2017; Trivedi et al., 2020) and is critical in the context of lysosomal storage diseases often associated with neurodegenerative diseases. Already, the missorting and secretion of PSAP is directly correlated with the accumulation of glycosphingolipids causing Gaucher's Disease (Kishimoto et al., 1992; Tayebi et al., 2020), or in case of PGRN the aggregation of ubiquitin-positive TDP-43 in inclusion bodies as seen for FTLD (Zhou et al. 2017b; Paushter et al., 2018).

The data presented in this section of the thesis imply that Cab45 is critical for transport of lysosomal proteins to lysosomes, PSAP and PGRN and to a lesser amount CatD, probably via influencing the recognition of lysosomal proteins by their receptors and propose that Cab45 also promotes the trafficking of other lysosomal proteins. In absence of Cab45, PSAP, PGRN and CatD are missorted, re-routed to the cell surface and secreted. In case of CatD the modest effects could represent a secondary effect of Cab45 depletion, as the loss of Cab45 causes hypersecretion of PSAP, which promotes pro-CatD trafficking (Gopalkrishnan et al., 2004). Additionally, the positioning of lysosomes is altered in Cab45 deleted cells from a distributed peripheral to an accumulated perinuclear localization, a fact which is especially interesting in context of neuronal cells, due to their extreme asymmetry and length of axons and dendrites (Pu et al., 2016) and high sensitivity to changes of lysosomal positioning.

The unexpected role of Cab45 in lysosomal protein sorting is additional to that published in former studies which demonstrate Cab45 as regulator of secretory cargo sorting at the TGN.

Future work has to gain a deeper molecular understanding of Cab45's role in this process. It could support the binding of the hydrolase to the receptor. Alternatively, it could be responsible for trafficking of these receptors to the right place in the TGN and act like a chaperoning component.

Part B - TGN46 influences the sorting of Cab45-dependent clients into sphingomyelin-rich vesicles

In the current model on Cab45-dependent sorting, influx of Ca^{2+} is induced by SPCA1 activation, leading to Ca^{2+} binding and Cab45 oligomerization and interaction with its client in large complex clusters, which are retained in the TGN lumen by their size (Crevenna et al., 2016). Newest studies show that phosphorylation of Cab45 by Golgi kinase Fam20C breaks the cluster for packaging it into sphingomyelin (SM)-rich vesicles (Hecht et al., 2020; Deng et al., 2018). The recognition of the phosphorylated Cab45-client-complex was hypothesized to be mediated directly or indirectly by TGN46, as it was found together with Cab45, client LyzC in SM-rich vesicles (Deng et. al., 2018).

4.6 TGN46 is found in SM-rich vesicles containing Cab45 and its client

Independent early screening experiments using BioID based proximity labelling indicate a participation of TGN45 in Cab45-dependent pathways due to immunoprecipitation of TGN46 among the proximity labeled potential Cab45 interaction partners (Fig. 3.4.1), although not consistently. BioID's long labelling time could lead to false positive results by labelling more than those in proximity. In addition to that, the combination with immunoprecipitation, a method of choice for interactome analysis, makes this method more susceptible to detergent and buffer. The sufficient washing steps remove unspecifically binding proteins, but on the other side also could lead to the loss of transient interactions (Chojnowski et al., 2018). Since the labeling time of biotin needs several hours with BioID (Roux et al., 2012; Kim et al., 2014), it gives a general overview of proteins that have been in proximity to the protein-of-interest, which in case of Cab45 can include proteins that are not directly participating in the sorting, recognition and packaging process and leads to false positives. As the process of Cab45-client-complex interaction with the TGN membrane is assumed to be transient, immunoprecipitation experiments can be insufficient to reflect the interaction between TGN46 and Cab45. However, follow-up BioID experiments with subsequent higher sensitive MS analysis instead of immunoblotting (data not shown) did not detect TGN46 among proximity labelled proteins. Interestingly, this is not excluding the possibility of participation of TGN46 in the Cab45-dependent sorting, as small amounts could be masked in MS where the sensitivity for all proteins is increased, although detection by western blotting was possible (Wakana et al., 2012). The usage of MS in combination with the more precise APEX based labelling is a more suitable screening method (Deng et al., 2018), as short times label more precisely although with lower sensitivity, which however, was not disadvantageous as isolated vesicles were analyzed *in vitro*. Analysis of APEX-labeled SM-vesicles contain TGN46, Cab45 and its client LyzC.

4.7 TGN46 participates in Cab45-dependent sorting in an unknown manner

The slightly increased secretion of Cab45 into supernatants of TGN46 depleted cells sparked the hypothesis of TGN46 binding Cab45 thereby supporting the interaction with client proteins for proper packaging into SM-rich vesicles. However, the overall mechanism of formation of post-Golgi vesicles was unchanged since the number of emerging vesicles in TGN46 deleted and control cells was similar to each other for LyzC-GFP-RUSH. Surprisingly, TGN46 has an influence on the client sorting into the correct, SM-rich, vesicles: knockdown of TGN46 led to decreased co-localization of Cab45 client LyzC and EQSM. Previous studies confirmed that Cab45, LyzC and EQSM are observed in the same punctae in immunofluorescence (Deng et al., 2018), therefore a decrease of co-localization of LyzC and EQSM indicates an impaired Cab45-dependent sorting. Without TGN46 LyzC is not correctly sorted into EQSM vesicles. The severity of TGN46 deletion is thereby important to note, as TGN46 siRNA treatment resulted in unchanged post-Golgi LyzC vesicle numbers compared to control siRNA treatment, but complete deletion of TGN46 did. In TGN46KO cells, the number of LyzC vesicles was lower than in control cells, particularly at 40 minutes after biotin addition, which is the time period when vesicle formation and budding happens primarily. Since TGN46 is a TGN-membrane spanning protein, it could be that a loss alters the morphology of the TGN, however, in immunofluorescence experiments (data not shown), the TGN morphology remained unchanged in cells without TGN46. The complete loss of TGN46 resulted in impaired LyzC-GFP-RUSH sorting, observed by reduced numbers of post-Golgi LyzC vesicles, which was previously associated with impeding of the Cab45-dependent sorting mechanism (Deng et al., 2018; Hecht et al. 2020). Not only the number of client vesicles was reduced but also the number of Cab45 punctae in a similar experiment. Both indicate that TGN46 deletion affects Cab45-dependent sorting.

4.7.1 TGN46 is not directly interacting with Cab45

Hypotheses that TGN46 is interacting via binding of Cab45 were rejected, after several immunoprecipitation experiments with recombinant Cab45 and recombinant TGN46 were unsuccessful (data not shown). Enrichment with recombinant Cab45 and endogenous TGN46 (with cell lysis) was similarly inconsistent and could not support the hypotheses. Interestingly, pulldown from cell lysates enriched with streptavidin in frame of BioID could show both TGN46 and Cab45 signals, which could be replicated in single experiments with Golgi membrane cell lysate, implying that if the two proteins are interacting with each other, at least one adaptor protein is necessary to promote the binding. If TGN46 is not interacting with Cab45 to support binding and vesicle budding, an indirect influence on Cab45 could be the participation in Cab45's recycling back to the Golgi after

secretion of the client. I tested this hypothesis but could not observe Cab45 on the cell surface of HeLa cells in surface biotinylation experiments in control cells (data not shown).

4.7.2 Does TGN46 support proper sorting into SM-rich vesicles by influencing TGN membrane composition

Despite the common usage of TGN46 as TGN marker protein in the last 30 years (Luzie et al., 1990), its function is unknown. In silico analysis described TGN46 as single span TGN membrane protein with a 20aa long transmembrane domain, which is slightly shorter than the mean (hydrophobic) residue length of transmembrane proteins in the TGN ($\approx$ 25-26 aa) (Sharpe et al., 2010; Singh and Mittal et al., 2015). A theory on how differential length of transmembrane domain (TMD) proteins can alter the local membrane composition in response to the cargo for vesicle formation and budding was originally proposed for post-Golgi membranes (PM, or organelle membranes) (Sharpe et al., 2010), but could be an interesting hypothesis for explanation of TGN46's role. First, the properties are defined as follows: longer TMDs are more lipid-like since their hydrophobic membrane domain is larger. The more similar the TMDs of the transmembrane proteins (TMPs) are in length and structure the higher is the probability for a potential attraction to each other. In this model, authors state that TMP with similar TMDs attract each other, so a membrane region in the TGN which contains more TMPs with thicker more ordered lipids could attract other TMPs with longer TMDs, which then attract a coat and lead to vesicle formation. Or on the other hand, a membrane region enriched with TMPs with shorter transmembrane domain than the cargo proteins, would sort lipids towards the cargo - away from the less hydrophobic TMPs with shorter TMD. Regarding TGN46, the loss of this protein could alter the hydrophobicity of the TGN membrane, so that either Cab45-client complexes are directed to membrane regions which are not SM-rich because of the missing (indirect) interaction to TGN46 (which would provide more hydrophobicity, thus sorting towards similarly high lipid, SM-rich domains). However, these are speculative ideas which need to be tested probably by expressing TGN46 mutants with varying length of the TMD and analysis of the Cab45-dependent sorting.

4.8 Cab45 regulates at least two independent sorting processes for soluble secretory cargo

Results from part A described the novel role of Cab45 participation in sorting and targeting of lysosomal hydrolases as well as lysosome positioning, while findings in part B revealed TGN46 as a potential component of the Cab45 receptor-independent machinery. Taking both results together, I

propose a dual-function of Cab45 as sorter in cargo-receptor independent and cargo-receptor-dependent pathways.
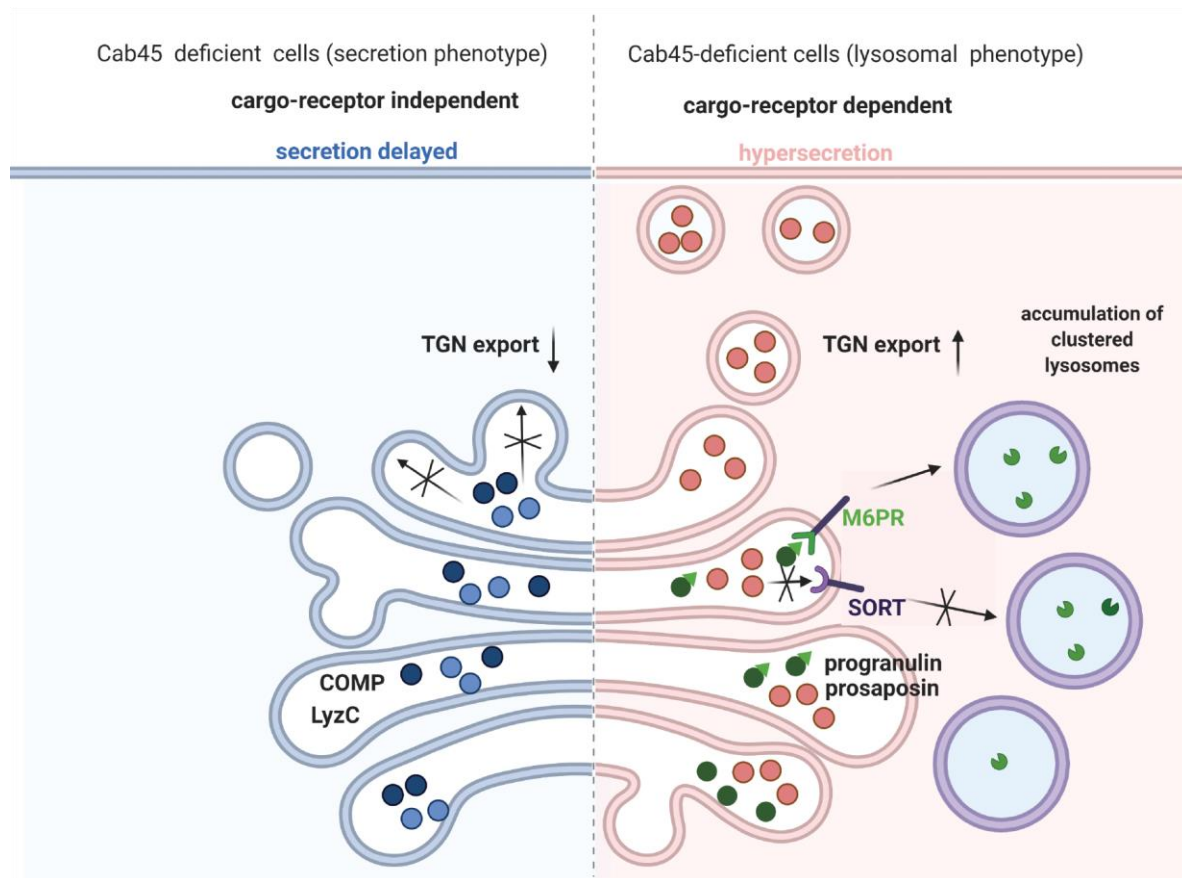
Fig. 4.8: Overview on Cab45 functions in sorting of soluble proteins. Left side, blue shade: The firstly described function of Cab45 to sort secretory soluble proteins, such as Lysozyme C (LyzC) and cartilage oligomeric matrix protein (COMP) at the TGN does not involve any receptors, but demands Ca^{2+}-induced oligomerization of Cab45 for sorting into SM-rich vesicle, possibly promoted via interaction with TGN46. The secretion in Cab45-deficient cells is delayed. Right side, red shade: The novel role of Cab45 in regulating sorting of lysosomal hydrolases, such as progranulin (PGRN) and prosaposin (PSAP) in a cargo-receptor-dependent manner at the TGN. In Cab45 deficient cells the recognition of lysosomal proteins by sortilin receptor (SORT) is impaired, which leads to partial compensation by other receptors (e.g., mannose-6-phosphate receptors, M6PRs) but hypersecretion of remaining PGRN or PSAP. Additionally, Cab45 depletion induces accumulation of lysosomes in clusters mostly seen at the perinuclear region.

5 Supplementary Data
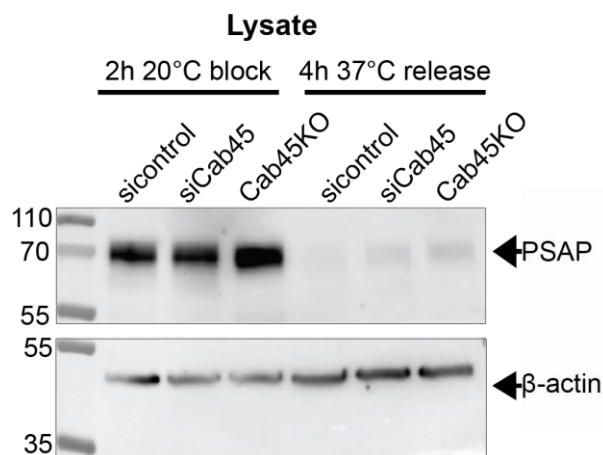
Fig. S1 (related to Fig. 3.1.1): Primary set-up of conditions for secretion assays for sicontrol, siCab45 and Cab45KO cells. A 20°C block experiment was performed to accumulate protein in the Golgi apparatus for 2h. Subsequent release at 37°C for 4h shows faint bands of PSAP in the lysate and no bands are observed in the supernatant (data not shown). As loading control β-actin is shown.
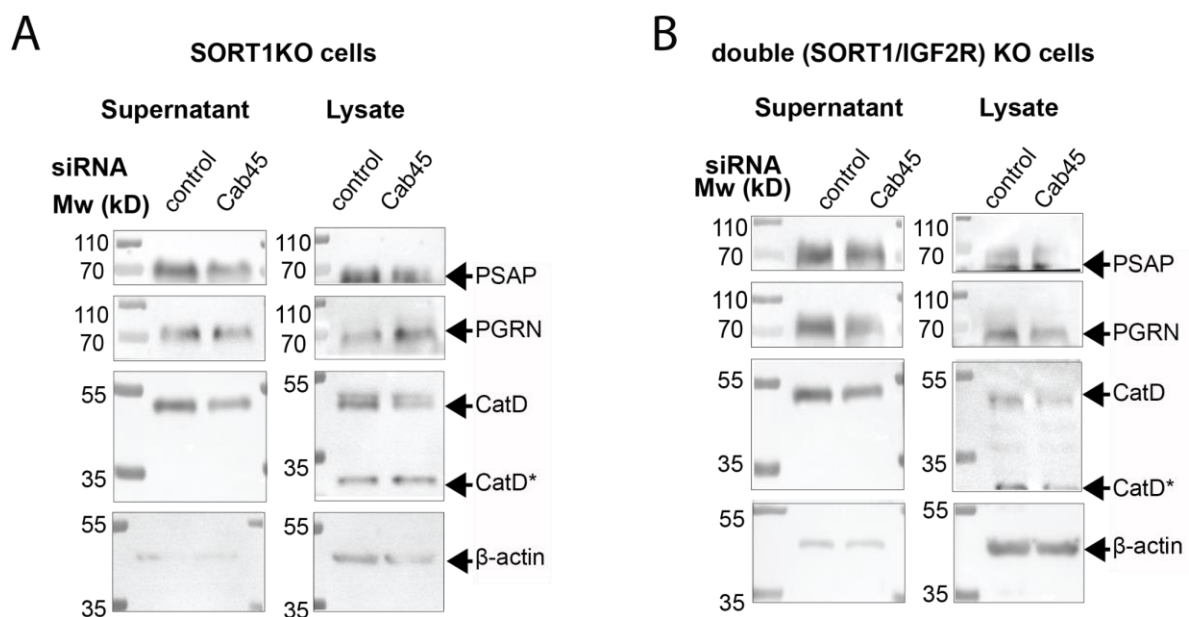
Fig. S2A, B (related to Fig. 3.1.3D,E): Secretion assays in receptor KO cell lines under siRNA treatment. Influence of Cab45 depletion on 24 h secretion of PSAP, PGRN and CatD in SORT1KO cell (A) and double (SORT1/IGF2R) KO cells (B). Representative western blot in **A.** SORT1KO cell lysate and supernatant indicate slightly decreased levels of PSAP and CatD, with depletion of Cab45. PGRN levels appear similar in control and Cab45 siRNA treated SORT1KO cell supernatant and lysate. **B.** Representative western blot of double KO cells show similar amounts of PSAP and CatD in the supernatant, while PGRN appears reduced in supernatant samples.

The detected protein bands for PSAP, PGRN and CatD levels similarly low in lysate for treatment with control or Cab45 siRNA.
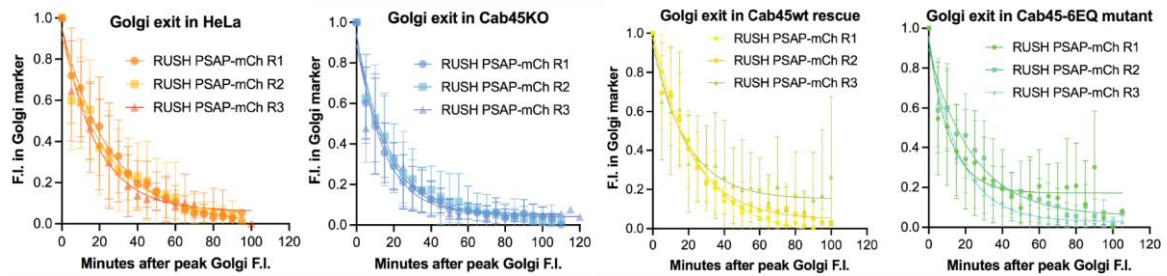
Fig. S3 (related to Fig. 3.2.3E): Golgi exit assay of PSAP-mCherry RUSH in triplicates for HeLa (orange), Cab45KO (blue), Cab45wt-rescue (yellow) and Cab45-6EQ mutant (green). Shown is the mean normalized fluorescence intensity (F.I.) of PSAP-mCherry RUSH in Golgi-marker region of BFP-GalT1 starting from the time when maximal PSAP-mCherry F.I. is reached. The triplicates were analyzed in non-linear regression in Fig.3.2.3E).

Table S1 (related to Fig. 3.1.1E): hiSPECS MS results. Significant hits are listed with gene names, protein names and fold change(KD/wt). -log(p-value) and log2(KD/wt) are corresponding to Fig. 3.1.1E. Hits with higher abundance in Cab45 depleted cell secretome compared to that of control cell and are listed in Fig. 3.1.1E are marked with *.

Protein names	Gene names	-LOG (P-value)	log2 (Difference (KD/wt))	fold change (KD/Ctr)
* Calsyntenin-1	CLSTN1	7,682	2,661	6,325
* Dipeptidyl peptidase 1	CTSC	6,739	1,432	2,697
* Legumain	LGMN	6,527	1,193	2,287
* Sialidase-1	NEU1	5,755	1,625	3,084
* Complement C1s subcomponent	C1S	5,513	1,162	2,238
* Procollagen-lysine,2-oxoglutarate 5-dioxygenase 2	PLOD2	5,386	1,379	2,600
* Prosaposin	PSAP	5,096	1,212	2,316
* Lysosomal alpha-mannosidase	MAN2B1	4,830	0,666	1,586
* Lysosomal acid lipase/cholesteryl ester hydrolase	LIPA	4,548	1,084	2,120
* Beta-hexosaminidase subunit beta	HEXB	4,479	0,909	1,878
Proteoglycan 4;Proteoglycan 4 C-terminal part	PRG4	4,327	-0,936	0,523
* Cathepsin L2	CTSV	4,311	0,732	1,661
Interleukin-6 receptor subunit beta	IL6ST	4,279	-0,947	0,519
* Gamma-glutamyl hydrolase	GGH	4,264	0,731	1,659
Tenascin-X	TNXB	4,236	-0,354	0,782
* Acid ceramidase	ASAH1	4,121	0,852	1,805
* Retinoid-inducible serine carboxypeptidase	SCPEP1	4,027	1,278	2,424
Glia-derived nexin	SERPINE2	4,024	-1,030	0,490
Apolipoprotein C-III	APOC3	3,928	-0,998	0,501
Exostosin-like 2	EXTL2	3,862	-0,824	0,565
Alpha-mannosidase 2x	MAN2A2	3,810	-1,118	0,461
N-acetyllactosaminide beta-1,6-N-acetylglucosaminyl-transferase, isoform A	GCNT2	3,808	-0,662	0,632
* Cathepsin Z	CTSZ	3,770	0,653	1,572
* Complement C3	C3	3,758	1,201	2,298
Peptidyl-prolyl cis-trans isomerase B	PPIB	3,676	-0,863	0,550
* Beta-hexosaminidase subunit alpha	HEXA	3,648	1,014	2,020
* N-acetylgalactosamine-6-sulfatase	GALNS	3,632	0,996	1,994
* Tripeptidyl-peptidase 1	TPP1	3,571	0,758	1,691
* Vasorin	VASN	3,558	0,723	1,650

* Ceroid-lipofuscinosis neuronal protein 5	CLN5	3,513	0,650	1,569
* Interleukin-1 receptor accessory protein	IL1RAP	3,503	0,560	1,474
Interleukin-1 receptor-like 1	IL1RL1	3,446	-1,210	0,432
* Neuronal pentraxin receptor	NPTXR	3,334	0,744	1,675
* Cathepsin D	CTSD	3,332	0,863	1,819
Plasminogen activator inhibitor 1	SERPINE1	3,314	-0,618	0,652
* Palmitoyl-protein thioesterase 1	PPT1	3,279	0,770	1,705
Golgi membrane protein 1	GOLM1	3,273	-0,708	0,612
* Cathepsin B	CTSB	3,269	0,501	1,415
Fibronectin;Anastellin;Ugl-Y1;Ugl-Y2;Ugl-Y3	FN1	3,257	-0,332	0,795
* Lysosomal Pro-X carboxypeptidase	PRCP	3,060	0,817	1,762
Ceruloplasmin	CP	2,997	-0,334	0,793
LIM and SH3 domain protein 1	LASP1	2,970	-0,398	0,759
Complement factor B	CFB	2,960	-0,796	0,576
* N-acetylglucosamine-6-sulfatase	GNS	2,941	1,050	2,070
Eukaryotic translation initiation factor 4B	EIF4B	2,866	-0,810	0,570
* Lysosomal protective protein	CTSA	2,842	0,701	1,626
* Beta-mannosidase	MANBA	2,841	1,112	2,161
Cyclic AMP-dependent transcription factor ATF-6 beta	ATF6B	2,833	-0,846	0,556
* Group XV phospholipase A2	PLA2G15	2,708	0,875	1,834
Insulin-like growth factor-binding protein 7	IGFBP7	2,707	-0,528	0,694
Deoxyribonuclease-2-alpha	DNASE2	2,631	0,508	1,422
Cell division control protein 42 homolog	CDC42	2,625	-0,452	0,731
Collagen alpha-3(VI) chain	COL6A3	2,593	-0,378	0,769
* Lysosomal thioesterase PPT2	PPT2	2,565	0,663	1,583
Mannosyl-oligosaccharide 1,2-alpha-mannosidase IA	MAN1A1	2,495	-0,873	0,546
Collagen alpha-1(XII) chain	COL12A1	2,420	-0,444	0,735
N-acetyllactosaminide beta-1,3-N-acetylglucosaminyltransferase 2	B3GNT2	2,397	-0,441	0,736
Ephrin-A1;Ephrin-A1, secreted form	EFNA1	2,376	0,678	1,600
Disintegrin and metalloproteinase domain-containing protein 9	ADAM9	2,372	0,488	1,403
Repulsive guidance molecule A	RGMA	2,361	-0,580	0,669
Cofilin-1	CFL1	2,357	-0,439	0,738
* Extracellular serine/threonine protein kinase FAM20C	FAM20C	2,354	0,491	1,406
Alpha-N-acetylglucosaminidase	NAGLU	2,327	0,825	1,771
Semaphorin-6D	SEMA6D	2,307	0,654	1,573

Stress-induced-phosphoprotein 1	STIP1	2,264	-0,628	0,647
Probable ATP-dependent RNA helicase DDX17	DDX17;DDX5	2,245	-0,395	0,761
Galectin-1	LGALS1	2,229	-0,715	0,609
Nucleolin	NCL	2,215	-0,662	0,632
Stanniocalcin-2	STC2	2,192	-0,687	0,621
Polypeptide N-acetylgalactosaminyltransferase 6	GALNT6	2,175	-0,407	0,754
Procollagen-lysine,2-oxoglutarate 5-dioxygenase 1	PLOD1	2,151	0,399	1,318
Beta-galactosidase	GLB1	2,145	0,763	1,697
Malate dehydrogenase, mitochondrial	MDH2	2,131	-0,518	0,698
Carboxypeptidase Q	CPQ	2,096	0,463	1,379
Arylsulfatase B	ARSB	2,054	0,722	1,649
Prostaglandin F2 receptor negative regulator	PTGFRN	2,054	-0,692	0,619
Protein NOV homolog	NOV	2,050	-0,592	0,663
EGF-containing fibulin-like extracellular matrix protein 1	EFEMP1	2,015	-0,448	0,733
D-glucuronyl C5-epimerase	GLCE	1,955	-0,519	0,698
High mobility group protein B1	HMGB1;HMGB1P1	1,929	-0,501	0,706
40S ribosomal protein S12	RPS12	1,928	-0,476	0,719
* Granulins (1-7);Acrogranin;Paragranulin	GRN	1,904	0,621	1,538
Putative phospholipase B-like 2 (32kDa, 45 kDa form)	PLBD2	1,893	0,873	1,831
Heterogeneous nuclear ribonucleoprotein R, Q	HNRNPR;SYNCRIP	1,892	-0,594	0,663
Protein disulfide-isomerase A3	PDIA3	1,887	-0,710	0,611
Granulocyte-macrophage colony-stimulating factor receptor subunit alpha	CSF2RA	1,873	-0,528	0,693
Complement C4-B	C4B	1,813	0,587	1,502
G-protein coupled receptor 126	GPR126	1,731	0,521	1,435
RNA-binding protein FUS	FUS	1,624	-0,619	0,651
60S ribosomal protein L10a	RPL10A	1,525	-0,721	0,607

6 Outlook and concluding remarks

During the course of my PhD studies on mechanisms of secretory cargo sorting at the trans-Golgi network I advanced the knowledge on Cab45-dependent sorting in revealing another component of the sorting machinery - the potential interaction partner TGN46 and extended the roles of Cab45 with another surprising involvement in lysosomal protein sorting and lysosomal positioning.

Part A in this thesis describes the cause of hypersecretion of lysosomal hydrolases upon depletion of Cab45 which is contrary to the secretion-delay-phenotype known for its clients in absence of Cab45. In this novel role of Cab45 the mechanism is unclear, but experiments indicated possible participation of Cab45 in the receptor-cargo interaction that sorts lysosomal hydrolases at the TGN into vesicles destined for the endolysosomal system. Results imply that a potential receptor pathway could involve SORT1 for transport of newly synthesized lysosomal proteins from the Golgi, as the loss of CI-M6PR together with Cab45 depletion leads to the hypersecretion phenotype, while loss of SORT1 does not. Other possible receptors could involve LRP1 which mediates PSAP uptake at the cell surface for endocytosis and which has to be evaluated in future experiments. Moreover, Cab45 seems to influence the export of lysosomal enzymes at the example of prosaposin (PSAP) from the TGN, possibly by supporting receptor-cargo interaction on the one hand and mediating the packing into transport vesicles on the other hand. Not only the direct involvement of Cab45 could regulate these processes but also secondary effects e.g. changes in Ca^{2+} concentration by the action of Cab45, that could mediate receptor-cargo interactions as well as vesicle budding and export mechanisms and therefore are an important target for future studies. In addition to these roles, Cab45 influences lysosomal positioning of LAMP1-positive endolysosomal compartments and the localization of PSAP within those. I could reveal the importance of Cab45 in maintaining correct sorting of lysosomal hydrolases to lysosomes and their positioning within the cells, which are ultimately essential for cellular homeostasis. Missorting leading to increased secretion and thereby loss of lysosomal hydrolases for proteolytic activities within the cell, causes formation of accumulated lysosomal enzyme substrates in lysosomal storage diseases which is often a pathological markers in neurodegenerative diseases. In this regard, it would be interesting to study the function auf Cab45 in more specialized cells, like neuronal derived cells.

Part B of this thesis described the continuation of studies on the already existing knowledge on the Cab45-dependent mechanism to sort other secretory soluble cargo like LyzC and COMP in a receptor-independent process. The current model is still under evaluation and could not give an explanation how Cab45 and its cargo is specifically recognized at the TGN membrane prior to vesicle budding. Findings in this thesis reveal the TGN transmembrane protein TGN46 as potential interactor to fulfill this role, possible by indirectly binding Cab45. Although mechanistic details could not be shown so far, it is clear that TGN46 participates on the Cab45-dependent sorting of clients like LyzC,

since the secretion-delay and missorting phenotype observed with loss of TGN46 resemble that of earlier studies, where other components of the mechanism were deleted or dysfunctional. Further studies could focus on the mode of targeting to SM-rich membrane regions at the TGN involving the structural features of TGN46. The use of mutants of TGN46's transmembrane domain and analysis of the hydrophobic, high repetitive region on its luminal domain could be points where either interaction could happen, or membrane composition can be altered for vesicle formation.

Overall, the study showed the complexity of Cab45-dependent sorting of soluble proteins within the secretory pathway in a receptor-independent and, as a novelty, receptor-dependent manner. Further studies on this mechanism will advance the field of sorting and secretion by answering how secretory soluble proteins without a tag can be sorted to their destinations.

7 Materials and Methods

Materials

Name	Manufacturer	Cat number	Notes
Antisera			
monoclonal antibodies (mABs) mouse β-actin	sigma	A-5441	1: 4000
Noncommercial rabbit Cab45 antibody	Published in Crevenna et al., 2016, Hecht et al., 2020		
mAB mouse β-integrin	BD Transduction Laboratories™	Clone18/CD29, 610467	1 : 1 000, 5% milk in TBS
Streptavidin-HRP	Cell Signaling	3999S	1: 5 000, 5% BSA in TBS
AB mouse prosaposin	Abnova	H0005660-M03	
mAB mouse progranulin	invitrogen	MA1-187	
mAB mouse cathepsin D	BD transduction Laboratories	610801	
polyclonal rabbit Sortilin/NT3	abcam	ab16640	
recombinant rabbit M6PR (cation independent)	abcam	ab124767	
mAB rabbit LAMP1 (clone D2D11)	cell signaling	9091S	
polyclonal antibody (pAB) sheep TGN46	Bio-Rad	AHP500G	
goat anti mouse poly HRP	ThermoScientific	32230	
goat anti rabbit poly HRP	ThermoScientific	32260	
Alexa Fluor donkey sheep488 (IgG H+L)	ThermoScientific	A11015	
Alexa Fluor donkey sheep594 (IgG H+L)	ThermoScientific	A11016	
Alexa Fluor donkey mouse488 (IgG H+L)	ThermoScientific	A21202	
Alexa Fluor donkey mouse594 (IgG H+L)	ThermoScientific	A21203	
Alexa Fluor donkey rabbit488 (IgG H+L)	ThermoScientific	A21206	
Alexa Fluor donkey rabbit 594 (IgG H+L)	ThermoScientific	A11037	

Cell Culture			
Bovine Serum Albumin (BSA)	sigma	A96-4-100G	
cOmplete mini Protease inhibitor tablets	Roche	11836170001	
Dulbecco's Phosphate-Buffered Saline	Gibco	14040133	
Dulbecco's Modified Eagle Medium (DMEM), high glucose	Gibco	11965118	
Trypsin EDTA	Gibco ThermoFisher	25300-054	0.05 %
Fetal Bovine Serum FBS	Gibco ThermoFisher	12306C-500mL	10%
penicillin/streptomycin	sigma	G1146-100mL	1%
PEI	Alfa Aesar	43896 CAS9002-96-6	1.25 mg/mL
Plasmids			
LyzC-eGFP RUSH; pIRESneo3_Str-KDEL-LyzC-FLAG-SBP-EGFP,	self-made		RUSH Construct: Str-KDEL and SBP-EGFP tagged LyzC-FLAG; cloned with AscI and EcoRI by restriction enzyme digest and ligation into Str-KDEL_ST-SBP-EGFP (Addgene:#65264), linker: Gly-Asn-Ser
pLPCX_SP-eGFP-HA-TGN46 (= TGN46 rescue)	self-made		Gibson assembly into pLPCX backbone (enzymes: EcoRI/NotI) with mCherry-TGNP-N-10 (Addgene:#54279) and eGFP-HA plasmid acquired by restriction enzyme digestion from a homemade eGFP-containing construct.
BirA-HA-Cab45	Received from the von Blume lab		Cloned with restriction digestion from ss-HA-Cab45 by B. Blank
BFP-GalT1	Kind gift from J.E. Rothman		
KDEL-Strep-PSAP-SBP-mCherry	Kind gift from S. Ferguson		
hiSPECS (Tueshaus et al., 2020)			
ManNAz	ThermoFisher	88904	
Concanavalin A beads	Sigma	C7555	
DBCO-beads	Jena Bioscience	CLK-1037	
EASY-nLC 1200 UHPLC system	Thermo Fisher Scientific		120 min gradient on a 30 cm long C18 column

C18 column (75 µm ReproSil-Pur 120 C18-AQ resin)	Self-packed, Dr. Maisch GmbH		
Q-Exactive™ HF Hybrid Quadrupole-Orbitrap™ mass spectrometer	Thermo Fisher Scientific		
Imaging			
Imaging media: DMEM with HEPES, no Phenol red	Gibco ThermoFisher	21063-029	
Glass bottom dishes: 35 mm, 20 mm bottom well #1.5 glass (0.16-0.19 mm),	cellVis	D35-20-1.5-N	35mm, 20 mm diameter, #1.5 glass (0.16-0.19 mm)
Paraformaldehyde PFA	EMS Electron Microscopy Sciences	50-980-487	Fresh diluted
Saponin	ChemCruz	SC280079	0.04%
Glass slides	EMS Electron Microscopy Sciences	72290-04	#1.5, 12mm diameter
ProLong Gold antifade reagent with DAPI	invitrogen	P36935	
D-Biotin	Fisher BioReagents	58-85-5	(40mM stock, usage: 1: 1000 dilution to 40 µM)
Lipofectamine®2000	Invitrogen	P/N 52887	
Opti-MEM™ I	Gibco ThermoFisher	31985-070	
HiPerfect	Qiagen	Cat. No. / ID: 301704	
Secretion assay and western blot			
siRNA Cab45	invitrogen	NM_01616 oligo	5′-GGTCACGTGTCTTGGGACGAGTATA-3′
AllStars Negative control siRNA	Qiagen	1027281	20nM
Cell scraper, 2-position blade,	Sarstedt	83.3950	
Amicon®Ultra (20 mL, Ultracel® - 10K	Millipore	UFC501096	
nitrocellulose membranes (0.2 µm)	Bio-Rad	1620112	
Pierce™ ECL Western Blotting solution	ThermoScientific	10590624	
ChemiDoc™ Touch Imaging system	Bio-Rad		
25mm 0.45 µM Acrodisc(R) filter	Pall Corporation	4614	

Bradford	Bio-Rad	5000006	
Nanodrop ONE(c)	ThermoScientific		
Live-cell-imaging			
confocal laser-scanning microscope (63x NA1.4 Plan-Apochromat oil objective)	Carl Zeiss	LSM 880	CFI Plan Apo Lambda 60x/NA 1.4 oil objective (Nikon)
spinning disk confocal microscope	Yokogawa	CSUXfw-06p-01	
imaging stage (Nikon eclipse Ti2)	Nikon		LWD NA=052m with stagetop Piezo
cycloheximide	dot-scientific inc.	66-81-9	100 µM
Avidin	Sigma-Aldrich	A9275	10 µM in DMSO (stock: 1 mg/ml)
qRT-PCR			
RNeasy Mini Kit (50)	Qiagen	Cat. No. / ID: 74104	
RevertAid RT Reverse Transcription Kit	Thermo Scientific™	K1691	
SYBR(R) green qPCR Readymix™ iQ (KiCqStart™)	sigma	KCQS03-230RXNLN 66186677	
Surface biotinylation and BioID			
NeutrAvidin agarose beads	Pierce	20353	
EZ-Link™ Sulfo-NHS-SS-biotin	Thermo Scientific™	21331	
Dynabeads™ MyOne™ Streptavidin C1	Invitrogen™	65-001	25µL bead slurry per sample
DynaMag™- Spin Magnet	Invitrogen™	12320D	
Software			
ImageLab Software	Bio-Rad	V.s.6.0.1	
Fiji ImageJ	Open source	Vers 1.0	
CFX Manager	Bio-Rad	Vers 3.0	

| PerlPrimer | Owen Marshall | v1.1.21 | |
| Prism9 | GraphPad Software, LLC | Version 9.2.0 (283) | |

Methods

Antisera

Antibodies used for the study are listed as follows: monoclonal antibodies (mABs) mouse β-actin (sigma, A-5441), mAB mouse prosaposin (Abnova, H0005660-M03), mAB mouse progranulin (invitrogen, MA1-187), mAB mouse cathepsin D (BD transduction Laboratories, 610801), polyclonal rabbit Sortilin/NT3 (abcam, ab16640), recombinant rabbit M6PR (cation independent) (abcam, ab124767), mAB rabbit LAMP1 (clone D2D11, 9091S, cell signaling), polyclonal antibody (pAB) sheep TGN46 (AHP500G, Bio-Rad). The Cab45 antibody was generated in rabbits as published in Crevenna et al., 2016. All primary antibodies for immunoblotting were diluted in 5% Bovine Serum Albumin (BSA, sigma) in TBS (1: 2 000). For application in immunostaining primary antibodies were used in 1:500 dilution (1:1 000 for Giantin and TGN46) in 4% BSA (in PBS) or 0.1% Saponin in 3% BSA (in PBS) respectively.

Secondary antibodies for immunoblotting goat anti mouse poly HRP (32230), goat anti rabbit poly HRP (32260) were purchased from ThermoScientific and used in 1:15 000 dilution in 5% BSA in TBS.

Secondary antibodies for immunostaining Alexa Fluor donkey sheep488 (IgG H+L) (A11015), Alexa Fluor donkey mouse488 (IgG H+L) (A21202), Alexa Fluor donkey mouse594 (IgG H+L) (A21203), Alexa Fluor donkey rabbit488 (IgG H+L) (A21206), Alexa Fluor donkey rabbit 594 (IgG H+L) (A11037) were purchased from ThermoScientific and used in 1: 500 dilution in 4% BSA in PBS.

Cell Culture and cell lines

Cell lines were cultured in Dulbecco's Modified Eagle Medium (DMEM) (high glucose, Gibco) with 10% fetal bovine serum (FBS, Gibco), 1% penicillin/streptomycin (sigma) at 37°C and 5% CO2. Passaging was performed with 0.05% Trypsin-EDTA every 2-3 days to maintain single layer growth. Stable cell line Cab45-HA-wt (Cab45wt-rescue) was generated by retrovirus transfection (Pfeifer et al., 2000) on Cab45 knockout (KO) cells as published previously (Crevenna et al., 2016). Cab45KO cell line was generated using CRISPR (Crevenna et al., 2016). SORT1KO, IGF2RKO, Sort1/IGF2R

double KO cell lines and parental HeLa were a gift from S. Ferguson (Yale School of Medicine, New Haven, CT, USA). TGN46KO and parental HeLa cell lines were a gift from C. Burd (Yale School of Medicine, New Haven).

DNA manipulation and plasmid engineering

RUSH constructs were cloned using Gibson assembly. pIRESneo3_Str-LyzC-KDEL-SBP-EGFP was published previously (Deng et al., 2018). Str-KDEL-Prosaposin-SBP-mCherry (Devireddy and Ferguson, 2021) was a gift from S. Ferguson (Yale School of Medicine, New Haven, CT, USA). BFP-GalT1 was received from C. Burd (Yale School of Medicine, New Haven, CT, USA) and gifted from J. Rothman (Yale School of Medicine, New Haven, CT, USA).

siRNA silencing

As negative control in all silencing experiments, AllStars negative control (20 nM, Qiagen) was used. Cab45 siRNA was purchased from Invitrogen as oligo:

5′-GGTCACGTGTCTTGGGACGAGTATA-3′ (Cab45 Oligo 2) and used in several publications before (von Blume et al., 2012; Deng et al., 2018)

TGN46 siRNA was purchased from siTOOLs Biotech (10618).

For general siRNA transfection 20 nM siRNA and 8 µL HiPerfect transfection reagent (Qiagen) were mixed in 100 µL Opti-MEM™I reduced serum medium (Gibco by Life Technologies) and added to 6-well-plates containing cells in growth media.

For Cab45 silencing in secretion assays using 15 cm dishes, 800 µL Opti-MEM containing 70 µL HiPerfect + 7 µL siRNA were added to cells grown to 60% confluency. Further experiments were performed after 24h of siRNA transfection.

Transfection with DNA plasmids

Transient transfection with engineered plasmids described above was performed using 12 µL PEI (1.25 mg/mL, Alfa Aesar) and 1.5 µg DNA for immunofluorescence experiments. The reagent was

incubated in 200 µL Opti-MEM reduced serum medium with 1.5 µg DNA for 15 min before adding to the cells cultured in 6-well-dishes (at least 60% confluent).

For Live Cell imaging cells (70-80 % confluent) were cultured in 3.5 mm glass bottom dishes and transfected using Lipofectamine®2000 transfection reagent (invitrogen). The mixtures containing each 150 µl Opti-MEM reduced serum medium with 3 µL Lipofectamine or with DNA (150 ng BFP-GalT1 and µg RUSH-construct) were incubated at room temperature for 5 min, then combined and incubated for 20 min. The solution was added to 1200 µL growth media on cells. After 5 h the supernatant was exchanged for new growth media with Avidin (1 mg/mL).

hiSPECS analysis

Secretome analysis was performed using the high-performance secretome protein enrichment with click sugars (hiSPECS) method as described in detail by Tüshaus et al, 2020. In brief, cells were cultured in cultivation media in the presence of 50 µM ManNAz (ThermoFisher, 88904) for 48h, condition media was collected and filtered to clear it from cellular debris. Glycoprotein enrichment was conducted with Concanavalin A (Sigma, C7555) beads prior to performing the click reaction of azide-modified glycoproteins to DBCO-beads (Jena Bioscience CLK-1037) overnight at 4°C. After washing the proteins with SDS, UREA and acetonitrile, they were digested with trypsin (on-bead). Desalted peptides were separated on an EASY-nLC 1200 UHPLC system (Thermo Fisher Scientific) using a 120 min gradient on a 30 cm long C18 column (self-packed, 75 µm ReproSil-Pur 120 C18-AQ resin Dr. Maisch GmbH). A Q-Exactive™ HF Hybrid Quadrupole-Orbitrap™ mass spectrometer (Thermo Fisher Scientific) was used for this study and data analysis was performed with MaxQuant software using standard settings besides a minimal peptide length of 6 (1% FDR on protein and peptide level).

Detection of proteins by immunostaining and immunoblotting

To detect proteins from cell lysate, cells were washed with PBS three times, then incubated with lysis buffer (1% Triton-X-100 in PBS) on ice. Secreted proteins were collected by concentration of cell culture supernatant with Amicon®Ultra (20 mL, Milipore, Ultracel® - 10K) centrifugal filters. For further analysis proteins were separated by size using SDS-PAGE and 10% Acrylamide gels.

For immunostaining, cells were grown on glass slides (#1.5, 12 mm diameter, EMS in 6-well dishes) to 60-70% confluency before transfection (see above). 24h after transfection, immunostaining was performed by fixing cells for 10 min with 4% fresh paraformaldehyde (PFA) (Electron Microscopy

Sciences) in Dulbecco's Phosphate Buffered Saline (Gibco), then permeabilized with 0.2%Triton-X-100 and 0.5% SDS in 4% BSA solution for 3 min. Cells were washed three times with DPBS after each step. Unspecific binding was blocked by 1h incubation with 4% BSA solution at room temperature or 2h at 4C. Subsequently, cells were incubated with primary antibody overnight at 4°C, and after washing with secondary antibody for 1h at room temperature (RT). The glass slides were mounted using ProLong Gold antifade reagent with DAPI (invitrogen) and imaged in confocal microscopy.

Immunostaining with LAMP1-antibody was changed according to the sensitivity of the antibody. Cells were grown as described above, then fixed with fresh 8% PFA in a 1:1 solution of DMEM and DPBS for 30 minutes at room temperature. Glass slides with the fixed cells were washed twice with DPBS. Permeabilization was performed with 0.1% saponin (ChemCruz) in DPBS for 15 minutes, followed by blocking with 3% BSA in DPS containing 0.1% saponin (20 min, RT). Primary and secondary antibodies were diluted in the blocking solution for overnight (primary) and 20 minute incubation (secondary), respectively. Glass slides were mounted as described above.

For immunoblotting SDS gels were transferred to nitrocellulose membranes (0.2 µm, Bio-Rad) by wet-blot system (Bio-Rad) in transfer buffer (25 mM Tris, 192 mM glycine, pH 8.3) containing 20% methanol at 105 V for 70 min. The membranes were blocked using 5% BSA in TBS for 1h, RT, before incubation with primary antibody (4C, overnight) and secondary antibody (1h, RT). Membranes were washed with TBS + 0.1% Tween-20 three times (each 10 min) after primary and secondary antibody incubation. Antibodies were diluted in 5% BSA in TBS as described above and detected using chemiluminescence (Pierce™ ECL Western Blotting solution) on a ChemiDoc™ Touch Imaging system (Bio-Rad) imaging system.

Analysis of LAMP1 localization

For analysis of confocal images with LAMP1 immunostaining ImageJ software was applied. The channels containing the LAMP1 fluorescent signal and a second channel in overexposure to visualize the outline of the whole cell were opened as separate images. The area of LAMP1 signal as well as the whole cell were manually selected and determined as regions of interest (ROIs), then measured with function 'Measure' in ROI manager. For quantification ROI (LAMP1) was divided by ROI (whole cell). The ratio in percent was plotted with GraphPad Prism9 and statistically analyzed using nonparametric multiple comparisons (Kruskal-Wallis test).

RUSH assay for fixed cell imaging

RUSH assays were performed as described in previous publications on fixed cells. Live-cell-imaging in combination with RUSH is described in detail as Golgi-exit assay. For RUSH assays with subsequent imaging of fixed cells, cells were grown on glass slides in 6-well-dishes. Transfection was done as described above and RUSH assay performed 24h after transfection. To start the experiment, cells were washed once in PBS before adding DMEM containing 40 µM D-biotin (Fisher BioReagents) for different time points (20. 40 and 60 min). For 0 min control no D-biotin was added. Cells were washed once with PBS before fixing with 4% paraformaldehyde in DPBS for 10 min. After three times washing with PBS, cells on glass slides were mounted with ProLong Gold antifade with DAPI and images acquired using a confocal laser-scanning microscope (Carl Zeiss; LSM 880; 63x NA1.4 Plan-Apochromat oil objective) with ZEN 2010 software in z-stacks (0.35 µM slices thickness).

Quantification of the number of post-Golgi vesicles was determined by using the ImageJ macro Count_Fixed_Vesicles_V1.3 (published on GitHub by M. Pakdel. 2019). The macro uses Fiji's *particle analyzer* function on generated binary images. Larger objects like fragments of organelles were omitted using a defined size of 4- 20 pixels for the recognized and counted objects.

RUSH assay for live-cell imaging (Golgi exit assay)

For the live-cell-imaging experiment with RUSH, cells were seeded on 35 mm dishes with 20 mm diameter glass bottom. Transfection was performed as described above. For the Golgi exit assay the culture media was exchanged with imaging media (DMEM without phenol-red + 10 % FBS). After setting up the imaging stage (Nikon eclipse Ti2, LWD NA=052m with stage top Piezo) and spinning disk confocal microscope (CSUXfw-06p-01, Yokogawa) including heating chamber to 37°C, the cells were imaged without D-biotin to determine the focal plane (locked with PFS) on a CFI Plan Apo Lambda 60x/NA 1.4 oil objective (Nikon). The RUSH assay started after washing the cells carefully three times with PBS and adding fresh imaging media containing 40 µM D-biotin, 100 µM cycloheximide (dot-scientific inc.). Images were acquired immediately in 5x6 fields of view with 10% tile stitching for 2h every 5 min. A laser combiner with 405, 488, 561, 640 nm (Agilent) was used for the respective fluorescence detection of mCherry or BFP. NIS element software was used to monitor imaging and save acquired images as stacked two-channel files. Images were further processed with ImageJ and BioFormats add-on. ImageJ threshold function (default setting) was used to transform image stacks of the Golgi marker (BFP-GalT1) into binary files for applying particle analyzer function. A size of 1-100 nM (include holes, exclude on edges) was set to recognize objects that

classify as Golgi elements in the BFP channel, which are then saved as regions of interest (ROI). ROIs were overlaid with the signal of the RUSH-construct and mean fluorescence intensity (F.I.) in this ROI measured. Data was saved and copied into Excel for refining and calculation of the mean signal intensity for each time point and cell. Maximal and minimal F.I. for each cell of all time points were subtracted and normalized by dividing by the highest value (= 1) and lowest value (= 0). Cells with intact and compact Golgi marker staining throughout the whole measurement were considered for analysis. For plotting the Golgi exit, the peak of F.I. in the Golgi marker ROI was set as t=0. All mean F.I. from that time point till the end of the measurement were plotted. Determination of the half-life of the RUSH construct in Golgi marker ROI was achieved by applying non-linear regression with exponential function. GraphPad Prism 9 built-in curve fit program was used for analysis with exponential one phase decay function.

Secretion assay

Cells were cultured in 15 cm tissue culture dishes and transfected with siRNA as described above. After 24h the media was exchanged to fresh culture media to recover cells before starting starvation when the cells are at least 75% confluent. Starvation was performed after three times washing in DPBS and changing to DMEM without FBS containing protease inhibitor (cOmplete mini protease inhibitor tablets, Roche). The cell culture supernatant was collected after 24h, filtered with 25mm 0.45 µM Acrodisc(R) filters (Pall Corporation), and concentrated to approximately 500 µL by using Amicon®Ultra (20 mL, Milipore, Ultracel® - 10K, catalog: UFC901096) at 4°C, 4347xg, 50 minutes. Volumes were equalized with DPBS and samples prepared according to protein levels of cell lysate.

Intracellular proteins in cell lysates were received after incubation with 500 µL lysis buffer (1x PBS + 1% Triton-X-100) for 20 min on ice. Cell debris was removed by centrifugation (20 min, 4°C, 21100 x g). Cleared lysate of each sample were equalized with lysis buffer to the same volume prior to measuring the relative protein concentration with Bradford (Bio-Rad) on Nanodrop ONE(c) (ThermoScientific).

The samples were denatured with 4x Laemmli buffer + 4% β-mercaptoethanol (95°C, 3 min) and separated by size using SDS-PAGE in 10% Acrylamide-SDS gels. Further protein detection was achieved with immunoblotting.

cDNA preparation for qRT-PCR

Total RNA was extracted from cells using RNeasy Mini Kit (Qiagen) according to the manufacturer's instructions. Concentrations were measured using Nanodrop® and used for cDNA preparation with RevertAid RT Reverse Transcription Kit (ThermoFisher Scientific) following the manufacturer's protocol.

The cDNA was stored at -80°C for further usage in qRT-PCR experiments.

qRT-PCR

Primer design was based on genome browser results for mRNA of the gene of interest. The sequence was copied into PerlPrimer software to receive following primer sequences:

SDF4 1F: 5'-CGCTGGATCATGGAGAAGAC-3'
SDF4 1R: 5'-GACTTCCTGTGTTTCCTCATCC-3'

PSAP 1F: 5'-AGAGCTGGACATGACTGAGG-3'
PSAP 1R: 5'-GTTCTTGCATATGTCGGCCA-3'

GRN 1F: 5'-CTTCTGGACAAATGGCCCAC-3'
GRN 1R: 5'-GGAGTTGTTACCTGATCTTTGGA-3'

Primer pairs for cathepsin D amplification were a gift from P. de Camille (Yale School of Medicine, New Haven, CT, USA):
CATD AS: 5'-CATTCTTCACGTAGGTGCTGGA-3'
CATD S: 5'-AACTGCTGGACATCGCTTGCT-3'

All RT-PCR experiments were performed using 5 µL SYBR(R) green qPCR Readymix™ iQ (KiCqStart™, sigma), 4 µL cDNA (5 nM), 0.6 µL (sense and antisense) primers (10 nM) and 0.4 µL DNase free water in duplicates. For preparing the calibration curves diluted cDNA from sicontrol, siCab45 and non-treated Hela were mixed equally in serial dilution. Amplification with the respective primers was performed and recorded with CFX96 and data further analyzed with CFX manager software version 3.0 (Bio-Rad).

Surface biotinylation

To check the expression of receptor proteins IGF2R and SORT1 on the cell surface in HeLa vs. Cab45KO cells, pulldown of biotinylated cell surface proteins in using NeutrAvidin agarose beads (Pierce, 20353) was performed. Cells were cultivated as described above and seeded in 10 cm culture dishes (150 000 cells per dish) until 70-80% confluent. After 18 – 24h cells were washed (2 times, 4 mL) carefully with ice-cold DPBS (1x) on ice. Cells from each cell line were labeled with Sulfo-NHS-SS-biotin (250 µg/mL, 2.5 mL per dish) for 90 min at 4°C (rocking platform). Excess biotin was removed by washing once with ice-cold glycine in DPBS (150 mM) before quenching the biotinylation reaction with incubation in the same glycine solution for 25 min (5 mL/ dish rocking platform). Cells were washed with ice-cold DPBS, subsequently collected with cell scrapers and lysed in 1mL Lysis buffer (100 mM Tris-HCL, 150 mM NaCl, 0.1 % SDS, 1% Triton, 1% deoxycholic acid, pH 7.4, incl. protease inhibitor tablet (Roche)) for 30 min on ice. Cell lysates were separated from membrane and cell debris by centrifugation for 15 min at 14000 rpm (4°C). NeutrAvidin beads were prepared for incubation by washing with 0.5 mL DPBS twice and 0.5 mL Lysis buffer twice (3400 rpm, 4°C, 3 min). After determination of total protein amount per cell lysate by Bradford (absorption λ = 595 nm) the equalized cell lysates were incubated with 150 µL NeutrAvidin bead slurry overnight at 4C (rotating wheel).

To reduce nonspecific protein binding, the beads were washed with lysis buffer (1 mL, 5 times) on ice by centrifugation (3400 rpm, 4 min, 3 min). Subsequently, biotinylated proteins were analyzed on SDS-PAGE in 80 µL Laemmli sample buffer containing 50 mM DTT (10 min, 95°C). Detection was performed by western blot after blocking in 5% BSA (in TBS) with antibodies recognizing IGF2R (abcam, ab124767, ERP6599, 1: 2 000, 5% BSA in TBS) and SORT1 (abcam, ab16640, GR3379711, 1: 2 000, 5% BSA in TBS), β-integrin (BD Transduction Laboratories ™ Clone 18/CD29, 1: 1 000, 5% milk in TBS).

BioID and pulldown

For application of the BioID method, Cab45KO cells were seeded into 10 cm tissue culture dishes and transfected with PEI as described above, at 60 - 70 % confluence with the construct BirA-Cab45. After 24 h growth medium was exchanged to medium containing 100 µM biotin in transfected or untransfected dishes respectively, for 3h, 6h or 22h. Transfected Cab45KO cells were treated without biotin as additional control cells. Cells were harvested using cell scrapers in 1 mL DPBS (collected with centrifugation at 500 rcf for 3 min, 4°C) and washed for 2 more times. Supernatant was discarded and cells incubated in 350 µL IP lysis buffer (50 mM TRIS, 100 mM NaCl, 0.1 % Triton-X-100, pH 7.4; cOmplete protease inhibitor tablet (Roche)). The lysate was separated by using a needle (27G) for 10 times and cleared from cell debris by centrifugation (13000 rpm, 20 min, 4°C). Protein concentrations

were determined with Bradford solution and equalized to 500 µL. Input of 50 µL was saved as a sample for analysis. Streptavidin magnetic beads (Invitrogen™ Dynabeads™ MyOne™ Streptavidin C1; 65-001; 25µL bead slurry per sample) were washed 3 times in 1 mL IP lysis buffer and separated from the beads using DynaMag-Spin (invitrogen, 12320D). The prepared biotinylated protein lysates were bound to washed magnetic beads (overnight, 4°C), then unbound samples taken before washing for 3 times with IP lysis buffer and 2 more times with 1x DPBS. Wash samples were taken for analysis. With the final washing step, the supernatant was removed completely in careful manner. Proteins were dissociated from the magnetic beads by boiling in Laemmli buffer (95°C, 10 min) and collected as IP sample. Subsequently, the biotinylated proteins in IP sample, Input, unbound and wash samples were analyzed via western blotting using anti-TGN46 antibody (Bio-Rad, AHP500G, 1: 1 500, 5% BSA in TBS).

8 References

Abed Rabbo, M., Y. Khodour, L.S. Kaguni, and J. Stiban. 2021. Sphingolipid lysosomal storage diseases: from bench to bedside. *Lipids Health Dis*. 20:44.

Abubakar, Y.S., W. Zheng, S. Olsson, and J. Zhou. 2017. Updated Insight into the Physiological and Pathological Roles of the Retromer Complex. *Int J Mol Sci*. 18.

Aguilera-Gomez, A., and C. Rabouille. 2017. Membrane-bound organelles versus membrane-less compartments and their control of anabolic pathways in Drosophila. *Dev Biol*. 428:310-317.

Akopian, D., K. Shen, X. Zhang, and S.O. Shan. 2013. Signal recognition particle: an essential protein-targeting machine. *Annu Rev Biochem*. 82:693-721.

Alberts, B. 2002. Molecular biology of the cell. Garland Science, New York. xxxiv, 1548 p. pp.

Alonso, M.T., J. Rojo-Ruiz, P. Navas-Navarro, M. Rodriguez-Prados, and J. Garcia- Sancho. 2017. Measuring Ca(2+) inside intracellular organelles with luminescent and fluorescent aequorin-based sensors. *Biochim Biophys Acta Mol Cell Res*. 1864:894-899.

Appenzeller-Herzog, C., and H.P. Hauri. 2006. The ER-Golgi intermediate compartment (ERGIC): in search of its identity and function. *J Cell Sci*. 119:2173-2183.

Arakel, E.C., and B. Schwappach. 2018. Correction: Formation of COPI-coated vesicles at a glance (doi:10.1242/jcs.209890). *J Cell Sci*. 131.

Arakel, E.C., and B. Schwappach. 2018. Formation of COPI-coated vesicles at a glance. *J Cell Sci*. 131.

Bajaj, L., P. Lotfi, R. Pal, A.D. Ronza, J. Sharma, and M. Sardiello. 2019. Lysosome biogenesis in health and disease. *J Neurochem*. 148:573-589.

Balla, T., N. Sengupta, and Y.J. Kim. 2020. Lipid synthesis and transport are coupled to regulate membrane lipid dynamics in the endoplasmic reticulum. *Biochim Biophys Acta Mol Cell Biol Lipids*. 1865:158461.

Banting, G., R. Maile, and E.P. Roquemore. 1998. The steady state distribution of humTGN46 is not significantly altered in cells defective in clathrin-mediated endocytosis. *J Cell Sci*. 111 (Pt 23):3451-3458.

Banting, G., and S. Ponnambalam. 1997. TGN38 and its orthologues: roles in post- TGN vesicle formation and maintenance of TGN morphology. *Biochim Biophys Acta*. 1355:209-217.

Barlowe, C. 2003. Signals for COPII-dependent export from the ER: what's the ticket out? *Trends Cell Biol*. 13:295-300.

Barlowe, C., and A. Helenius. 2016. Cargo Capture and Bulk Flow in the Early Secretory Pathway. *Annu Rev Cell Dev Biol*. 32:197-222.

Barlowe, C., and R. Schekman. 1993. SEC12 encodes a guanine-nucleotide- exchange factor essential for transport vesicle budding from the ER. *Nature*. 365:347-349.

Berninsone, P.M., and C.B. Hirschberg. 2000. Nucleotide sugar transporters of the Golgi apparatus. *Curr Opin Struct Biol*. 10:542-547.

Berridge, M.J., P. Lipp, and M.D. Bootman. 2000. The versatility and universality of calcium signalling. *Nat Rev Mol Cell Biol*. 1:11-21.

Beznoussenko, G.V., S. Parashuraman, R. Rizzo, R. Polishchuk, O. Martella, D. Di Giandomenico, A. Fusella, A. Spaar, M. Sallese, M.G. Capestrano, M. Pavelka, M.R. Vos, Y.G. Rikers, V. Helms, A.A. Mironov, and A. Luini. 2014. Transport of soluble proteins through the Golgi occurs by diffusion via continuities across cisternae. *elife*. 3.

Blank, B., and J. von Blume. 2017. Cab45-Unraveling key features of a novel secretory cargo sorter at the trans-Golgi network. *Eur J Cell Biol*. 96:383-390.

Boncompain, G., and F. Perez. 2012. Synchronizing protein transport in the secretory pathway. *Curr Protoc Cell Biol*. Chapter 15:Unit 15 19.

Bonifacino, J.S., and B.S. Glick. 2004. The mechanisms of vesicle budding and fusion. *Cell*. 116:153-166.

Bonifacino, J.S., and J. Neefjes. 2017. Moving and positioning the endolysosomal system. *Curr Opin Cell Biol*. 47:1-8.

Bonifacino, J.S., and R. Rojas. 2006. Retrograde transport from endosomes to the trans-Golgi network. *Nat Rev Mol Cell Biol*. 7:568-579.

Borgonovo, B., J. Ouwendijk, and M. Solimena. 2006. Biogenesis of secretory granules. *Curr Opin Cell Biol*. 18:365-370.

Botta, R., S. Lisi, A. Pinchera, F. Giorgi, C. Marcocci, A.R. Taddei, A.M. Fausto, N. Bernardini, C. Ippolito, L. Mattii, L. Persani, T. de Filippis, D. Calebiro, P. Madsen, C.M. Petersen, and M. Marino. 2009. Sortilin is a putative postendocytic receptor of thyroglobulin. *Endocrinology*.

150:509-518.

Braulke, T., and J. S. Bonifacino. 2009. Sorting of lysosomal proteins. *Biochim Biophys Acta.* 1793:605-614.

Campelo, F., J. van Galen, G. Turacchio, S. Parashuraman, M.M. Kozlov, M.F. Garcia- Parajo, and V. Malhotra. 2017. Sphingomyelin metabolism controls the shape and function of the Golgi cisternae. *Elife.* 6.

Carreras-Sureda, A., P. Pihan, and C. Hetz. 2018. Calcium signaling at the endoplasmic reticulum: fine-tuning stress responses. *Cell Calcium.* 70:24-31.

Carrasquillo, M. M., Nicholson, A. M., Finch, N., Gibbs, J. R., Baker, M., Rutherford, N. J., Hunter, T. A., DeJesus-Hernandez, M., Bisceglio, G. D., Mackenzie, I. R., Singleton, A., Cookson, M. R., Crook, J. E., Dillman, A., Hernandez, D., Petersen, R. C., Graff-Radford, N. R., Younkin, S. G., and R. Rademakers. 2010. Genome-wide screen identifies rs646776 near sortilin as a regulator of progranulin levels in human plasma. *Am. J. Hum. Genet.* 87:890–897.

Chanat, E., and W.B. Huttner. 1991. Milieu-induced, selective aggregation of regulated secretory proteins in the trans-Golgi network. *J Cell Biol.* 115:1505-1519.

Cheng, X.T., Y.X. Xie, B. Zhou, N. Huang, T. Farfel-Becker, and Z.H. Sheng. 2018. Characterization of LAMP1-labeled nondegradative lysosomal and endocytic compartments in neurons. *J Cell Biol.* 217:3127-3139.

Cherepanova, N., Shrimal, S., Gilmore R. N-linked glycosylation and homeostasis of the endoplasmic reticulum. 2016. *Curr Opin Cell Biol.* 41:57-65.

Chojnowski, A., R.M. Sobota, P.F. Ong, W. Xie, X. Wong, O. Dreesen, B. Burke, and C.L. Stewart. 2018. 2C-BioID: An Advanced Two Component BioID System for Precision Mapping of Protein Interactomes. *iScience.* 10:40-52.

Cool, D.R., and Y.P. Loh. 1998. Carboxypeptidase E is a sorting receptor for prohormones: binding and kinetic studies. *Mol Cell Endocrinol.* 139:7-13.

Coutinho, M.F., M.J. Prata, and S. Alves. 2012. A shortcut to the lysosome: the mannose-6-phosphate-independent pathway. *Mol Genet Metab.* 107:257-266.

Cowley, D.J., Y.R. Moore, D.S. Darling, P.B. Joyce, and S.U. Gorr. 2000. N- and C- terminal domains direct cell type-specific sorting of chromogranin A to secretory granules. *J Biol Chem.* 275:7743-7748.

Crevenna, A.H., B. Blank, A. Maiser, D. Emin, J. Prescher, G. Beck, C. Kienzle, K. Bartnik, B. Habermann, M. Pakdel, H. Leonhardt, D.C. Lamb, and J. von Blume. 2016. Secretory cargo sorting by Ca2+-dependent Cab45 oligomerization at the trans-Golgi network. *J Cell Biol.* 213:305-314.

Curwin, A.J., J. von Blume, and V. Malhotra. 2012. Cofilin-mediated sorting and export of specific cargo from the Golgi apparatus in yeast. *Mol Biol Cell.* 23:2327-2338.

de Duve, C. 2005. The lysosome turns fifty. *Nat Cell Biol.* 7:847-849.

Dell'Angelica, E.C., Mullins, C., Caplan, S. and J. S. Bonifacino. 2000. Lysosome-related organelles. *FASEB J.* 14:1265-1278.

Deng, Y., M. Pakdel, B. Blank, E.L. Sundberg, C.G. Burd, and J. von Blume. 2018. Activity of the SPCA1 Calcium Pump Couples Sphingomyelin Synthesis to Sorting of Secretory Proteins in the Trans-Golgi Network. *Dev Cell.* 47:464-478 e468.

Desnick, R.J., and E.H. Schuchman. 2012. Enzyme replacement therapy for lysosomal diseases: lessons from 20 years of experience and remaining challenges. *Annu Rev Genomics Hum Genet.* 13:307-335.

Di Martino, R., L. Sticco, and A. Luini. 2019. Regulation of cargo export and sorting at the trans-Golgi network. *FEBS Lett.* 593:2306-2318.

Dittie, A.S., J. Klumperman, and S.A. Tooze. 1999. Differential distribution of mannose-6-phosphate receptors and furin in immature secretory granules. *J Cell Sci.* 112 (Pt 22):3955-3966.

Dittmer, F., and K. von Figura. 1999. Phosphorylation of arylsulphatase A occurs through multiple interactions with the UDP-N-acetylglucosamine-1- phosphotransferase proximal and distal to its retrieval site by the KDEL receptor. *Biochem J.* 340 (Pt 3):729-736.

Doray, B., P. Ghosh, J. Griffith, H.J. Geuze, and S. Kornfeld. 2002. Cooperation of GGAs and AP-1 in packaging MPRs at the trans-Golgi network. *Science.* 297:1700-1703.

Dowhan, W. 2017. Understanding phospholipid function: Why are there so many lipids? *J Biol Chem.* 292:10755-10766.

Dunphy, W.G., and J.E. Rothman. 1985. Compartmental organization of the Golgi stack. *Cell.* 42:13-

21.

Dupree, P., and D.J. Sherrier. 1998. The plant Golgi apparatus. *Biochim Biophys Acta*. 1404:259-270.

Duran, J.M., F. Campelo, J. van Galen, T. Sachsenheimer, J. Sot, M.V. Egorov, C. Rentero, C. Enrich, R.S. Polishchuk, F.M. Goni, B. Brugger, F. Wieland, and V. Malhotra. 2012. Sphingomyelin organization is required for vesicle biogenesis at the Golgi complex. *EMBO J*. 31:4535-4546.

Elias, S., C. Delestre, M. Courel, Y. Anouar, and M. Montero-Hadjadje. 2010. Chromogranin A as a crucial factor in the sorting of peptide hormones to secretory granules. *Cell Mol Neurobiol*. 30:1189-1195.

Ellgaard, L., and A. Helenius. 2001. ER quality control: towards an understanding at the molecular level. *Curr Opin Cell Biol*. 13:431-437.

Evers, B.M., C. Rodriguez-Navas, R.J. Tesla, J. Prange-Kiel, C.R. Wasser, K.S. Yoo, J. McDonald, B. Cenik, T.A. Ravenscroft, F. Plattner, R. Rademakers, G. Yu, C.L. White, 3rd, and J. Herz. 2017. Lipidomic and Transcriptomic Basis of Lysosomal Dysfunction in Progranulin Deficiency. *Cell Rep*. 20:2565-2574.

Fagerberg, L., K. Jonasson, G. von Heijne, M. Uhlen, and L. Berglund. 2010. Prediction of the human membrane proteome. *Proteomics*. 10:1141-1149.

Farquhar, M.G., and G.E. Palade. 1981. The Golgi apparatus (complex)-(1954-1981)- from artifact to center stage. *J Cell Biol*. 91:77s-103s.

Fass, D., S. Blacklow, P.S. Kim, and J.M. Berger. 1997. Molecular basis of familial hypercholesterolaemia from structure of LDL receptor module. *Nature*. 388:691-693.

Feige, M.J., and L.M. Hendershot. 2011. Disulfide bonds in ER protein folding and homeostasis. *Curr Opin Cell Biol*. 23:167-175.

Franzusoff, A., K. Redding, J. Crosby, R.S. Fuller, and R. Schekman. 1991. Localization of components involved in protein transport and processing through the yeast Golgi apparatus. *J Cell Biol*. 112:27-37.

Fuentealba, R.A., Q. Liu, J. Zhang, T. Kanekiyo, X. Hu, J.M. Lee, M.J. LaDu, and G. Bu. 2010. Low-density lipoprotein receptor-related protein 1 (LRP1) mediates neuronal Abeta42 uptake and lysosomal trafficking. *PLoS One*. 5:e11884.

Funato, K., H. Riezman, and M. Muniz. 2020. Vesicular and non-vesicular lipid export from the ER to the secretory pathway. *Biochim Biophys Acta Mol Cell Biol Lipids*. 1865:158453.

Futai, M., G.H. Sun-Wada, Y. Wada, N. Matsumoto, and M. Nakanishi-Matsui. 2019. Vacuolar-type ATPase: A proton pump to lysosomal trafficking. *Proc Jpn Acad Ser B Phys Biol Sci*. 95:261-277.

Gary-Bobo, M., P. Nirde, A. Jeanjean, A. Morere, and M. Garcia. 2007. Mannose 6- phosphate receptor targeting and its applications in human diseases. *Curr Med Chem*. 14:2945-2953.

Ghosh, P., N.M. Dahms, and S. Kornfeld. 2003. Mannose 6-phosphate receptors: new twists in the tale. *Nat Rev Mol Cell Biol*. 4:202-212.

Ghosh, R.N., W.G. Mallet, T.T. Soe, T.E. McGraw, and F.R. Maxfield. 1998. An endocytosed TGN38 chimeric protein is delivered to the TGN after trafficking through the endocytic recycling compartment in CHO cells. *J Cell Biol*. 142:923-936.

Gillingham, A.K., and S. Munro. 2016. Finding the Golgi: Golgin Coiled-Coil Proteins Show the Way. *Trends Cell Biol*. 26:399-408.

Gleeson, P.A., J.G. Lock, M.R. Luke, and J.L. Stow. 2004. Domains of the TGN: coats, tethers and G proteins. *Traffic*. 5:315-326.

Glick, B.S., T. Elston, and G. Oster. 1997. A cisternal maturation mechanism can explain the asymmetry of the Golgi stack. *FEBS Lett*. 414:177-181.

Glick, B.S., and A. Luini. 2011. Models for Golgi traffic: a critical assessment. *Cold Spring Harb Perspect Biol*. 3:a005215.

Goldberg, D.E., and S. Kornfeld. 1983. Evidence for extensive subcellular organization of asparagine-linked oligosaccharide processing and lysosomal enzyme phosphorylation. *J Biol Chem*. 258:3159-3165.

Gomez-Navarro, N., and E. Miller. 2016. Protein sorting at the ER-Golgi interface. *J Cell Biol*. 215:769-778.

Gopalakrishnan, M.M., H.W. Grosch, S. Locatelli-Hoops, N. Werth, E. Smolenova, M. Nettersheim, K. Sandhoff, and A. Hasilik. 2004. Purified recombinant human prosaposin forms oligomers that bind procathepsin D and affect its autoactivation. *Biochem J*. 383:507-515.

Griffiths, G., and K. Simons. 1986. The trans Golgi network: sorting at the exit site of the Golgi complex.

Science. 234:438-443.

Hanada, K., K. Kumagai, S. Yasuda, Y. Miura, M. Kawano, M. Fukasawa, and M. Nishijima. 2003. Molecular machinery for non-vesicular trafficking of ceramide. *Nature*. 426:803-809.

Hannun, Y.A., and L.M. Obeid. 2002. The Ceramide-centric universe of lipid-mediated cell regulation: stress encounters of the lipid kind. *J Biol Chem*. 277:25847-25850.

Harayama, T., and H. Riezman. 2018. Understanding the diversity of membrane lipid composition. *Nat Rev Mol Cell Biol*. 19:281-296.

Hariri, H., N. Bhattacharya, K. Johnson, A.J. Noble, and S.M. Stagg. 2014. Insights into the mechanisms of membrane curvature and vesicle scission by the small GTPase Sar1 in the early secretory pathway. *J Mol Biol*. 426:3811-3826.

Hasilik, A., C. Wrocklage, and B. Schroder. 2009. Intracellular trafficking of lysosomal proteins and lysosomes. *Int J Clin Pharmacol Ther*. 47 Suppl 1:S18-33.

Hassan, A.J., J. Zeng, X. Ni, and C.R. Morales. 2004. The trafficking of prosaposin (SGP-1) and GM2AP to the lysosomes of TM4 Sertoli cells is mediated by sortilin and monomeric adaptor proteins. *Mol Reprod Dev*. 68:476-483.

Hecht, T.K., B. Blank, M. Steger, V. Lopez, G. Beck, B. Ramazanov, M. Mann, V. Tagliabracci, and J. von Blume. 2020. Fam20C regulates protein secretion by Cab45 phosphorylation. *J Cell Biol*. 219.

Heijne, G.v. 1994. Signal peptidases. R.G. Landes Co., Austin. xi, 127 p. pp. Hiesberger, T., S. Huttler, A. Rohlmann, W. Schneider, K. Sandhoff, and J. Herz. 1998. Cellular uptake of saposin (SAP) precursor and lysosomal delivery by the low density lipoprotein receptor-related protein (LRP). *EMBO J*. 17:4617-4625.

Hineno, T., Sano, A., Kondoh, K., Ueno, S., Kakimoto, Y., and K. Yoshida. 1991. Secretion of sphingolipid hydrolase activator precursor, prosaposin. *Biochem Biophys Res Commun*. 176:668–74.

Hirokawa, N., and Y. Noda. 2008. Intracellular transport and kinesin superfamily proteins, KIFs: structure, function, and dynamics. *Physiol Rev*. 88:1089-1118.

Hishikawa, D., T. Hashidate, T. Shimizu, and H. Shindou. 2014. Diversity and function of membrane glycerophospholipids generated by the remodeling pathway in mammalian cells. *J Lipid Res*. 55:799-807.

Honore, B., and H. Vorum. 2000. The CREC family, a novel family of multiple EF- hand, low-affinity Ca(2+)-binding proteins localised to the secretory pathway of mammalian cells. *FEBS Lett*. 466:11-18.

Hu, F., T. Padukkavidana, C.B. Vaegter, O.A. Brady, Y. Zheng, I.R. Mackenzie, H.H. Feldman, A. Nykjaer, and S.M. Strittmatter. 2010. Sortilin-mediated endocytosis determines levels of the frontotemporal dementia protein, progranulin. *Neuron*. 68:654-667.

Hutchings, J., V.G. Stancheva, N.R. Brown, A.C.M. Cheung, E.A. Miller, and G. Zanetti. 2021. Structure of the complete, membrane-assembled COPII coat reveals a complex interaction network. *Nat Commun*. 12:2034.

Irwin, D.M. 2015. Genomic organization and evolution of ruminant lysozyme c genes. *Dongwuxue Yanjiu*. 36:1-17.

James, M. N. G., and A. R. Siedecki. 1986. Molecular structure of an aspartic proteinase zymogen porcine pepsinogen, at 1.8 A resolution. *Nature*. 319:33-38.

Jensen, D., and R. Schekman. 2011. COPII-mediated vesicle formation at a glance. *J Cell Sci*. 124:1-4.

Jessop, C.E., T.J. Tavender, R.H. Watkins, J.E. Chambers, and N.J. Bulleid. 2009. Substrate specificity of the oxidoreductase ERp57 is determined primarily by its interaction with calnexin and calreticulin. *J Biol Chem*. 284:2194-2202.

Johnson, N., K. Powis, and S. High. 2013. Post-translational translocation into the endoplasmic reticulum. *Biochim Biophys Acta*. 1833:2403-2409.

Johnson, N., F. Vilardi, S. Lang, P. Leznicki, R. Zimmermann, and S. High. 2012. TRC40 can deliver short secretory proteins to the Sec61 translocon. *J Cell Sci*. 125:3612-3620.

Jones, S.M., J.R. Crosby, J. Salamero, and K.E. Howell. 1993. A cytosolic complex of p62 and rab6 associates with TGN38/41 and is involved in budding of exocytic vesicles from the trans-Golgi network. *J Cell Biol*. 122:775-788.

Kakhlon, O., P. Sakya, B. Larijani, R. Watson, and S.A. Tooze. 2006. GGA function is required for maturation of neuroendocrine secretory granules. *EMBO J*. 25:1590-1602.

Karamysheva, Z.N., E.B. Tikhonova, and A.L. Karamyshev. 2019. Granulin in Frontotemporal Lobar

Degeneration: Molecular Mechanisms of the Disease. *Front Neurosci*. 13:395.

Kienzle, C., N. Basnet, A.H. Crevenna, G. Beck, B. Habermann, N. Mizuno, and J. von Blume. 2014. Cofilin recruits F-actin to SPCA1 and promotes Ca^{2+}- mediated secretory cargo sorting. *J Cell Biol*. 206:635-654.

Kim, D.I., K.C. Birendra, W. Zhu, K. Motamedchaboki, V. Doye, and K.J. Roux. 2014. Probing nuclear pore complex architecture with proximity-dependent biotinylation. *Proc Natl Acad Sci U S A*. 111:E2453-2461.

Kishimoto, Y., M. Hiraiwa, and J.S. O'Brien. 1992. Saposins: structure, function, distribution, and molecular genetics. *J Lipid Res*. 33:1255-1267.

Kleizen, B., and I. Braakman. 2004. Protein folding and quality control in the endoplasmic reticulum. *Curr Opin Cell Biol*. 16:343-349.

Klumperman, J. 2011. Architecture of the mammalian Golgi. *Cold Spring Harb Perspect Biol*. 3.

Klumperman, J., A. Hille, T. Veenendaal, V. Oorschot, W. Stoorvogel, K. von Figura, and H.J. Geuze. 1993. Differences in the endosomal distributions of the two mannose 6-phosphate receptors. *J Cell Biol*. 121:997-1010.

Kornfeld, S., and I. Mellman. 1989. The biogenesis of lysosomes. *Annu Rev Cell Biol*. 5:483-525.

Korolchuk, V.I., S. Saiki, M. Lichtenberg, F.H. Siddiqi, E.A. Roberts, S. Imarisio, L. Jahreiss, S. Sarkar, M. Futter, F.M. Menzies, C.J. O'Kane, V. Deretic, and D.C. Rubinsztein. 2011. Lysosomal positioning coordinates cellular nutrient responses. *Nat Cell Biol*. 13:453-460.

Koval, M., and R. E. Pagano 1991. Intracellular transport and metabolism of sphingomyelin. *Biochim Biophys Acta*. 1082:113-125.

Kuhlbrandt, W. 2004. Biology, structure and mechanism of P-type ATPases. *Nat Rev Mol Cell Biol*. 5:282-295.

Kuhn, P.H., K. Koroniak, S. Hogl, A. Colombo, U. Zeitschel, M. Willem, C. Volbracht, U. Schepers, A. Imhof, A. Hoffmeister, C. Haass, S. Rossner, S. Brase, and S.F. Lichtenthaler. 2012. Secretome protein enrichment identifies physiological BACE1 protease substrates in neurons. *EMBO J*. 31:3157-3168.

Kurokawa, K., and A. Nakano. 2019. The ER exit sites are specialized ER zones for the transport of cargo proteins from the ER to the Golgi apparatus. *J Biochem*. 165:109-114.

Ladinsky, M.S., D.N. Mastronarde, J.R. McIntosh, K.E. Howell, and L.A. Staehelin. 1999. Golgi structure in three dimensions: functional insights from the normal rat kidney cell. *J Cell Biol*. 144:1135-1149.

Ladinsky, M.S., C.C. Wu, S. McIntosh, J.R. McIntosh, and K.E. Howell. 2002. Structure of the Golgi and distribution of reporter molecules at 20 degrees C reveals the complexity of the exit compartments. *Mol Biol Cell*. 13:2810-2825.

Lang, L., T. Takahashi, J. Tang, and S. Kornfeld. 1985. Lysosomal enzyme phosphorylation in human fibroblasts. Kinetic parameters offer a biochemical rationale for two distinct defects in the uridine diphospho-N- acetylglucosamine:lysosomal enzyme precursor N-acetylglucosamine-1-phosphotransferase. *J Clin Invest*. 76:2191-2195.

Laurent-Matha, V., D. Derocq, C. Prebois, N. Katunuma, and E. Liaudet-Coopman. 2006. Processing of human cathepsin D is independent of its catalytic function and auto-activation: involvement of cathepsins L and B. *J Biochem*. 139:363-371.

Laurent-Matha, V., A. Lucas, S. Huttler, K. Sandhoff, M. Garcia, and H. Rochefort. 2002. Procathepsin D interacts with prosaposin in cancer cells but its internalization is not mediated by LDL receptor-related protein. *Exp Cell Res*. 277:210-219.

Lee, M.C., L. Orci, S. Hamamoto, E. Futai, M. Ravazzola, and R. Schekman. 2005. Sar1p N-terminal helix initiates membrane curvature and completes the fission of a COPII vesicle. *Cell*. 122:605-617.

Lefrancois, S., J. Zeng, A.J. Hassan, M. Canuel, and C.R. Morales. 2003. The lysosomal trafficking of sphingolipid activator proteins (SAPs) is mediated by sortilin. *EMBO J*. 22:6430-6437.

Lev, S. 2010. Non-vesicular lipid transport by lipid-transfer proteins and beyond. *Nat Rev Mol Cell Biol*. 11:739-750.

Li, J., E. Ahat, and Y. Wang. 2019. Golgi Structure and Function in Health, Stress, and Diseases. *Results Probl Cell Differ*. 67:441-485.

Lingappa, V.R., and G. Blobel. 1980. Early events in the biosynthesis of secretory and membrane proteins: the signal hypothesis. *Recent Prog Horm Res*. 36:451-475.

Lippincott-Schwartz, J., T.H. Roberts, and K. Hirschberg. 2000. Secretory protein trafficking and organelle dynamics in living cells. *Annu Rev Cell Dev Biol*. 16:557-589.

Lissandron, V., P. Podini, P. Pizzo, and T. Pozzan. 2010. Unique characteristics of Ca^{2+} homeostasis of the trans-Golgi compartment. *Proc Natl Acad Sci U S A*. 107:9198-9203.

Lou, H., S.K. Kim, E. Zaitsev, C.R. Snell, B. Lu, and Y.P. Loh. 2005. Sorting and activity-dependent secretion of BDNF require interaction of a specific motif with the sorting receptor carboxypeptidase e. *Neuron*. 45:245-255.

Lowe, M. 2011. Structural organization of the Golgi apparatus. *Curr Opin Cell Biol*. 23:85-93.

Lupashin, V., and E. Sztul. 2005. Golgi tethering factors. *Biochim Biophys Acta*. 1744:325-339.

Luzio, J.P., B. Brake, G. Banting, K.E. Howell, P. Braghetta, and K.K. Stanley. 1990. Identification, sequencing and expression of an integral membrane protein of the trans-Golgi network (TGN38). *Biochem J*. 270:97-102.

Luzio, J.P., P.R. Pryor, and N.A. Bright. 2007. Lysosomes: fusion and function. *Nat Rev Mol Cell Biol*. 8:622-632.

Maccioni, H.J., R. Quiroga, and W. Spessott. 2011. Organization of the synthesis of glycolipid oligosaccharides in the Golgi complex. *FEBS Lett*. 585:1691-1698.

Mallet, W.G., and F.R. Maxfield. 1999. Chimeric forms of furin and TGN38 are transported with the plasma membrane in the trans-Golgi network via distinct endosomal pathways. *J Cell Biol*. 146:345-359.

Mancias, J.D., and J. Goldberg. 2005. Exiting the endoplasmic reticulum. *Traffic*. 6(4):278-285.

Margittai, E., B. Enyedi, M. Csala, M. Geiszt, and G. Banhegyi. 2015. Composition of the redox environment of the endoplasmic reticulum and sources of hydrogen peroxide. *Free Radic Biol Med*. 83:331-340.

McCrossan, M., M. Windsor, S. Ponnambalam, J. Armstrong, and T. Wileman. 2001. The trans Golgi network is lost from cells infected with African swine fever virus. *J Virol*. 75:11755-11765.

Meldolesi, J., and T. Pozzan. 1998. The endoplasmic reticulum Ca^{2+} store: a view from the lumen. *Trends Biochem Sci*. 23:10-14.

Mendes, L.F.S., M.R.B. Batista, E. Kava, L. Bleicher, M.C. Micheletto, and A.J. Costa- Filho. 2022. Resurrecting Golgi proteins to grasp Golgi ribbon formation and self-association under stress. *Int J Biol Macromol*. 194:264-275.

Meyer, R.C., M.M. Giddens, B.M. Coleman, and R.A. Hall. 2014. The protective role of prosaposin and its receptors in the nervous system. *Brain Res*. 1585:1-12.

Mindell, J.A. 2012. Lysosomal acidification mechanisms. *Annu Rev Physiol*. 74:69-86.

Molinari, M., C. Galli, V. Piccaluga, M. Pieren, and P. Paganetti. 2002. Sequential assistance of molecular chaperones and transient formation of covalent complexes during protein degradation from the ER. *J Cell Biol*. 158:247-257.

Morgan, D.O., J.C. Edman, D.N. Standring, V.A. Fried, M.C. Smith, R.A. Roth, and W.J. Rutter. 1987. Insulin-like growth factor II receptor as a multifunctional binding protein. *Nature*. 329:301-307.

Mostov, K.E., and M.H. Cardone. 1995. Regulation of protein traffic in polarized epithelial cells. *Bioessays*. 17:129-138.

Munro, S. 1995. An investigation of the role of transmembrane domains in Golgi protein retention. *EMBO J*. 14:4695-4704.

Munro, S. 2011. The golgin coiled-coil proteins of the Golgi apparatus. *Cold Spring Harb Perspect Biol*. 3.

Nakano, A., and A. Luini. 2010. Passage through the Golgi. *Curr Opin Cell Biol*. 22:471-478.

Nguyen, A.D., T.A. Nguyen, L.H. Martens, L.L. Mitic, and R.V. Farese, Jr. 2013. Progranulin: at the interface of neurodegenerative and metabolic diseases. *Trends Endocrinol Metab*. 24:597-606.

Ni, X., M. Canuel, and C.R. Morales. 2006. The sorting and trafficking of lysosomal proteins. *Histol Histopathol*. 21:899-913.

Novikoff, A. B., and S. Goldfischer. 1961. Nucleosidediphosphatase activity in the Golgi apparatus and its usefulness for cytological studies. *Proc Natl Acad Sci U S A*. 47:802-810.

Ohno, H., J. Stewart, M.C. Fournier, H. Bosshart, I. Rhee, S. Miyatake, T. Saito, A. Gallusser, T. Kirchhausen, and J.S. Bonifacino. 1995. Interaction of tyrosine- based sorting signals with clathrin-associated proteins. *Science*.

269:1872-1875.

Okreglak, V., and D.G. Drubin. 2007. Cofilin recruitment and function during actin- mediated endocytosis dictated by actin nucleotide state. *J Cell Biol*. 178:1251-1264.

Olivari, S., and M. Molinari. 2007. Glycoprotein folding and the role of EDEM1, EDEM2 and EDEM3 in degradation of folding-defective glycoproteins. *FEBS Lett*. 581:3658-3664.

Pacheco-Fernandez, N., M. Pakdel, and J. Von Blume. 2021. Retention Using Selective Hooks (RUSH) Cargo Sorting Assay for Protein Vesicle Tracking in HeLa Cells. *Bio Protoc*. 11:e3936.

Pagano, R.E., V. Puri, M. Dominguez, and D.L. Marks. 2000. Membrane traffic in sphingolipid storage diseases. *Traffic*. 1:807-815.

Pakdel, M., N. Pacheco-Fernandez, and J. von Blume. 2021. Retention Using Selective Hooks (RUSH) Cargo Sorting Assay for Live-cell Vesicle Tracking in the Secretory Pathway Using HeLa Cells. *Bio Protoc*. 11:e3958.

Pakdel, M., and J. von Blume. 2018. Exploring new routes for secretory protein export from the trans-Golgi network. *Mol Biol Cell*. 29:235-240.

Palade, G. 1975. Intracellular aspects of the process of protein synthesis. *Science*. 189:347-358.

Pantazopoulou, A., and B.S. Glick. 2019. A Kinetic View of Membrane Traffic Pathways Can Transcend the Classical View of Golgi Compartments. *Front Cell Dev Biol*. 7:153.

Papanikou, E., and B.S. Glick. 2009. The yeast Golgi apparatus: insights and mysteries. *FEBS Lett*. 583:3746-3751.

Paraan, M., Mendez, J., Sharum, S., Kurtin, D., He, H., and S.M. Stagg. 2020. The structures of natively assembled clathrin-coated vesicles. *Sci Adv*. 6:eaba8397.

Park, K., S. Ju, N. Kim, and S.Y. Park. 2021. The Golgi complex: a hub of the secretory pathway. *BMB Rep*. 54:246-252.

Parton, R.G., C.G. Dotti, R. Bacallao, I. Kurtz, K. Simons, and K. Prydz. 1991. pH- induced microtubule-dependent redistribution of late endosomes in neuronal and epithelial cells. *J Cell Biol*. 113:261-274.

Paschal, B.M., and R.B. Vallee. 1987. Retrograde transport by the microtubule-associated protein MAP 1C. *Nature*. 330:181-183.

Patterson, G.H., K. Hirschberg, R.S. Polishchuk, D. Gerlich, R.D. Phair, and J. Lippincott-Schwartz. 2008. Transport through the Golgi apparatus by rapid partitioning within a two-phase membrane system. *Cell*. 133:1055-1067.

Pelham, H.R., and J.E. Rothman. 2000. The debate about transport in the Golgi--two sides of the same coin? *Cell*. 102:713-719.

Pfeffer, S.R. 2010. How the Golgi works: a cisternal progenitor model. *Proc Natl Acad Sci U S A*. 107:19614-19618.

Pfeffer, S.R. 2012. Cargo carriers from the Golgi to the cell surface. *EMBO J*. 31:3954-3955.

Pizzo, P., V. Lissandron, P. Capitanio, and T. Pozzan. 2011. Ca($^{2+}$) signalling in the Golgi apparatus. *Cell Calcium*. 50:184-192.

Pohlmann, R., M.W. Boeker, and K. von Figura. 1995. The two mannose 6-phosphate receptors transport distinct complements of lysosomal proteins. *J Biol Chem*. 270:27311-27318.

Ponnambalam, S., M. Girotti, M.L. Yaspo, C.E. Owen, A.C. Perry, T. Suganuma, T. Nilsson, M. Fried, G. Banting, and G. Warren. 1996. Primate homologues of rat TGN38: primary structure, expression and functional implications. *J Cell Sci*. 109 (Pt 3):675-685.

Potere, N., M.G. Del Buono, A.G. Mauro, A. Abbate, and S. Toldo. 2019. Low Density Lipoprotein Receptor-Related Protein-1 in Cardiac Inflammation and Infarct Healing. *Front Cardiovasc Med*. 6:51.

Preissler, S., J.E. Chambers, A. Crespillo-Casado, E. Avezov, E. Miranda, J. Perez, L.M. Hendershot, H.P. Harding, and D. Ron. 2015. Physiological modulation of BiP activity by trans-protomer engagement of the interdomain linker. *Elife*. 4:e08961.

Preissler, S., C. Rato, Y. Yan, L.A. Perera, A. Czako, and D. Ron. 2020. Calcium depletion challenges endoplasmic reticulum proteostasis by destabilising BiP- substrate complexes. *Elife*. 9.

Prescott, A.R., J.M. Lucocq, J. James, J.M. Lister, and S. Ponnambalam. 1997. Distinct compartmentalization of TGN46 and beta 1,4-galactosyltransferase in HeLa cells. *Eur J Cell Biol*. 72:238-246.

Press, B., Y. Feng, B. Hoflack, and A. Wandinger-Ness. 1998. Mutant Rab7 causes the accumulation of cathepsin D and cation-independent mannose 6- phosphate receptor in an early endocytic compartment. *J Cell Biol*. 140:1075-1089.

Preuss, D., J. Mulholland, A. Franzusoff, N. Segev, and D. Botstein. 1992. Characterization of the Saccharomyces Golgi complex through the cell cycle by immunoelectron microscopy. *Mol Biol Cell*. 3:789-803.

Pryor, P.R., B.M. Mullock, N.A. Bright, S.R. Gray, and J.P. Luzio. 2000. The role of intraorganellar Ca($2+$) in late endosome-lysosome heterotypic fusion and in the reformation of lysosomes from hybrid organelles. *J Cell Biol*. 149:1053-1062.

Pu, J., C.M. Guardia, T. Keren-Kaplan, and J.S. Bonifacino. 2016. Mechanisms and functions of lysosome positioning. *J Cell Sci*. 129:4329-4339.

Puertollano, R., R.C. Aguilar, I. Gorshkova, R.J. Crouch, and J.S. Bonifacino. 2001. Sorting of mannose 6-phosphate receptors mediated by the GGAs. *Science*. 292:1712-1716.

Puertollano, R., N.N. van der Wel, L.E. Greene, E. Eisenberg, P.J. Peters, and J.S. Bonifacino. 2003. Morphology and dynamics of clathrin/GGA1-coated carriers budding from the trans-Golgi network. *Mol Biol Cell*. 14:1545-1557.

Puri, S., C. Bachert, C.J. Fimmel, and A.D. Linstedt. 2002. Cycling of early Golgi proteins via the cell surface and endosomes upon lumenal pH disruption. *Traffic*. 3:641-653.

Qian, M., D.E. Sleat, H. Zheng, D. Moore, and P. Lobel. 2008. Proteomics analysis of serum from mutant mice reveals lysosomal proteins selectively transported by each of the two mannose 6-phosphate receptors. *Mol Cell Proteomics*. 7:58-70.

Quistgaard, E.M., P. Madsen, M.K. Groftehauge, P. Nissen, C.M. Petersen, and S.S. Thirup. 2009. Ligands bind to Sortilin in the tunnel of a ten-bladed beta- propeller domain. *Nat Struct Mol Biol*. 16:96-98.

Rabouille, C., N. Hui, F. Hunte, R. Kieckbusch, E.G. Berger, G. Warren, and T. Nilsson. 1995. Mapping the distribution of Golgi enzymes involved in the construction of complex oligosaccharides. *J Cell Sci*. 108 (Pt 4):1617-1627.

Ramazanov, B.R., M.L. Tran, and J. von Blume. 2021. Sending out molecules from the TGN. *Curr Opin Cell Biol*. 71:55-62.

Reaves, B.J., G. Banting, and J.P. Luzio. 1998. Lumenal and transmembrane domains play a role in sorting type I membrane proteins on endocytic pathways. *Mol Biol Cell*. 9:1107-1122.

Reczek, D., M. Schwake, J. Schroder, H. Hughes, J. Blanz, X. Jin, W. Brondyk, S. Van Patten, T. Edmunds, and P. Saftig. 2007. LIMP-2 is a receptor for lysosomal mannose-6-phosphate-independent targeting of beta-glucocerebrosidase. *Cell*. 131:770-783.

Reily, C., T.J. Stewart, M.B. Renfrow, and J. Novak. 2019. Glycosylation in health and disease. *Nat Rev Nephrol*. 15:346-366.

Reitman, M.L., and S. Kornfeld. 1981. UDP-N-acetylglucosamine:glycoprotein N-acetylglucosamine-1-phosphotransferase. Proposed enzyme for the phosphorylation of the high mannose oligosaccharide units of lysosomal enzymes. *J Biol Chem*. 256:4275-4281.

Reitman, M.L., A. Varki, and S. Kornfeld. 1981. Fibroblasts from patients with I-cell disease and pseudo-Hurler polydystrophy are deficient in uridine 5'- diphosphate-N-acetylglucosamine: glycoprotein N- acetylglucosaminylphosphotransferase activity. *J Clin Invest*. 67:1574-1579.

Reynders, E., F. Foulquier, W. Annaert, and G. Matthijs. 2011. How Golgi glycosylation meets and needs trafficking: the case of the COG complex. *Glycobiology*. 21:853-863.

Rijnboutt, S., Aerts, H.M.F.G., Geuze, H.J., Tager, J.M., and G.J. Strous. 1991. *J. Biol. Chem*. 266:4862-4868.

Rink, J., E. Ghigo, Y. Kalaidzidis, and M. Zerial. 2005. Rab conversion as a mechanism of progression from early to late endosomes. *Cell*. 122:735-749.Roberts, D.L., D.J. Weix, N.M. Dahms, and J.J. Kim. 1998. Molecular basis of lysosomal enzyme recognition: three-dimensional structure of the cation- dependent mannose 6-phosphate receptor. *Cell*. 93:639-648.

Rocha, N., C. Kuijl, R. van der Kant, L. Janssen, D. Houben, H. Janssen, W. Zwart, and J. Neefjes. 2009. Cholesterol sensor ORP1L contacts the ER protein VAP to control Rab7-RILP-p150 Glued and late endosome positioning. *J Cell Biol*. 185:1209-1225.

Roux, K.J., D.I. Kim, M. Raida, and B. Burke. 2012. A promiscuous biotin ligase fusion protein identifies proximal and interacting proteins in mammalian cells. *J Cell Biol*. 196:801-810.

Saftig, P., and J. Klumperman. 2009. Lysosome biogenesis and lysosomal membrane proteins: trafficking meets function. *Nat Rev Mol Cell Biol*. 10:623-635.

Saraste, J., and M. Marie. 2018. Intermediate compartment (IC): from pre-Golgi vacuoles to a semi-

autonomous membrane system. *Histochem Cell Biol*. 150:407-430.

Saraste, J., G.E. Palade, and M.G. Farquhar. 1986. Temperature-sensitive steps in the transport of secretory proteins through the Golgi complex in exocrine pancreatic cells. *Proc Natl Acad Sci U S A*. 83:6425-6429.

Sato, K., and A. Nakano. 2004. Reconstitution of coat protein complex II (COPII) vesicle formation from cargo-reconstituted proteoliposomes reveals the potential role of GTP hydrolysis by Sar1p in protein sorting. *J Biol Chem*. 279:1330-1335.

Schein, S. 2009. Architecture of clathrin fullerene cages reflects a geometric constraint--the head-to-tail exclusion rule--and a preference for asymmetry. *J Mol Biol*. 387:363-375.

Scherer, P.E., G.Z. Lederkremer, S. Williams, M. Fogliano, G. Baldini, and H.F. Lodish. 1996. Cab45, a novel (Ca2+)-binding protein localized to the Golgi lumen. *J Cell Biol*. 133:257-268.

Schrag, J.D., D.O. Procopio, M. Cygler, D.Y. Thomas, and J.J. Bergeron. 2003. Lectin control of protein folding and sorting in the secretory pathway. *Trends Biochem Sci*. 28:49-57.

Schuhmacher, M., A.T. Grasskamp, P. Barahtjan, N. Wagner, B. Lombardot, J.S. Schuhmacher, P. Sala, A. Lohmann, I. Henry, A. Shevchenko, U. Coskun, A.M. Walter, and A. Nadler. 2020. Live-cell lipid biochemistry reveals a role of diacylglycerol side-chain composition for cellular lipid dynamics and protein affinities. *Proc Natl Acad Sci U S A*. 117:7729-7738.

Schutz, I., T. Lopez-Hernandez, Q. Gao, D. Puchkov, S. Jabs, D. Nordmeyer, M. Schmudde, E. Ruhl, C.M. Graf, and V. Haucke. 2016. Lysosomal Dysfunction Caused by Cellular Accumulation of Silica Nanoparticles. *J Biol Chem*. 291:14170-14184.

Sevlever, D., P. Jiang, and S.H. Yen. 2008. Cathepsin D is the main lysosomal enzyme involved in the degradation of alpha-synuclein and generation of its carboxy-terminally truncated species. *Biochemistry*. 47:9678-9687.Sharpe, H.J., T.J. Stevens, and S. Munro. 2010. A comprehensive comparison of transmembrane domains reveals organelle-specific properties. *Cell*. 142:158-169.

Singh, S., and A. Mittal. 2016. Transmembrane Domain Lengths Serve as Signatures of Organismal Complexity and Viral Transport Mechanisms. *Sci Rep*. 6:22352.

Sleat, D.E., M.C. Della Valle, H. Zheng, D.F. Moore, and P. Lobel. 2008. The mannose 6-phosphate glycoprotein proteome. *J Proteome Res*. 7:3010-3021.

Sleat, D.E., J.A. Wiseman, I. Sohar, M. El-Banna, H. Zheng, D.F. Moore, and P. Lobel. 2012. Proteomic analysis of mouse models of Niemann-Pick C disease reveals alterations in the steady-state levels of lysosomal proteins within the brain. *Proteomics*. 12:3499-3509.

Stalder, D., and D.C. Gershlick. 2020. Direct trafficking pathways from the Golgi apparatus to the plasma membrane. *Semin Cell Dev Biol*. 107:112-125.

Stanley, K.K., and K.E. Howell. 1993. TGN38/41: a molecule on the move. *Trends Cell Biol*. 3:252-255.

Stanley, P. 2011. Golgi glycosylation. *Cold Spring Harb Perspect Biol*. 3.

Staudt, C., E. Puissant, and M. Boonen. 2016. Subcellular Trafficking of Mammalian Lysosomal Proteins: An Extended View. *Int J Mol Sci*. 18.

Stefan, C.J., W.S. Trimble, S. Grinstein, G. Drin, K. Reinisch, P. De Camilli, S. Cohen, A.M. Valm, J. Lippincott-Schwartz, T.P. Levine, D.B. Iaea, F.R. Maxfield, C.E. Futter, E.R. Eden, D. Judith, A.R. van Vliet, P. Agostinis, S.A. Tooze, A. Sugiura, and H.M. McBride. 2017. Membrane dynamics and organelle biogenesis-lipid pipelines and vesicular carriers. *BMC Biol*. 15:102.

Sun, G., H. Zhao, B. Kalyanaraman, and N.M. Dahms. 2005. Identification of residues essential for carbohydrate recognition and cation dependence of the 46-kDa mannose 6-phosphate receptor. *Glycobiology*. 15:1136-1149.

Suzuki, C.K., J.S. Bonifacino, A.Y. Lin, M.M. Davis, and R.D. Klausner. 1991. Regulating the retention of T-cell receptor alpha chain variants within the endoplasmic reticulum: Ca(2+)-dependent association with BiP. *J Cell Biol*. 114:189-205.

Tagliabracci, V.S., J.L. Engel, J. Wen, S.E. Wiley, C.A. Worby, L.N. Kinch, J. Xiao, N.V. Grishin, and J.E. Dixon. 2012. Secreted kinase phosphorylates extracellular proteins that regulate biomineralization. *Science*. 336:1150-1153.

Tagliabracci, V.S., S.E. Wiley, X. Guo, L.N. Kinch, E. Durrant, J. Wen, J. Xiao, J. Cui, K.B. Nguyen, J.L. Engel, J.J. Coon, N. Grishin, L.A. Pinna, D.J. Pagliarini, and J.E. Dixon. 2015. A Single Kinase Generates the Majority of the Secreted Phosphoproteome. *Cell*. 161:1619-1632.

Tang, B.L. 2001. Protein trafficking mechanisms associated with neurite outgrowth and polarized sorting in neurons. *J Neurochem*. 79:923-930.

Tatu, U., and A. Helenius. 1997. Interactions between newly synthesized glycoproteins, calnexin and a network of resident chaperones in the endoplasmic reticulum. *J Cell Biol*. 136:555-565.

Tayama, M., S. Soeda, Y. Kishimoto, B.M. Martin, J.W. Callahan, M. Hiraiwa, and J.S. O'Brien. 1993. Effect of saposins on acid sphingomyelinase. *Biochem J*. 290 (Pt 2):401-404.

Tayebi, N., G. Lopez, J. Do, and E. Sidransky. 2020. Pro-cathepsin D, Prosaposin, and Progranulin: Lysosomal Networks in Parkinsonism. *Trends Mol Med*. 26:913-923.

Thurberg, B.L., C. Lynch Maloney, C. Vaccaro, K. Afonso, A.C. Tsai, E. Bossen, P.S. Kishnani, and M. O'Callaghan. 2006. Characterization of pre- and post- treatment pathology after enzyme replacement therapy for Pompe disease. *Lab Invest*. 86:1208-1220.

Tooze, J., and M. Hollinshead. 1991. Tubular early endosomal networks in AtT20 and other cells. *J Cell Biol*. 115:635-653.

Tooze, S.A. 1998. Biogenesis of secretory granules in the trans-Golgi network of neuroendocrine and endocrine cells. *Biochim Biophys Acta*. 1404:231-244.

Towler, M.C., A.R. Prescott, J. James, J.M. Lucocq, and S. Ponnambalam. 2000. The manganese cation disrupts membrane dynamics along the secretory pathway. *Exp Cell Res*. 259:167-179.

Trivedi, P.C., J.J. Bartlett, and T. Pulinilkunnil. 2020. Lysosomal Biology and Function: Modern View of Cellular Debris Bin. *Cells*. 9.

Tushaus, J., S.A. Muller, E.S. Kataka, J. Zaucha, L. Sebastian Monasor, M. Su, G. Guner, G. Jocher, S. Tahirovic, D. Frishman, M. Simons, and S.F. Lichtenthaler. 2020. An optimized quantitative proteomics method establishes the cell type- resolved mouse brain secretome. *EMBO J*. 39:e105693.

van Galen, J., F. Campelo, E. Martinez-Alonso, M. Scarpa, J.A. Martinez-Menarguez, and V. Malhotra. 2014. Sphingomyelin homeostasis is required to form functional enzymatic domains at the trans-Golgi network. *J Cell Biol*. 206:609-618.

van Meer, G., D.R. Voelker, and G.W. Feigenson. 2008. Membrane lipids: where they are and how they behave. *Nat Rev Mol Cell Biol*. 9:112-124.

Vandecaetsbeek, I., Vangheluwe, P., Raeymaekers, L., Wuytack, F., and J. Vanoevelen. 2011. The Ca^{2+} pumps of the endoplasmic reticulum and Golgi apparatus. *Cold Spring Harb Perspect Biol*. 3:a004184.

Vangheluwe, P., M.R. Sepulveda, L. Missiaen, L. Raeymaekers, F. Wuytack, and J. Vanoevelen. 2009. Intracellular Ca^{2+}- and Mn^{2+}-transport ATPases. *Chem Rev*. 109:4733-4759.

Varki, A., and S. Kornfeld. 1981. Purification and characterization of rat liver alpha-N- acetylglucosaminyl phosphodiesterase. *J Biol Chem*. 256:9937-9943.

Venditti, R., Wilson, C., and M.A. de Matteis. 2013. Exiting the ER: what we know and what we don't. *Trends Cell Biol*. 24:9-18.

Voeltz, G.K., M.M. Rolls, and T.A. Rapoport. 2002. Structural organization of the endoplasmic reticulum. *EMBO Rep*. 3:944-950.

von Blume, J., A.M. Alleaume, G. Cantero-Recasens, A. Curwin, A. Carreras-Sureda, T. Zimmermann, J. van Galen, Y. Wakana, M.A. Valverde, and V. Malhotra. 2011. ADF/cofilin regulates secretory cargo sorting at the TGN via the Ca^{2+} ATPase SPCA1. *Dev Cell*. 20:652-662.

von Blume, J., A.M. Alleaume, C. Kienzle, A. Carreras-Sureda, M. Valverde, and V. Malhotra. 2012. Cab45 is required for Ca(2+)-dependent secretory cargo sorting at the trans-Golgi network. *J Cell Biol*. 199:1057-1066.

von Blume, J., J.M. Duran, E. Forlanelli, A.M. Alleaume, M. Egorov, R. Polishchuk, H. Molina, and V. Malhotra. 2009. Actin remodeling by ADF/cofilin is required for cargo sorting at the trans-Golgi network. *J Cell Biol*. 187:1055-1069.von Blume, J., and A. Hausser. 2019. Lipid-dependent coupling of secretory cargo sorting and trafficking at the trans-Golgi network. *FEBS Lett*. 593:2412-2427.

Voorhees, R.M., and R.S. Hegde. 2016. Structure of the Sec61 channel opened by a signal sequence. *Science*. 351:88-91.

Vorum, H., H. Hager, B.M. Christensen, S. Nielsen, and B. Honore. 1999. Human calumenin localizes to the secretory pathway and is secreted to the medium. *Exp Cell Res*. 248:473-481.

Voss, M., B. Schroder, and R. Fluhrer. 2013. Mechanism, specificity, and physiology of signal peptide peptidase (SPP) and SPP-like proteases. *Biochim Biophys Acta*. 1828:2828-2839.

Wakana, Y., R. Kotake, N. Oyama, M. Murate, T. Kobayashi, K. Arasaki, H. Inoue, and

M. Tagaya. 2015. CARTS biogenesis requires VAP-lipid transfer protein complexes functioning at the endoplasmic reticulum-Golgi interface. *Mol Biol Cell*. 26:4686-4699.

Wakana, Y., J. van Galen, F. Meissner, M. Scarpa, R.S. Polishchuk, M. Mann, and V. Malhotra. 2012. A new class of carriers that transport selective cargo from the trans Golgi network to the cell surface. *EMBO J*. 31:3976-3990.

Wandinger-Ness, A., and M. Zerial. 2014. Rab proteins and the compartmentalization of the endosomal system. *Cold Spring Harb Perspect Biol*. 6:a022616.

Watson, P., and D.J. Stephens. 2005. ER-to-Golgi transport: form and formation of vesicular and tubular carriers. *Biochim Biophys Acta*. 1744:304-315.

Wilbur, J.D., P.K. Hwang, J.A. Ybe, M. Lane, B.D. Sellers, M.P. Jacobson, R.J. Fletterick, and F.M. Brodsky. 2010. Conformation switching of clathrin light chain regulates clathrin lattice assembly. *Dev Cell*. 18:841-848.

Willnow, T.E., C.M. Petersen, and A. Nykjaer. 2008. VPS10P-domain receptors - regulators of neuronal viability and function. *Nat Rev Neurosci*. 9:899-909.

Witkos, T.M., and M. Lowe. 2015. The Golgin Family of Coiled-Coil Tethering Proteins. *Front Cell Dev Biol*. 3:86.

Wuytack, F., L. Raeymaekers, and L. Missiaen. 2002. Molecular physiology of the SERCA and SPCA pumps. *Cell Calcium*. 32:279-305.

Xiang, Y., and Y. Wang. 2010. GRASP55 and GRASP65 play complementary and essential roles in Golgi cisternal stacking. *J Cell Biol*. 188:237-251.

Xiang, Y., and Y. Wang. 2011. New components of the Golgi matrix. *Cell Tissue Res*. 344:365-379.

Yabe, D., M. Taniwaki, T. Nakamura, N. Kanazawa, K. Tashiro, and T. Honjo. 1998. Human calumenin gene (CALU): cDNA isolation and chromosomal mapping to 7q32. *Genomics*. 49:331-333.

Yadav, S., and A.D. Linstedt. 2011. Golgi positioning. *Cold Spring Harb Perspect Biol*. 3.

Yamamoto, Y., and T. Sakisaka. 2012. Molecular machinery for insertion of tail- anchored membrane proteins into the endoplasmic reticulum membrane in mammalian cells. *Mol Cell*. 48:387-397.

Yang, Y., M. Lee, and G.D. Fairn. 2018. Phospholipid subcellular localization and dynamics. *J Biol Chem*. 293:6230-6240.

Zaidi, N., A. Maurer, S. Nieke, and H. Kalbacher. 2008. Cathepsin D: a cellular roadmap. *Biochem Biophys Res Commun*. 376:5-9.

Zempel, H., and E. Mandelkow. 2014. Lost after translation: missorting of Tau protein and consequences for Alzheimer disease. *Trends Neurosci*. 37:721-732.

Zhang, X., and S.O. Shan. 2014. Fidelity of cotranslational protein targeting by the signal recognition particle. *Annu Rev Biophys*. 43:381-408.

Zhang, X., L. Wang, B. Lak, J. Li, E. Jokitalo, and Y. Wang. 2018. GRASP55 Senses Glucose Deprivation through O-GlcNAcylation to Promote Autophagosome- Lysosome Fusion. *Dev Cell*. 45:245-261 e246.

Zhang, Z., P. Yue, T. Lu, Y. Wang, Y. Wei, and X. Wei. 2021. Role of lysosomes in physiological activities, diseases, and therapy. *J Hematol Oncol*. 14:79.

Zheng, Y., O.A. Brady, P.S. Meng, Y. Mao, and F. Hu. 2011. C-terminus of progranulin interacts with the beta-propeller region of sortilin to regulate progranulin trafficking. *PLoS One*. 6:e21023.

Zhou, X., D.H. Paushter, T. Feng, C.M. Pardon, C.S. Mendoza, and F. Hu. 2017c. Regulation of cathepsin D activity by the FTLD protein progranulin. *Acta Neuropathol*. 134:151-153.

Zhou, X., P.M. Sullivan, L. Sun, and F. Hu. 2017b. The interaction between progranulin and prosaposin is mediated by granulins and the linker region between saposin B and C. *J Neurochem*. 143:236-243.

Zhou, X., L. Sun, F. Bastos de Oliveira, X. Qi, W.J. Brown, M.B. Smolka, Y. Sun, and F. Hu. 2015. Prosaposin facilitates sortilin-independent lysosomal trafficking of progranulin. *J Cell Biol*. 210:991-1002.

Zhou, X., L. Sun, O. Bracko, J.W. Choi, Y. Jia, A.L. Nana, O.A. Brady, J.C.C. Hernandez, N. Nishimura, W.W. Seeley, and F. Hu. 2017a. Impaired prosaposin lysosomal trafficking in frontotemporal lobar degeneration due to progranulin mutations. *Nat Commun*. 8:15277.

Zimmermann, R., M. Sagstetter, M.J. Lewis, and H.R. Pelham. 1988. Seventy- kilodalton heat shock proteins and an additional component from reticulocyte lysate stimulate import of M13 procoat protein into microsomes. *EMBO J*. 7:2875-2880.

9 Acknowledgements

roommate since the time we started our 'collaborative' adventurous move from Germany to the US.

Thanks to my former lab members in Munich Renate Gautsch and Gisela Beck for immaculate cell culture work, lab management and cloning help, Dr. Mehrshad Pakdel and Dr. Natalia Pacheco-Fernandez for a wonderful working environment, fun breaks, and conversations, also after the lab time.

Of course, I want to thank all my old and new friends who supported me throughout my US stay, in particular Melanie, Thuy and Muimui. Also, I want to thank the Yale Badminton team, especially Pei Hua, Mel, Ed and Ian for all the fun training and practice sessions, competitions, gatherings and pot-lucks - a much needed balance and off-time from the lab. In this regard, a special thanks to Dr. Derek Feng, who supported me with guidance, advice for the PhD and beyond. Thanks also to Dr. Yuki Yasumoto for Japanese-learning sessions and cooking evenings.

A very special acknowledgement to my partner Ayato for the patience, emotional support, motivation and happy moments that were essential to finish the thesis alone in a different country.

Last but not least, I want to acknowledge my family, in particular my sister for the endless support and reassurance, affirmation and conversations.

Để bài luận án tiến sĩ này cố thế hoàn thành, con xin cảm ơn Bố Mẹ và em Mai Linh đã bên cạnh, luôn động viên, ủng hộ.